REPORT DOCUMENTATION PAGE

AFRL-SR-AR-TR-05-

00876

1. REPORT DATE (DD-MM-YYYY)	2. REPORT TYPE	3. DATES COVERED (From - To)
22/11/2004	Final Technical	07/15/99-07/14/04

4. TITLE AND SUBTITLE
"Center for Radiation Studies and Solutions "

5a. CONTRACT NUMBER

5b. GRANT NUMBER
F49620-99-1-0296

5c. PROGRAM ELEMENT NUMBER

6. AUTHOR(S)
Dr. Umesh K. Mishra

5d. PROJECT NUMBER

5e. TASK NUMBER

5f. WORK UNIT NUMBER

7. PERFORMING ORGANIZATION NAME(S) AND ADDRESS(ES)
University of California, Santa Barbara
Santa Barbara, CA 93106-2050

8. PERFORMING ORGANIZATION REPORT NUMBER

9. SPONSORING/MONITORING AGENCY NAME(S) AND ADDRESS(ES)
AFOSR
4015 Wilson Blvd., Room 713
Arlington, VA 22203

NE

10. SPONSOR/MONITOR'S ACRONYM(S)

11. SPONSOR/MONITOR'S REPORT NUMBER(S)

12. DISTRIBUTION/AVAILABILITY STATEMENT
Distribution Unlimited, approved for public release

13. SUPPLEMENTARY NOTES

14. ABSTRACT
The influence of the radiation to the performance of the GaN-based and GaAs-based electronic devices was investigated extensively. In order to study the effects upon various devices, several novel device structures (such as p-capped AlGaN/GaN HEMTs and GOI GaAs pHEMTs) as well as new processing techniques were developed. The radiation induced traps, the forward and reserved biased currents of the diodes and the DC current-voltage characteristics of HEMTs and HBTs were investigated as a function of gamma-ray and proton radiation energy and total dose. The degradation mechanisms were discussed. The research indicated that GaN has an intrinsically low susceptibility to radiation-induced material degradation and GaN-based electronic devices appear to be excellent candidates for use in space systems.

15. SUBJECT TERMS
AlGaN, GaN, AlGaAs, GaAs, FET, HEMT, HBT, diode, microwave power devices, gamma radiation effects, proton radiation effects

16. SECURITY CLASSIFICATION OF:			17. LIMITATION OF ABSTRACT	18. NUMBER OF PAGES	19a. NAME OF RESPONSIBLE PERSON
a. REPORT	b. ABSTRACT	c. THIS PAGE			Dr. Umesh K. Mishra
unclassified	unclassified	unclassified	UL	114	19b. TELEPHONE NUMBER (Include area code) 805-893-3586

Final Technical Report

Air force grant number: F49620-99-1-0296

Title "*Center for the Radiation Studies and Solutions*"

Attn: Dr. Gerald L. Witt
AFOSR
4015 Wilson Blvd, Room 713
Arlington, VA 22203
Tel: (703)696-8571
Fax: (703)696-8481

Dr. Umesh K. Mishra
Electrical and Computer Engineering Department
University of California, Santa Barbara
Santa Barbara, CA 93106
Tel: (805)893-3586

Table of Contents

Part I Device Development

Part 2 Radiation Study

Part I Device development

To study the effects of radiation upon the various devices, different types of GaAs and GaN-based electronic devices were developed. The growth, fabrication and characterization were investigated in detail.

Oxidized GaAs pHEMT was studied. The growth was optimized to minimize the charge loss and partially oxidized pHEMT showed improved power added efficiency(PAE). Oxidation technique was also applied to GaAs-based HBTs. Oxide aperture GaAs HBT showed an increased f_{max} due to the reduced base-collector capacitance.

As to the GaN-based electronic devices, DC-to-RF dispersion phenomenon and its suppression were investigated. The temperature dependence of the DC and pulsed I-V characteristics were measured and related trapping mechanism was discussed. A p-GaN capped AlGaN/GaN HEMT was developed to reduce the dispersion without any surface passivation. Additionally, some GaN processing techniques were developed. Digital etching of GaN HEMTs provides a highly reproducible, high quality (i.e., low damage) gate recess process with no selectivity between AlGaN and GaN. A high temperature and high pressure thermal processing was also studied for the ion implantation.

GaAs-based devices

GaAs on Insulator (GOI) metal-semiconductor field effect transistors (MESFETs) have shown low substrate leakage current and high power added efficiency. It is of great interest to extend this technology to pHEMTs, but high charge loss after the oxidation has been a serious problem for the application of GOI technology. Most of the efforts focused on the development of low charge loss, high quality epi materials. The growth of low temperature (LT) GaAs or AlGaAs and its' in-situ annealing conditions are critical for low charge loss. Unoxidized, partially and fully oxidized devices were built on the same wafer at the same time for comparison. Partially oxidized devices showed improved power added efficiency. On the other hand fully oxidized devices suffered from impact ionization and low thermal conductance of the oxide.

Oxide aperture HBTs have recently been fabricated. These devices show an increased f_{max} as a result of the reduced base-collector capacitance, but due to parasitic capacitance at the base-emitter their f_{τ} is limited.

1.1. GOI MESFETs and pHEMTs

1.1.1. Optimized Growth

Optimized the MBE growth conditions for low charge loss and high mobility, high sheet charge density MESFET and pHEMT structures (Figure 1).

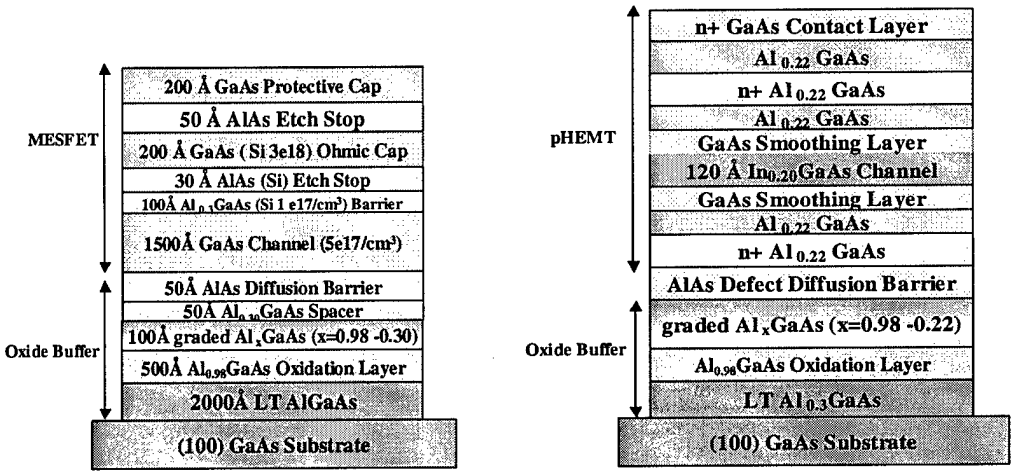

Figure 1 MBE grown GOI MESFET and pHEMT structures

The 2000Å low temperature (LT) grown GaAs or $Al_{0.30}GaAs$ underneath the oxidation layer is believed to expedite the oxidation process since the As precipitates in this LT grown layer act as gathering centers for As byproducts produced in the oxidation process. Further more, LT GaAs or AlGaAs has been shown to have very short lifetime on the order of ps due to high defect density in the material. Electron hole pairs induced by high-energy particles can recombine quickly in this LT grown layer, thus improving the radiation hardness of the devices. Due to the low surface mobility of Al, LT grown $Al_{0.3}GaAs$ tends to grow rough and even polycrystalline at 270°C. Its' growth temperature was increased to 300~400°C, which gave smooth LT layer and lowered charge loss of 6 ~15%, without slowing down the oxidation rate. Annealing at 600°C for 10 minutes is the optimized in-situ LT (Al)GaAs annealing condition. Hall measurements of MESFET structures showed sheet charge densities of 3 ~ 6 x $10^{12}/cm^2$ and room temperature mobilities of 2500 ~ 3000 $cm^2/V{\cdot}s$. pHEMT structures achieved sheet charge densities of 3 ~ 4.7 x $10^{12}/cm^2$ and room temperature mobilities of 5000 ~ 6800 $cm^2/V{\cdot}s$.

1.1.2. Partially Oxidized GOI FETs with improved PAE

Fully oxidized pHEMTs with LT GaAs buffer showed transconductance peaking as high as 50% compared with the unoxidized devices due to impact ionization in the InGaAs channel, as well as charge loss up to 30% due to back depletion caused by defects at the oxide-semiconductor interface (Figure 2).

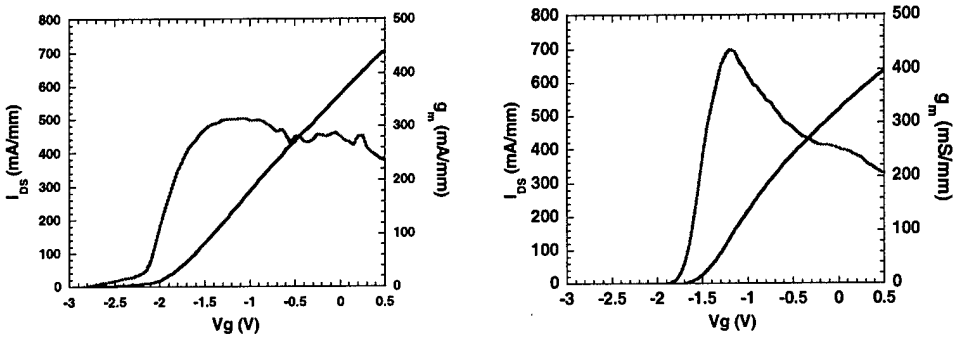

Figure 2 Drain current and transconductance versus gate bias at 2.5 V drain bias of (left) unoxidized sample with maximum g_m of 313 mS/mm and (right) oxidized sample with peaked transconductance as high as 437 mS/mm.

Partial oxidation was investigated to solve these problems. A series of partially to fully oxidized pHEMTs were fabricated with the oxidation front extending from below the source edge to beyond the drain edge. Device layout was shown in Figure 3. It was found that the largest transconductance peaking and charge loss occurred for devices with an

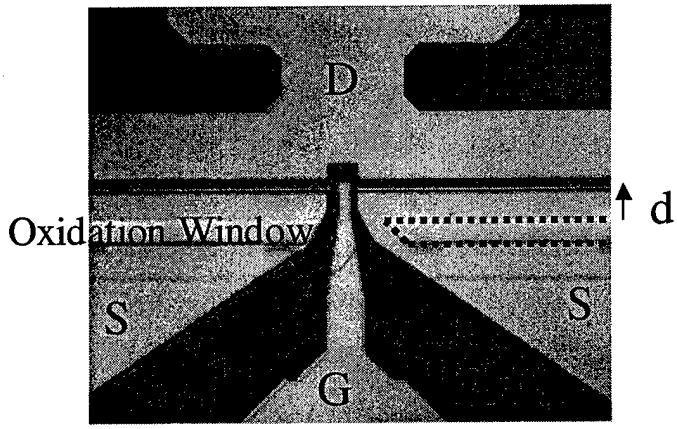

Figure 3 pHEMT device layout with varying distance between the oxidation window and device source edge.

oxidation front extending beyond the gate region (Figure 4). Devices with the oxidation front stopped around the source edge showed flat transconductance curves and negligible charge loss. As shown in Figure 5, improved PAEs as high as 55% have been achieved at

8 GHz, class AB bias condition, compared with a PAE of 32.5% for an unoxidized control sample on the same wafer and fabricated at the same time. The associated power

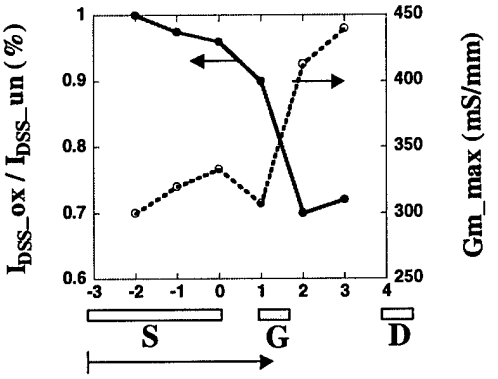

I_{DSS}_unoxidized = 667 mA/mm

Gm_max_unoxidized = 341 mS/mm

Figure 4 Normalized I_{DSS} and maximum transconductance at 2.5 V of partially oxidized pHEMTs.

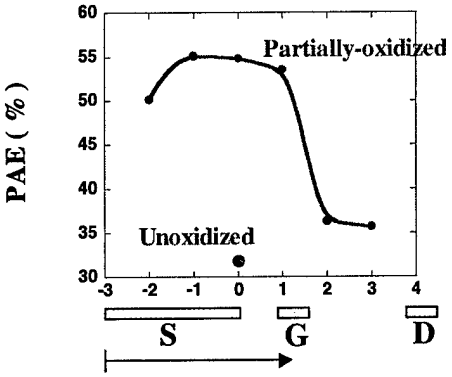

PAE_unoxidized = 32.5 %

Figure 5 Power added efficiency of pHEMTs at 8 GHz with a bias near class AB operation. The drain bias was 3.5 V.

gains were around 15 to 17 dB at a low V_{DS} bias of 3.5V. The preliminary results indicated partially oxidized pHEMTs are promising for high efficiency low voltage wireless application.

MESFET devices with LT $Al_{0.30}GaAs$ buffer showed minimized charge loss and similar trend in terms of RF performance (Figure 6). Partially oxidized devices obtained 62% PAE compared with unoxidized devices with 55% PAE at 4 GHz, class AB bias condition.

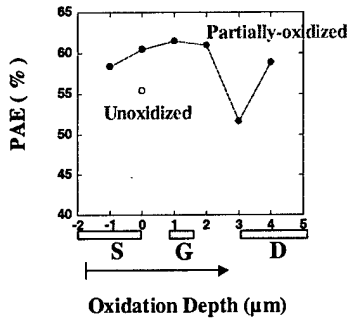

Figure 6 Power added efficiency of MESFETs at 8 GHz with a bias near class AB operation. The drain bias was 3 ~ 4 V.

1.2. Oxide Aperture HBT

1.2.1. Oxide Aperture Diode

Oxide aperture diodes, similar to those used in the base-emitter junction of the oxide aperture transistor, were fabricated and studied to better understand the role and potential effect of the oxide aperture on diode performance, and thus transistor performance.

The layer structure, accompanied by its band structure, used in the fabrication of the oxide aperture diodes (oxide diodes) is shown in Figure 7; the thickness of the base-emitter grade (t_{BE}) was varied between 100 Å, 500 Å, and 1000 Å with the thickness of the emitter grade held at 500 Å. The diodes were fabricated using a standard airbridge, mesa diode structure. The process, in essence, consisted of etching the diode mesa down to the sub-emitter to expose the $AlAs_{0.56}Sb_{0.44}$ layer for oxidation. After the $AlAs_{0.56}Sb_{0.44}$ layer was oxidized to form the aperture, base and emitter contacts were deposited. Devices were completed with an isolation etch and airbridge process.

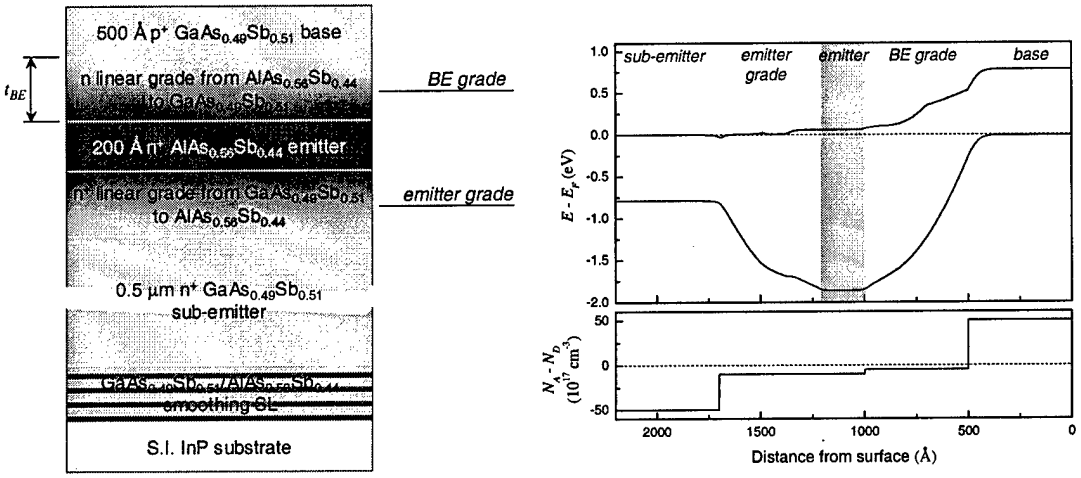

Figure 7 Layer structure and band diagram of the oxide aperture diodes used in this dissertation. The band diagram is for a diode with a 500 Å base-emitter grade. The shaded region indicates the location of the oxide aperture.

A summary of the dominant active geometry and diode ideality factor for diodes fabricated in this dissertation, extracted from current-voltage characteristics, are presented in Table 1. A plot of ideality factor versus base-emitter grade thickness, t_{BE}, is shown in Figure 8. The ideality factor is found to be a minimum for oxide diodes with t_{BE} = 500 Å.

t_{BE} (Å)	Dominant active geometry	Ideality factor, η
unoxidized	Mesa area, A_{mesa}	~1
100	Aperture perimeter, $P_{aperture}$	1.88
500	Aperture area, $A_{aperture}$	1.01
1000	Between $A_{aperture}$ and A_{mesa}	1.36

Table 1 Summary of active geometry and ideality factor for diodes fabricated in this dissertation.

Figure 9 presents an illustration of the hypothesized physics underlying the observed characteristics, which are similar to those seen in conventional emitter-up heterojunction bipolar transistors (HBTs) with emitter ledges. For oxide diodes with t_{BE} = 100 Å, the close proximity of the oxide surface to the depletion region of the *pn* junction results in carrier recombination along the inner periphery of the oxide aperture (Figure 9a). If t_{BE} is increased, the oxide is removed away from the *pn* junction depletion region, removing its

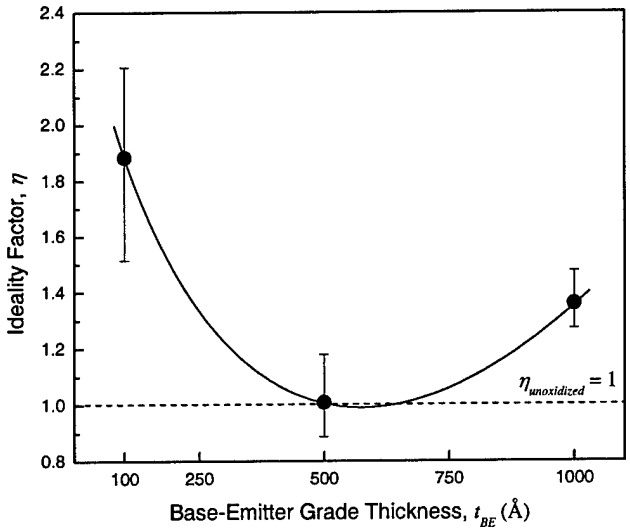

Figure 8 Plot of ideality factor, η, versus base-emitter grade thickness, t_{BE}. The average η as a function of bias for each thickness found using with the error bars indicating the maximum and minimum measured η.

influence on the junction's carrier dynamics (Figure 9b and c). In the t_{BE} = 1000 Å case, the region above the oxide aperture becomes undepleted, allowing for lateral diffusion of carriers outside of the aperture area, reducing the effectiveness of the aperture, and resulting in injection of carriers outside of the aperture area (Figure 9c).

To properly channel the carriers injected into the base from the emitter, the material above the oxide aperture must remain depleted, in order to prevent lateral carrier diffusion. Therefore, the base-emitter grade must be sufficiently thick to remove the

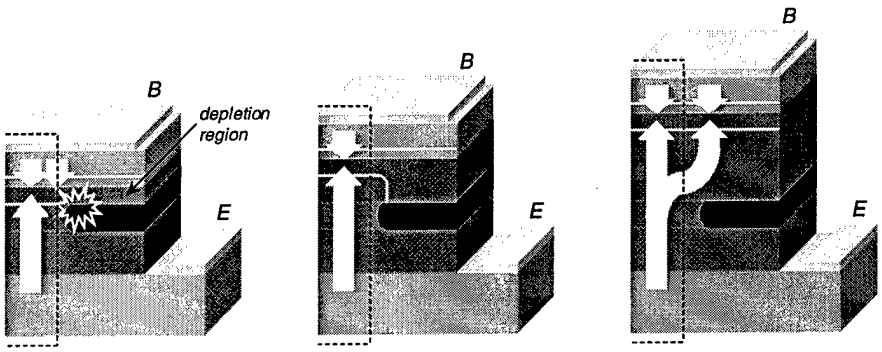

(a) t_{BE} = 100 Å (b) t_{BE} = 500 Å (c) t_{BE} = 1000 Å

Figure 9 Illustration of oxide aperture half-diodes with (a) t_{BE} = 100 Å, (b) t_{BE} = 500 Å, and (c) t_{BE} = 1000 Å. The dashed line outlines the region bounded by the oxide aperture.

oxide's influence on the *pn* junction's carrier dynamics, but not so thick that the region above the aperture becomes undepleted, allowing diffusion outside of the aperture area (Figure 9b).

Simulations of the oxide aperture diodes using ATLAS Device Simulation Software[6] support these conclusions (Figure 10).[7]

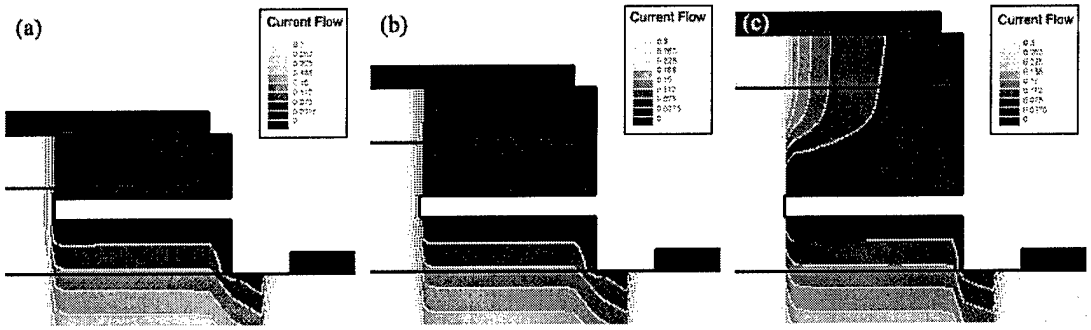

Figure 10 Simulations of the oxide aperture diodes: (a) t_{BE} = 100 Å (without recombination), (b) t_{BE} = 500 Å, and (c) t_{BE} = 1000 Å. The light regions indicate areas of high current density; the dark, low current density.

1.2.2. Oxide Aperture HBT

The layer structure and band diagram for the Generation II oxide aperture HBTs fabricated in this dissertation is presented in Figure 11. The structure (from substrate to surface) consisted of a semi-insulating (SI) InP substrate, a 0.5 μm n^+ $GaAs_{0.49}Sb_{0.51}$ sub-emitter (Te: 1×10^{19} cm^{-3}), a 500 Å n+ linear grade from $GaAs_{0.49}Sb_{0.51}$ to $AlAs_{0.56}Sb_{0.44}$ (Te: 1×10^{19} cm^{-3}), a 200 Å n^+ $AlAs_{0.56}Sb_{0.44}$ emitter (source layer for the oxide aperture) (Te: 5×10^{18} cm^{-3}), a 500 Å n linear grade from $AlAs_{0.56}Sb_{0.44}$ to $GaAs_{0.49}Sb_{0.51}$ (Te:

1×10^{18} cm^{-3}), a 500 Å p^+ $GaAs_{0.49}Sb_{0.51}$ base (Be: 5×10^{19} cm^{-3}), and a 3000 Å n^- $In_{0.53}Ga_{0.47}As$ collector (Te: 5×10^{16} cm^{-3}).

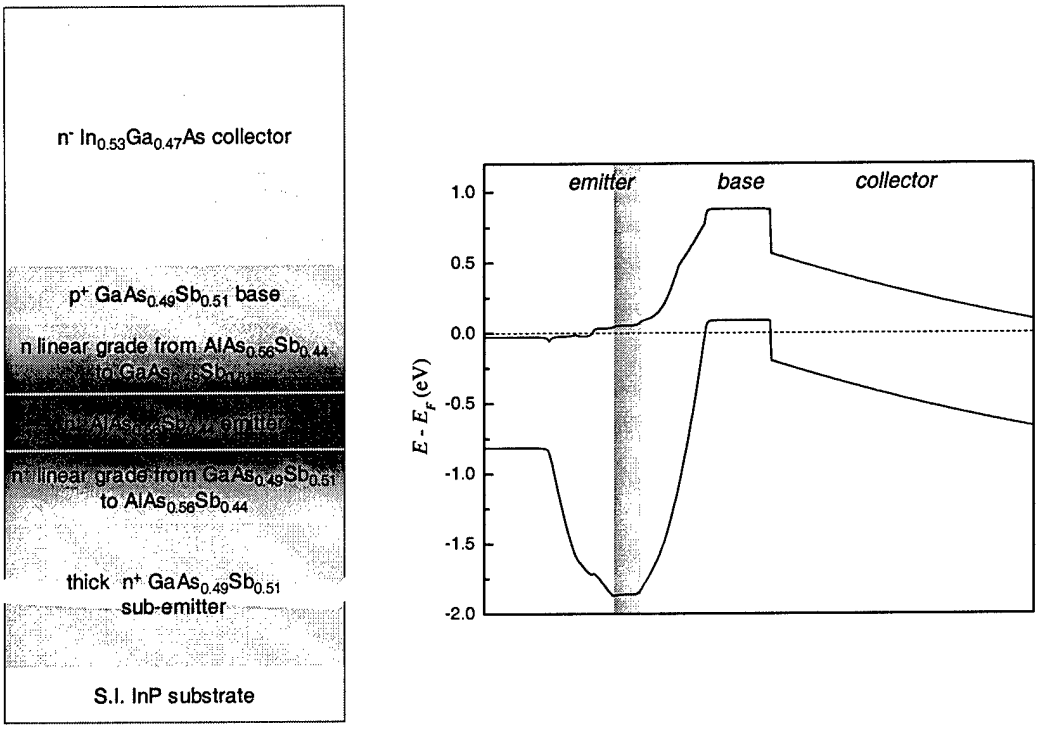

Figure 11 Layer structure and band diagram of the oxide aperture HBT.

The fabrication of the oxide aperture HBT is not that different from most conventional three-tiered mesa RF HBTs, which makes the device attractive from a production point-of-view. The fabrication process began with the deposition of a 1 μm SiO_2 dummy collector by standard photolithography, SiO_2 e-beam evaporation, and lift-off. The base mesa was then defined using photolithography and a phosphoric acid-based etch. The mesa was etched down to the sub-emitter with the intention of exposing the $AlAs_{0.56}Sb_{0.44}$ emitter for oxidation. After the $AlAs_{0.56}Sb_{0.44}$ emitter was oxidized to form the oxide aperture, the collector mesa was defined using a selective citric acid-based etch. The base and emitter contacts were deposited next by e-beam evaporation. An emitter mesa etch down to the SI InP electrically isolates the device. A co-planar waveguide (CPW) transmission line structure and microwave probe pads are deposited on the SI InP to facilitate microwave measurements. The wafer is then planarized for subsequent airbridge/interconnect processing. After airbridge posts are deposited by e-beam evaporation, the planarization resist is blanket etched to expose the SiO_2 dummy

collector. Following the airbridge lithography, the SiO_2 dummy collector is removed in buffered hydrofluoric acid to expose the collector. The airbridge metal is deposited by e-beam evaporation, forming a Schottky contact on the collector. The fabrication is completed by opening vias for contacting the CPW lines. Figure 12 shows a photograph of a completed device.

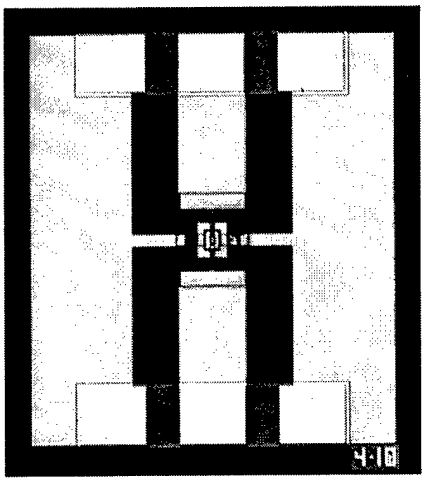

Figure 12 Photo of a completed oxide aperture HBT. The device here has a 4×10 μm^2 collector contact.

Gummel and common-emitter characteristics for three sizes of Generation II HBTs are shown in Figure 13: a transistor with a 3.5×9.5 μm^2 emitter area and 4×10 μm^2 collector area (referred to as a 4×10 transistor), a transistor with $A_E = 1.5 \times 9.5$ μm^2 and $A_C = 2 \times 10$ μm^2 (2×10 transistor), and a transistor with $A_E = 0.5 \times 9.5$ μm^2 and $A_C = 1 \times 10$ μm^2 (1×10 transistor). These devices, like the previous generation, show a considerably high gain. In strong contrast to the previous generations' characteristics, this generation displays excellent ideality factors for the base and collector currents ($\eta_B = 1.18$, $\eta_C = 1$). The low breakdown and increased output conductance, especially at higher current densities, is believed to be due to impact ionization in the collector and not the Early Effect.

The short circuit current gain (h_{21}) and unilateral power gain (U) corresponding for maximum measured f_{max} a 2×10 HBT is shown in Figure 14.

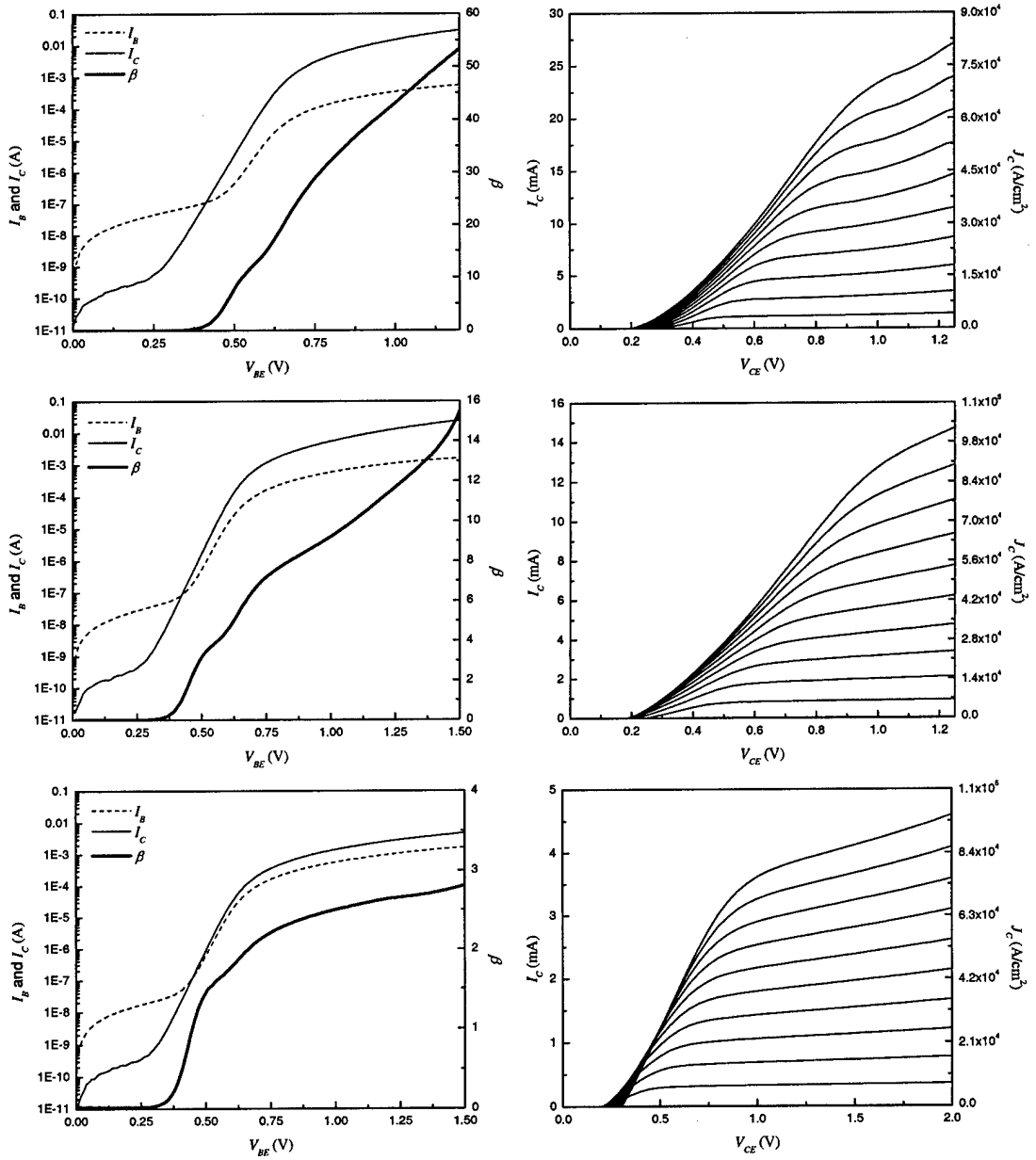

Figure 13 Gummel and common-emitter characteristic plots of (a) a $A_C = 4 \times 10$ μm^2 ($A_E = 3.5 \times 9.5$ μm^2) HBT ($I_B = 0 \sim 0.5$ mA at 50 μA steps), (b) a $A_C = 2 \times 10$ μm^2 ($A_E = 1.5 \times 9.5$ μm^2) HBT ($I_B = 0 \sim 1.25$ mA at 125 μA steps), and (c) a $A_C = 1 \times 10$ μm^2 ($A_E = 0.5 \times 9.5$ μm^2) HBT ($I_B = 0 \sim 1.5$ mA at 150 μA steps).

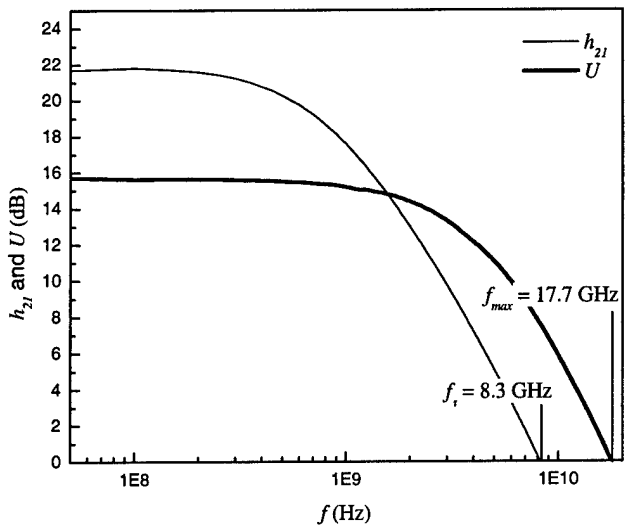

Figure 14 Plot of h_{21} and U versus frequency. The measured f_t and f_{max} are 8.3 GHz and 17.7 GHz, respectively.

2. GaN-based devices

Recent work in GaN electronics has centered on examining the source of RF dispersion and effective technological schemes to removing it from GaN HEMTs. Through temperature dependent measurements of GaN HEMTs, it is hypothesized that RF dispersion is a results from surface potential fluctuations arising from the conduction of gate electrons through a mini-band of traps, located within the bandgap of the $Al_xGa_{1-x}N$ cap layer, along the surface of the gate-drain access region. In order to remove dispersion from the devices, methods to de-couple the surface fluctuations from the channel have been examined.

In addition to work related to RF dispersion, the general processing of GaN electronics has been examined with the goal of increased reproducibility and flexibility in mind, and the development of a semi-insulating (SI) GaN buffer for reduced leakage has been pursued.

2.1. RF Dispersion: Temperature Dependence

It is well known that unpassivated GaN HEMTs suffer from RF dispersion, leading to reduced power at high frequencies. This is clearly shown in Figure 15. This observed RF dispersion is a result of surface potential fluctuations that cannot keep pace with the applied gate signal (Figure 16).

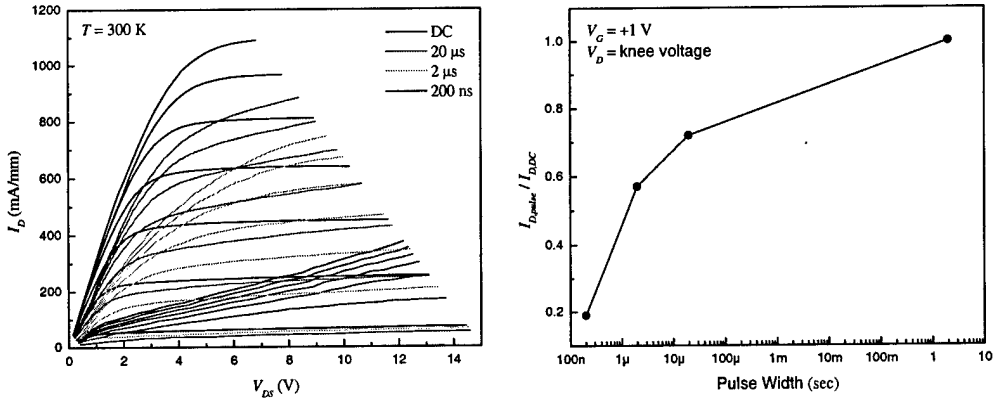

Figure 15 Plots of FET characteristics as a function of gate-pulse width and the relative drain current as a function of gate-pulse width.

There are three possible sources of the RF dispersion:

1 **Single energy level trap:**
- Around 1.5 eV (Fermi level pinning position)
- Too deep to show this pulse width dependent current

2 **A range of different energy levels of traps:**
- Experiments showed most of the current can be recovered by ~80 μs pulse
- Centroid should be around 1.5 eV
- Too deep to achieve this pulse width dependent current

3 **A range of traps various distances from the gate**
- RC Network
- Different time response

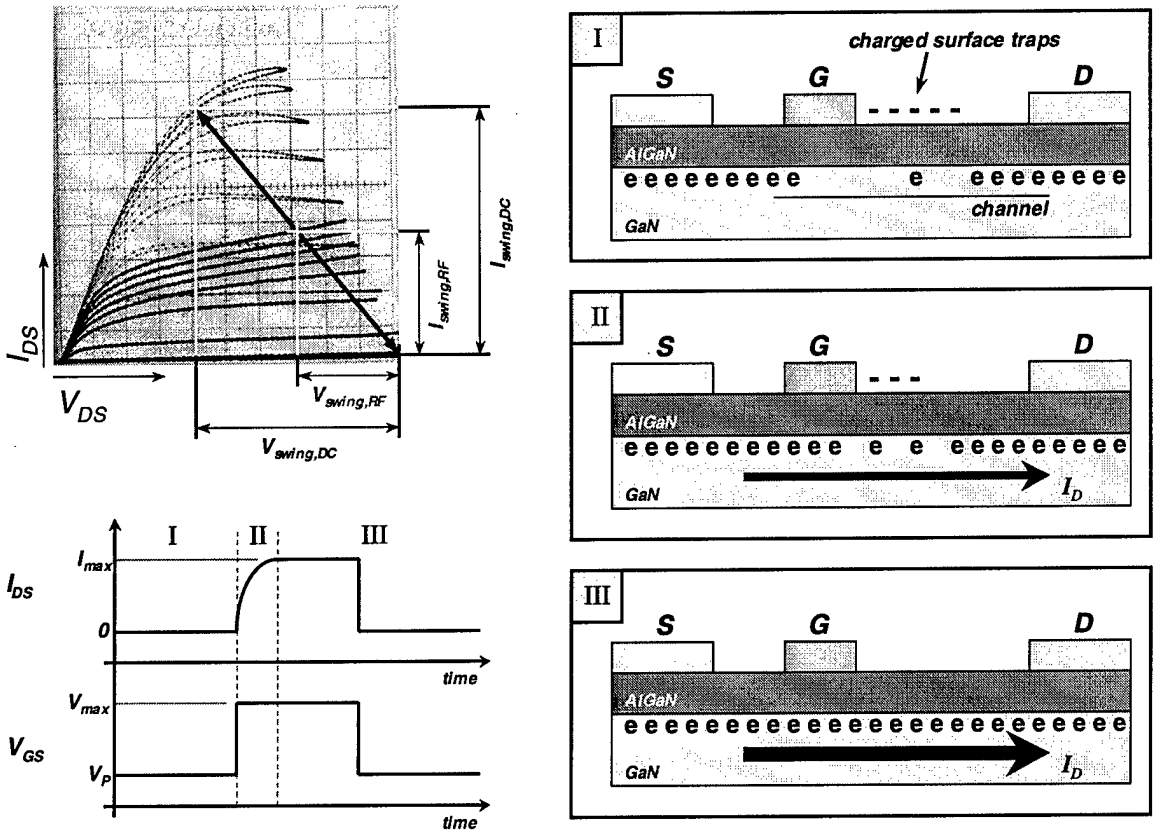

Figure 16 Illustration of RF dispersion arising from surface potential fluctuations.

The dependence of the dispersion on gate-pulse width suggests that the dispersion observed in GaN HEMTs is a result of (**3**) a range of traps various distances from the gate. A high density of traps would result in a mini-band within the bandgap of the surface $Al_xGa_{1-x}N$ layer, similar to LT GaAs. This mini-band would allow electrons to travel laterally by means of hopping conduction. The resulting lateral conduction and natural capacitance of the HEMT structure would result in a distributed *RC* network, with traps located closer to the gate having a shorter response time (Figure 17).

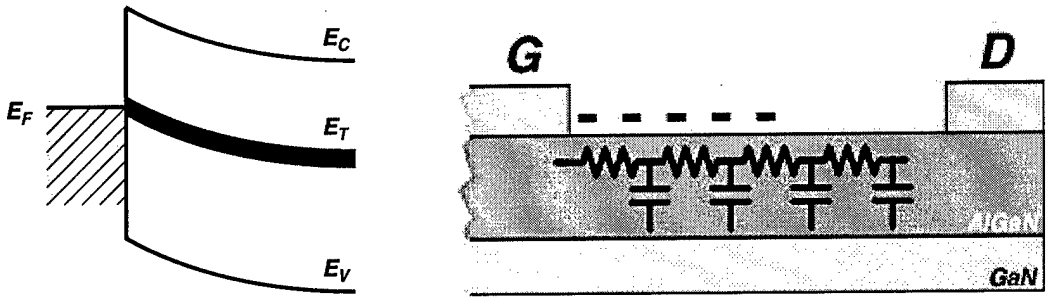

Figure 17 Illustration of the trap mini-band and resultant *RC* network.

Even in passivated device, with no dispersion at room temperature, show dispersion as temperature decreases (Figure 18). The loss in current resulting from dispersion is determined by the ratio of the charge density in the gate-drain access region (n_{access}) and the charge density under the gate (n_{gate}). Low temperature decreases the electron hopping conductivity through the trap mini-band, resulting in more traps remaining charged and less electrons in the channel in the access region and, therefore, more dispersion at low temperatures (Figure 19).

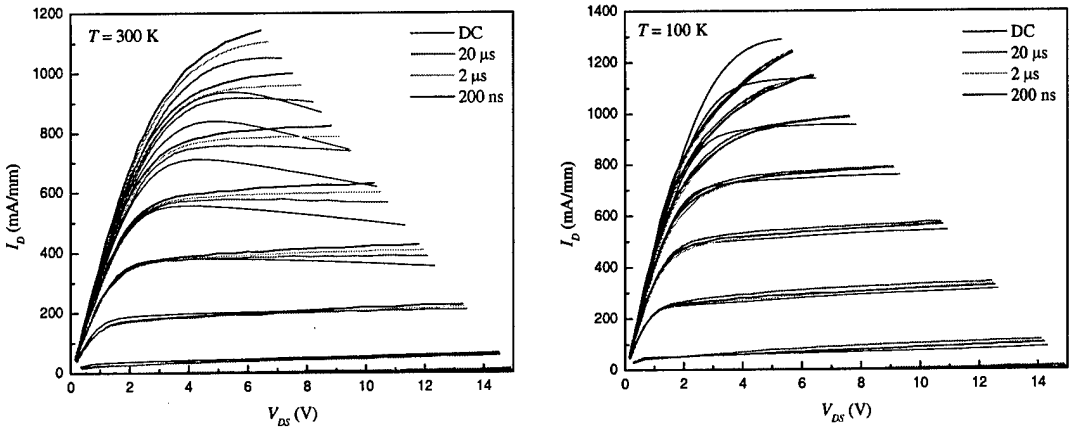

Figure 18 FET characteristics of a passivated GaN HEMT on sapphire at 300 K and 100 K as a function of gate-pulse width.

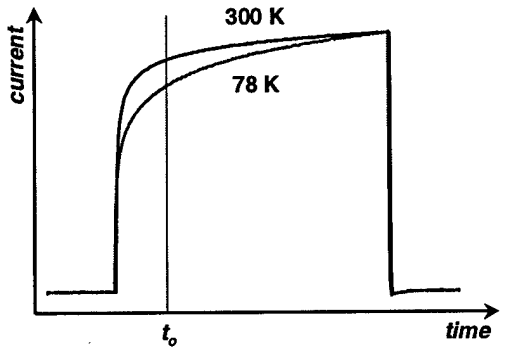

Figure 19 Example of the increased dispersion observed in the drain current at low temperature. For similar pulse widths, where the drain current is sampled at the same time (t_o), the lower temperature measurement results in an increase of the observed dispersion.

2.2. RF Dispersion: p-capped GaN HEMTs

In order to produce a more repeatable and reliable microwave performance AlGaN/GaN HEMT (specifically at X-band), the RF-DC dispersion caused by surface potential fluctuations need to be eliminated. Therefore, some form of reliable surface passivation must be achieved.

In standard HEMTs, fluctuations in the surface potential can radically affect the charge density in the channel. By placing a p-GaN layer at the surface of the device, the channel can be screened from fluctuations in the surface potential, resulting in no change in channel charge with surface potential fluctuation (Figure 20).

Figure 21 shows the material and device structure for the p-capped GaN HEMTs. These devices showed excellent DC characteristics (Figure 22). Comparison of a p-capped GaN HEMT and a standard HEMT shows that the p-capped HEMT removes dispersion with gate-pulse widths up to 80 μs (Figure 23). Shorter gate-pulse widths show some dispersion, but with greatly reduced effects.

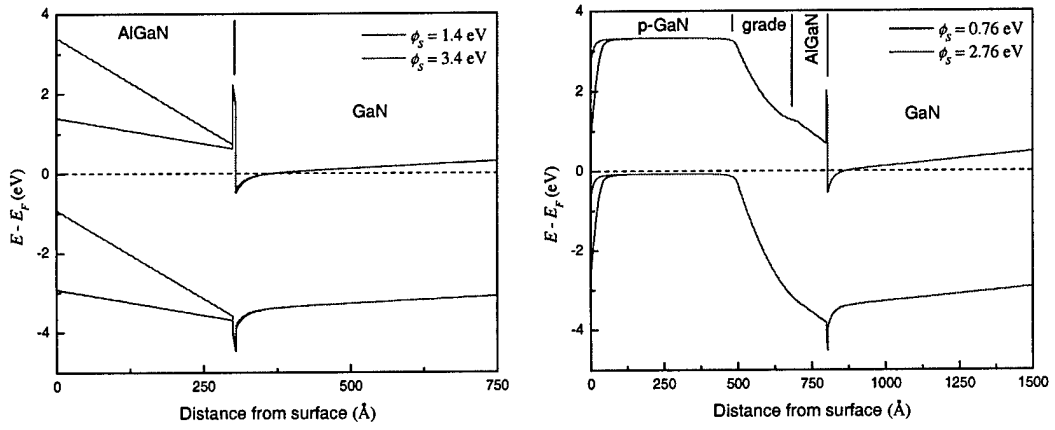

Figure 20 Band diagram of a standard HEMT and p-GaN capped HEMT. The standard HEMT sees a decrease in channel charge of 20 % for a 2 V increase in surface potential. For the same change in surface potential, the p-GaN capped sample sees no change in charge density.

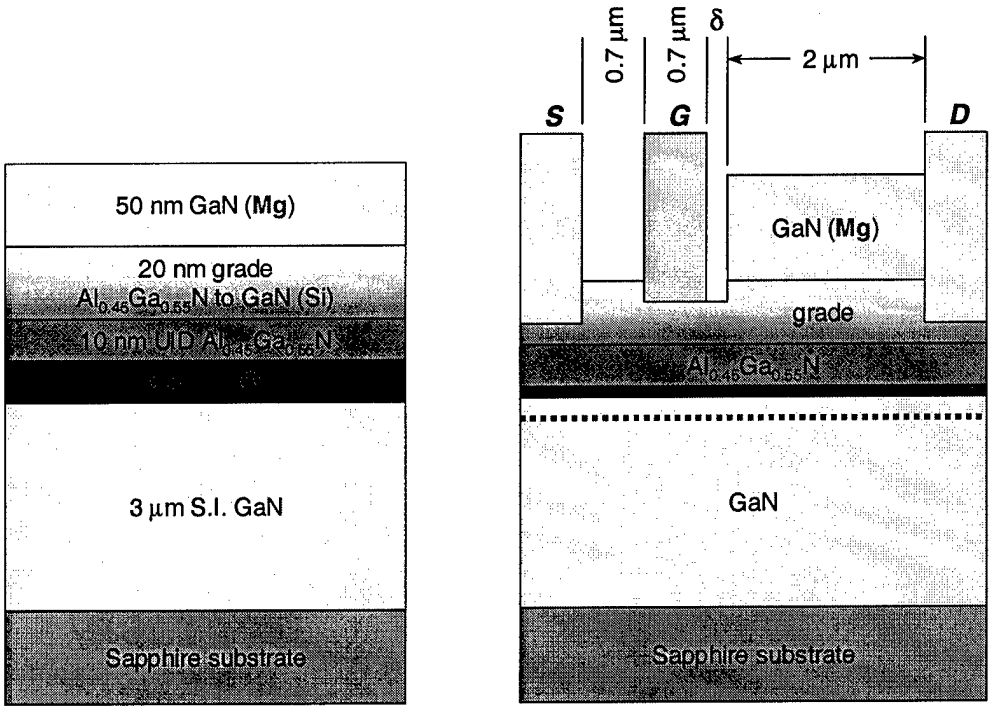

Figure 21 Material and device structure of the p-capped GaN HEMT (μ = 1475 cm^2/Vsec, n_{sh} = 1.35 × 10^{13} cm^{-2}). δ is approximately 0.1 μm.

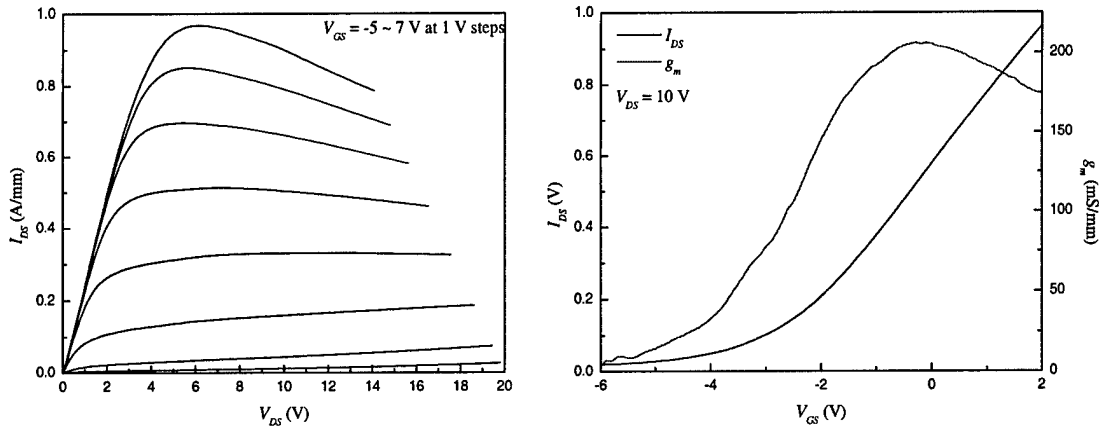

Figure 22 FET characteristic and gm vs. VGS plot for a p-capped GaN HEMT ($I_{DS,max}$ = 1 mA/mm, V_P = -5 V, $g_{m,max}$ = 205 mS/mm, V_{BD} = 50 V).

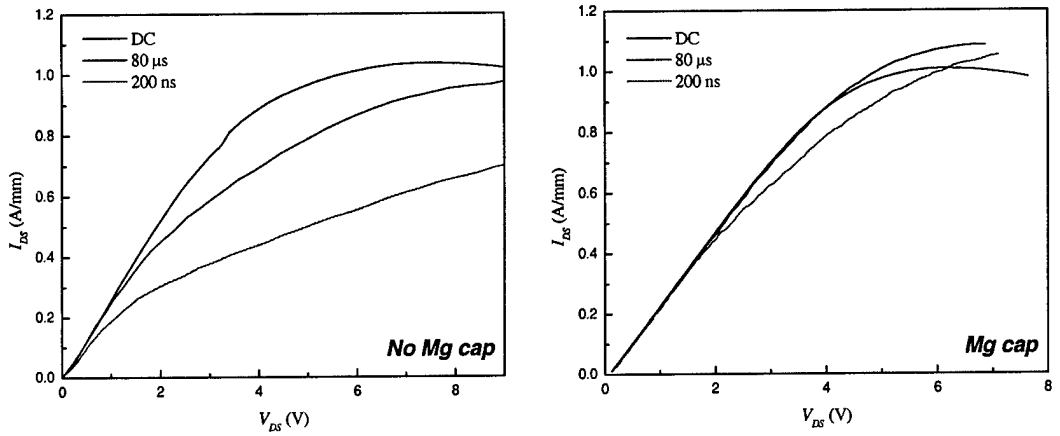

Figure 23 Comparison of a standard HEMT and a p-capped GaN HEMT vs gate-pulse width. The p-capped HEMT shows far less dispersion.

Small signal and power measurements are shown in Figure 24.

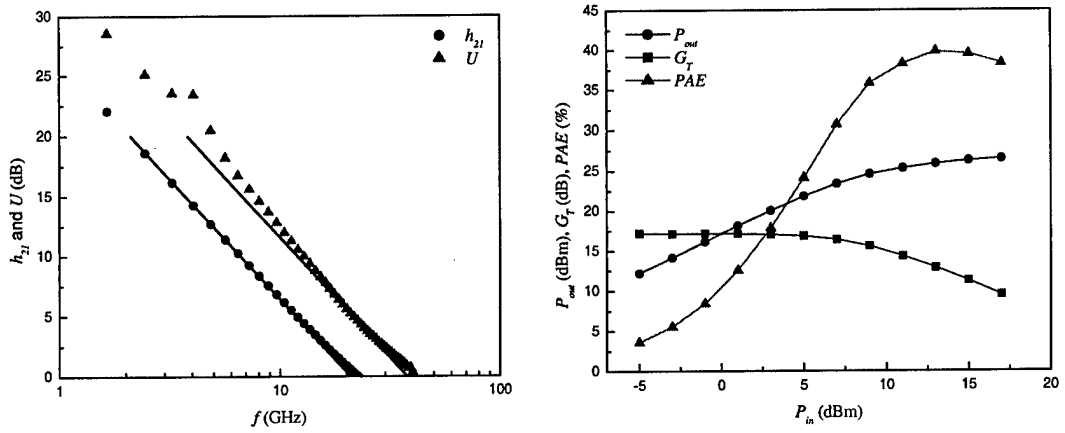

Figure 24 Small signal and power measurements for a p-capped GaN HEMT (f_τ = 20 GHz, f_{max} = 38 GHz; $P_{out,max}$ = 3 W/mm, PAE = 40 % at V_{DS} = 20 V, I_{DS} = 150 A/mm, and 4.2 GHz).

2.3. Processing: Digital Gate Recess Etching

Due to GaN's (and its related materials) chemical robustness, wet chemical etching for gate recessing in HEMT structures is effectively impossible. Also, achieving a high quality (i.e., smooth), reproducible etch using dry chemistries has also proven difficult due to the lack of chemical reactivity and high physical nature of these etches (Figure 25, Figure 26, Figure 27).

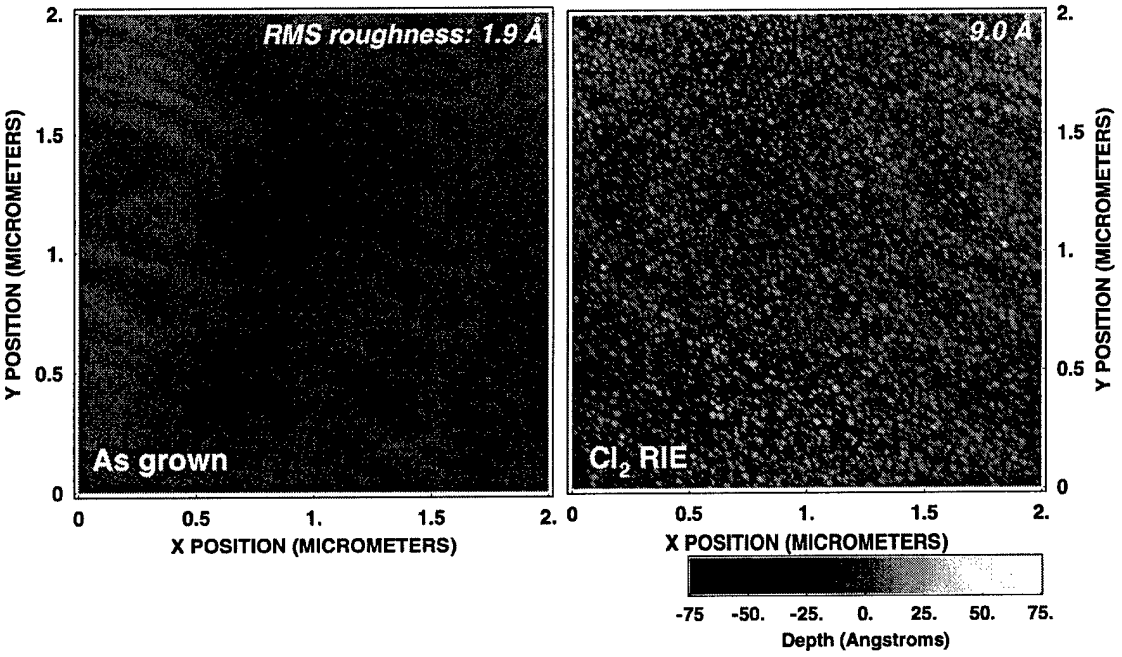

Figure 25 AFM scans of GaN, before and after a Cl_2 RIE (*Power* = 15 W, *pressure* = 15 mTorr, Cl_2 *flow* = 15 sccm, *time* = 200 sec).

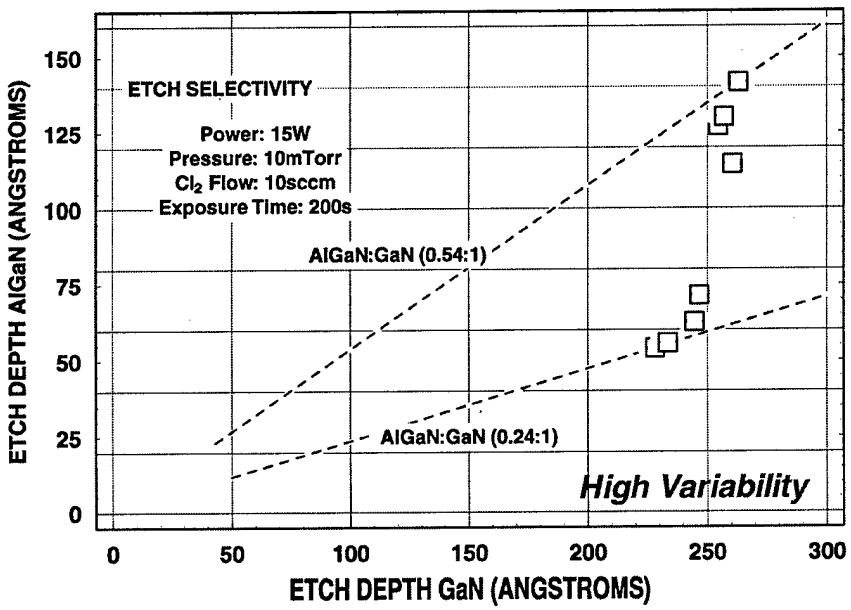

Figure 26 Plot of AlGaN etch depth vs GaN etch depth. This plot shows the high variability in etch selectivity for a given set of conventional etch conditions.

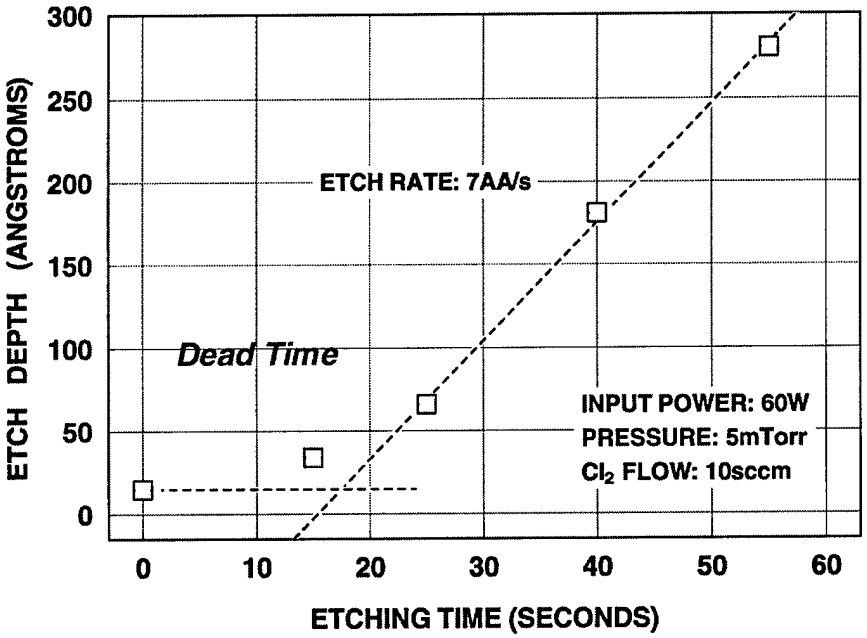

Figure 27 Plot of etch depth vs etch time showing poor linearity of the Cl_2 RIE.

For these reasons, achieving a reproducible, high quality gate-recess technology for GaN HEMTs using conventional processing has proven to be impossible. Therefore, an alternative method to producing a reliable, highly reproducible gate-recess has been pursued. The process of digital etching GaN offers this alternative.

A comparison of conventional etching and digital etching is shown in Figure 28. Experimental results from the digital etching of GaN HEMTs shows that this method

results in a highly reproducible, high quality (i.e., low damage) gate recess process with no selectivity between AlGaN and GaN (Figure 29, Figure 30, Figure 31).

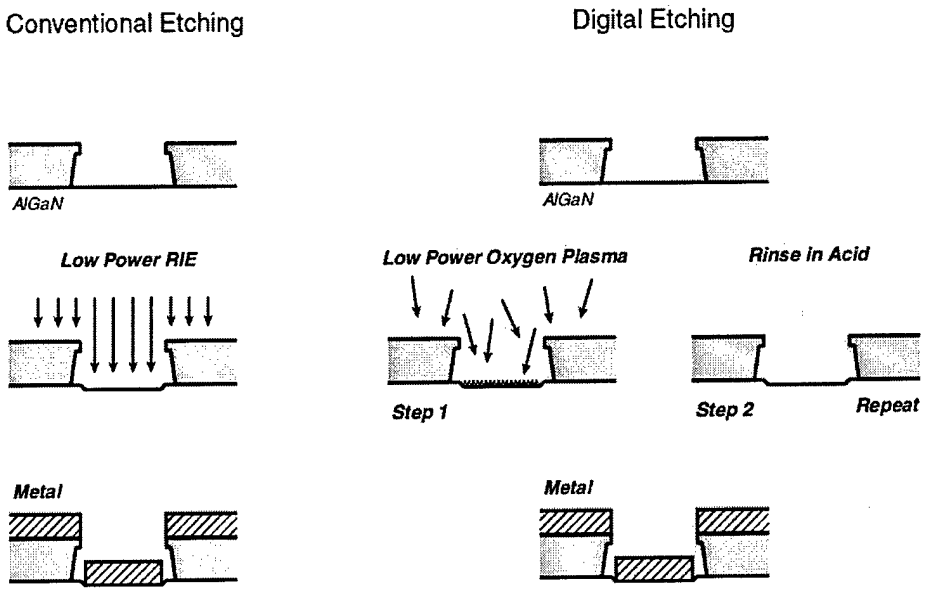

Figure 28 Illustration of the comparison between conventional etching and digital etching.

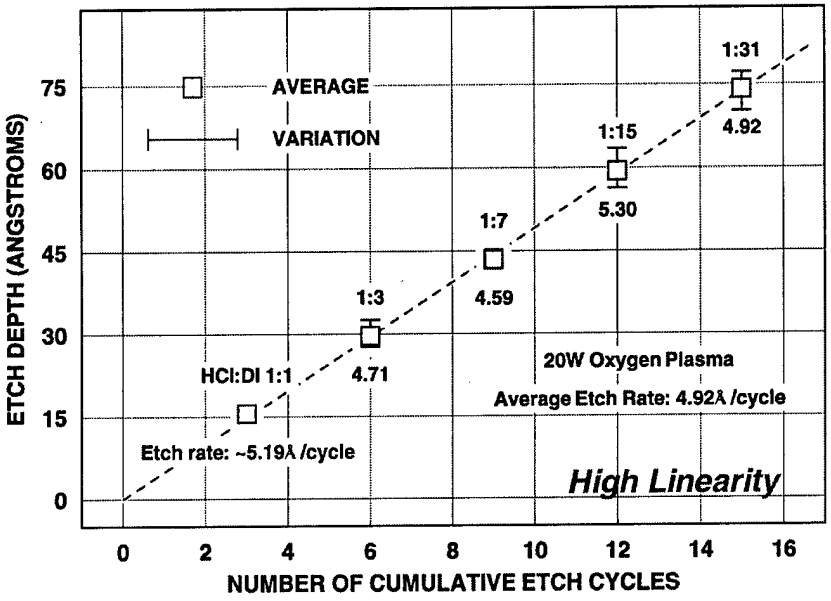

Figure 29 Plot of etch depth vs etch cycles. The digital etch is very linear.

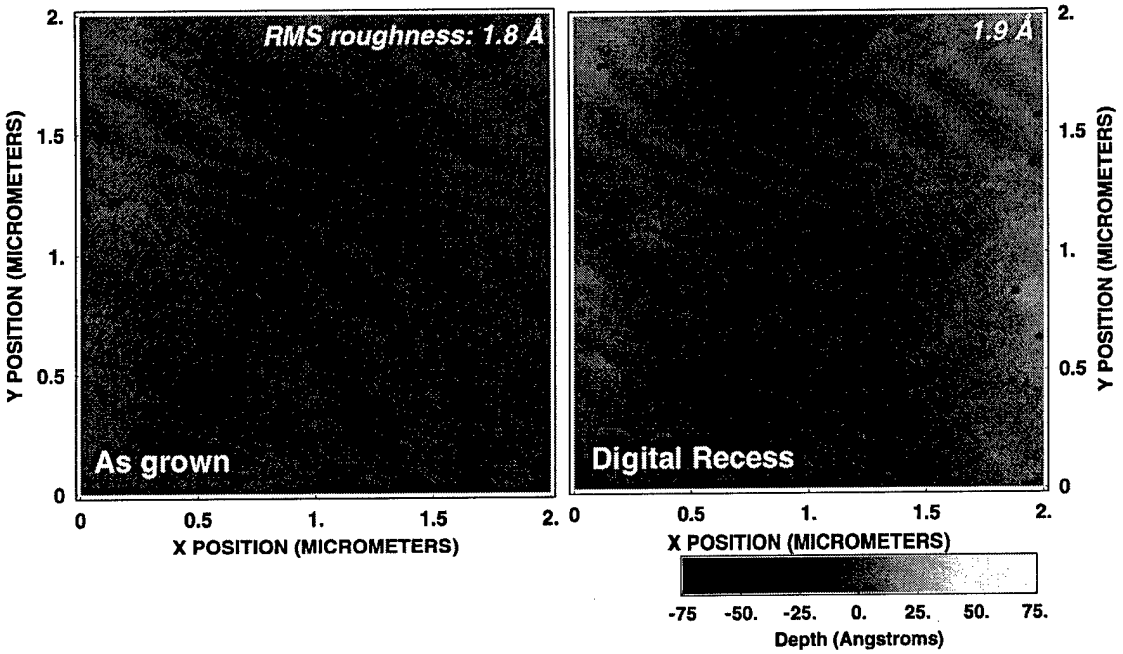

Figure 30 AFM scans of GaN, before and after a digital etch series. The surface remains as smooth as compared to the as grown surface.

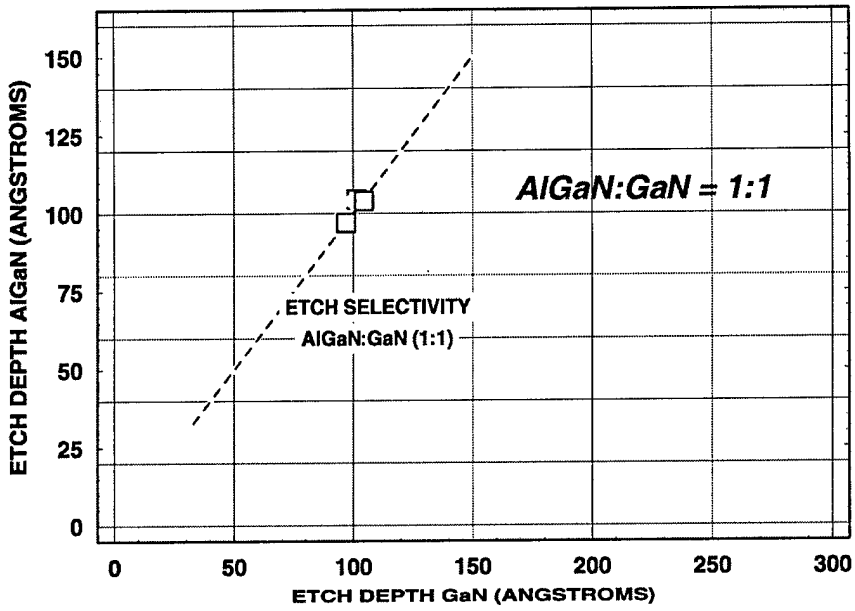

Figure 31 Plot of AlGaN etch depth vs GaN etch depth. The digital etch is highly reproducible.

2.4. Processing: High Temperature, High Pressure Thermal Processing

Conventional GaN processing currently uses thermal processes chiefly to improve ohmic contacts and to activate Mg acceptors in p-type GaN. Temperatures for these processes (< 1000 °C) are commonly limited by desorption at the surface. Thermal processes at much higher temperatures (~ 1500 °C +) could possibly allow for the development of emerging implant and defect reduction technologies, as well as simply extending conventional thermal processes. In order to maintain crystal quality and surface stability at these high temperatures, increased operating pressures are required.

Preliminary results with a new high pressure, high temperature annealing station (RF inductive heating: 1500 °C +, 1500 psi capable with NH_3, H_2, and/or N_2 ambient available) are promising. GaN samples (capped with AlN) annealed at over 1200 °C at 1500 psi N_2 for 45 seconds show improved material characteristics (Figure 32).

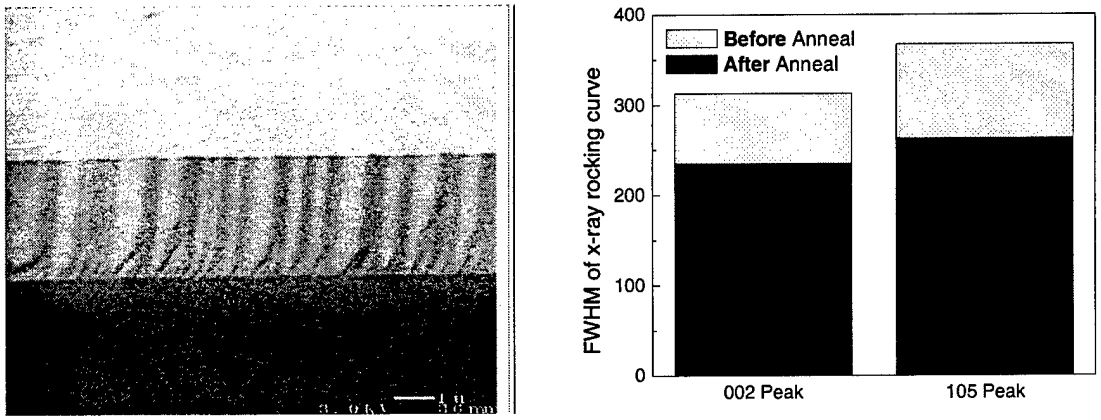

Figure 32 Cross-sectional SEM of an AlN capped GaN sample annealed at over 1200 °C at 1500 psi N_2 for 45 seconds, and the corresponding x-ray results.

Part 2 Radiation Study

To do an extensive investigation of the radiation response of the GaAs and GaN-based electronic devices, the various radiations, the γ–ray and proton, were used.

Charge trapping centers in the GaN prior to the radiation were studied as well as their change after low dose of the radiation. The properties of the Schottky diode on n-type GaN, including barrier height, I-V characteristics and the effect of the annealing, before and after ^{60}Co γ–ray radiation were investigated in detail. The results indicated that - irradiation induced an increase in the effective Schottky barrier height extracted from *C–V* measurements. Increasing radiation dose was found to degrade the reverse leakage current, whereas its effect on the forward *I–V* characteristics was negligible. Low temperature post-irradiation annealing after a cumulative irradiation dose of 21 Mrad(Si) was found to restore the reverse *I–V* characteristics to pre-irradiation levels. Some radiation-induced defect centers were found. The results indicated that epitaxial GaN has an intrinsically low susceptibility to radiation-induced material degradation. However, radiation hardness of GaN devices is more likely to be limited by susceptibility of the metal-GaN interface to radiation-induced damage and by the deleterious effect of a high density dislocations.

The effects of γ–ray and proton radiation to the DC performance of the AlGaN/GaN HEMTs were also investigated. The change of the drain current as a function of proton energies indicated that the degradation is very little when the proton energy is larger than 15MeV. The degradation of the drain current is also limited with the relatively low dose of low energy proton radiation. AlGaN/GaN HEMTS appear to be excellent candidates for use in space systems. At the proton energies encountered in actual systems, the amount of degradation at typical mission fluences should be negligible for these kinds of devices.

The AlGaAs/GaAs HBT was also checked by the proton radiation. Significant gradation was found the proton energy is low while relatively little degradation due to high energy protons.

3. GaN buffer and GaN-based diodes

3.1. Charge trapping centers in GaN grown by MOCVD

Deep-level transient capacitance measurements (DLTS) were performed on Schottky diodes fabricated on undoped MOCVD-grown GaN epitaxial layers before and after exposure to different doses of ^{60}Co gamma-irradiation. The DLTS measurements were performed from 77 to 300 K, and the samples exposed to accumulated doses of 200, 500 and 1000 krad(Si). Three deep-levels were found in the sample prior to irradiation with thermal activation energies of 241 ± 5, 294 ± 32 and 575 ± 2 meV. Our measurements indicate that for low doses (<= 1Mrad(Si)) no new traps have been induced, and that the traps present in the unirradiated material do not experience any significant change in their characteristics.

The detail investigation can be found in Appendix A.

3.2. ^{60}Co gamma irradiation effects on n-GaN Schottky diodes

The effect of γ-ray exposure on the electrical characteristics of Ni/n-GaN Schottky barrier diodes has been investigated using current-voltage (I-V), capacitance-voltage (C-V), and deep-level transient spectroscopy (DLTS) measurements. The results indicate that γ-irradiation induces an increase in the effective Schottky barrier height extracted from C-V measurements. Increasing radiation dose was found to degrade the reverse leakage current, whereas its effect on the forward I-V characteristics was negligible. Low temperature (<=50°C) post-irradiation annealing after a cumulative irradiation dose of 21 Mrad(Si) was found to restore the reverse I-V characteristics to pre-irradiation levels without significantly affecting the radiation-induced changes in C-V and forward I-V characteristics. Three shallow radiation-induced defect centers with thermal activation energies of 88 104 and 144 meV were detected by DLTS with a combined production rate of 2.12×10^{-3} cm^{-1}. These centers are likely to be related to nitrogen-vacancies. The effect of high-energy radiation exposure on device characteristics is discussed taking into account possible contact inhomogeneities arising from dislocations and interfacial defects. The DLTS results indicate that GaN has an intrinsically low susceptibility to radiation-induced material degradation, yet the effects observed in the Schottky diode I-V and C-V characteristics indicate that the total-dose radiation hardness of GaN devices may be limited by susceptibility of the metal-GaN interface to radiation-induced damage.

The detail investigation can be found in Appendix B.

3.3. Annealing behavior of radiation-induced damage in n-GaN Schottky diodes

The effect of isochronal thermal annealing on ^{60}Co gamma-irradiated Ni/n-GaN Schottky barrier diodes, which had previously been exposed to 21 Mrad(Si) total dose, has been investigated using capacitance-voltage (C–V) and current-voltage (I–V) measurements, whereas capacitance deep-level transient spectroscopy (DLTS) has been employed to monitor the evolution and annihilation of radiation-induced defects during thermal annealing. While a relatively low temperature anneal at 50°C has been shown to restore the reverse bias I–V characteristics to pre-irradiation levels without any significant effect on the C–V and forward I–V characteristics, subsequent thermal annealing up to 160°C is shown to further improve device characteristics. However, annealing above 250°C is found to degrade both forward and reverse I–V characteristics and induce a reduction in the free carrier concentration obtained from C–V characteristics. Detailed analysis of the forward current and C–V characteristics indicate that the apparent reduction in Schottky barrier height after annealing above 250°C, is associated with dislocation-related to annealing effects. Annealing at temperatures above 250°C were found to result in the annihilation of radiation-induced defects, as evidenced by DLTS measurements. From the detailed analysis of the radiation-induced defect concentrations, the dominant annealing process is characterized by an activation energy in the range of 1.77 eV to 1.92 eV. The physical origin of radiation-induced defects, and of defects involved in their annihilation process, is discussed in the perspective of recent theoretical calculations of native defect diffusion mechanisms in GaN.

The detail investigation can be found in Appendix C.

4. GaN-based HEMTs

4.1. Magnetoresistance characteristics of gamma-irradiated AlGaN/GaN HEMTs

The effect of ^{60}Co gamma-irradiation on the device characteristics of $Al_{0.35}Ga_{0.65}N$-GaN heterojunction field effect transistors (HFET) has been investigated using DC and geometrical magnetoresistance measurements. Cumulative gamma-ray doses up to 20 Mrad(Si) are shown to induce drain current degradation, negative threshold voltage shifts and reverse gate leakage current degradation. Analysis of drain magneto-conductance characteristics measured at 80 K indicated an increase in two-dimensional electron gas (2DEG) sheet concentration with accumulated radiation dose. More importantly, the 2DEG mobility-concentration characteristics are noted to remain approximately constant for total gamma-radiation doses up to 20 Mrad(Si), indicating that the areal density of radiation-induced defects at the heterointerface is likely to be negligible. The threshold voltage shifts are therefore attributable to the introduction of relatively shallow radiation-induced defects in the AlGaN barrier region and/or to defects introduced at the gate-barrier interface. Although the drain conductance characteristics manifested similar degradation trends at 80 and 300 K, the 2DEG parameters obtained at 300 K exhibited significant scatter with increasing dose, possibly a manifestation of device instabilities induced by radiation-induced surface defects in the ungated access region near the edge of the gate. Device failure due to severe gate leakage and loss of gate control over the 2DEG charge, occurred after a total dose of 30 Mrad(Si).

The detail investigation can be found in Appendix D.

4.2. The energy dependence of proton-induced degradation in AlGaN/GaN HEMTs

The effects of proton irradiation at various energies are reported for AlGaN/GaN high electron mobility transistors (HEMTs). The devices exhibit little degradation when irradiated with 15-, 40-, and 105-MeV protons at fluences up to 10^{13} cm^{-2}, and the damage completely recovers after annealing at room temperature. For 1.8-MeV proton irradiation, the drain saturation current decreases 10.6% and the maximum transconductance decreases 6.1% at a fluence of 10^{12} cm^{-2}. The greater degradation measured at the lowest proton energy considered here is caused by the much larger nonionizing energy loss of the 1.8-MeV protons.

The detail investigation can be found in Appendix E.

4.3. Characterization of Proton-Irradiated AlGaN/GaN HEMTs by DLTS

Spatially resolved cathodoluminescence spectroscopy studies of AlGaN/GaN MODFET and MBE-grown layered HFET transistor structures reveal spectral differences corresponding to spatially localized changes in electronic properties after 1.8-MeV proton irradiation. These changes indicate a reduction in internal electric-field strength within the AlGaN layers and the formation of charged defects. These localized electronic changes and the associated reduction in charge density induced at the AlGaN/GaN 2DEG interface channel can account for the decreases in MODFET saturation current, drain current, and transconductance observed electrically.

The detail investigation can be found in Appendix F.

4.4. Proton-irradiation effects on AlGaN/AlN/GaN HEMTs

The degradation of AlGaN/AlN/GaN high electron mobility transistors due to 1.8-MeV proton irradiation was measured at fluences up to 3×10^{15} cm^{-2}. The devices have much higher mobility than AlGaN/GaN devices, but they possess similarly high radiation tolerance, exhibiting little degradation at fluences up to 1×10^{14} cm^{-2}. Decreased sheet carrier mobility due to increased carrier scattering and decreased sheet carrier density due to carrier removal are the primary damage mechanisms. The device degradation is observed as a decrease in the maximum transconductance, an increase in the threshold voltage, and a decrease in the drain saturation current.

The detail investigation can be found in Appendix G.

5. GaAs-based HBTs

5.1. Proton-Induced Degradation in AlGaAs/GaAs HBTs

GaAs HBTs were irradiated with protons at energies of 1.8 MeV and 105 MeV and at fluences ranging from $3\times10^{11}cm^{-2}$ to 3×10^{13} cm^{-2}. For 1.8-MeV proton irradiation, the increase of the base current and the large decrease of collector current both contribute to the degradation of the device. The increase of the base current is due to displacement damage-induced traps, which decrease the minority carrier lifetime. However, the collector current decrease appears to be mainly due to degradation of the emitter–base diode, which decreases the electron injection efficiency. Although these HBT devices show significant degradation for 1.8-MeV proton irradiation, they are good candidates for applications in space systems because they exhibit relatively little degradation due to high-energy (105 MeV) protons, which are much more representative of space than are 1.8-MeV protons.

The detail investigation can be found in Appendix H.

Publication List

[1] Umana-Membreno G, Dell J.M., Parish G., Nener B.D., Faraone L., Ventury R., Mishra U.K., "Effect of gamma-radiation on two-dimensional electron gas transport and device characteristics of $Al_xGa_{1-x}N$/GaN HEMTs", 2004 MRS International Workshop on Nitride Semiconductors, 19-23 July 2004, Pittsburgh, PA, USA (2004) - to be published also in Physica Status Solidi.

[2] X. Hu, B. Choi, H. Barnaby, D. Fleetwood, R. Schrimpf, S. Lee, S. Shojah-Ardalan, R. Wilkins, U. Mishra, and R. Dettmer, "The Energy Dependence of Proton-Induced Degradation in AlGaN/GaN High Electron Mobility Transistors" IEEE Transactions on Nuclear Science, Vol. 51, No. 2, pp. 293-297, April, 2004.

[3] Umana-Membreno G.A., Dell J.M., Parish, G., Nener B.D., Faraone L., Ventury R., Mishra U.K, "Magnetoresistance characteristics of gamma-irradiated $Al_{0.35}Ga_{0.65}N$ / GaN HFETs", SPIE 2003 Internat. Symp. "Microelectronics, MEMS, and Nanotechnology" Perth, Australia, 10-12 Dec. 2003, SPIE Proc. 5274, pp. 152-162 (2004).

[4] X Hu, A. Karmarkar, B. Jun, D. Fleetwood, R. Schrimpf, R. Geil, R. Weller, B. White, M. Bataiev, L. Brillson, and U. Mishra, "Proton-Irradiation Effects on AlGaN/AlN/GaN High Electron Mobility Transistors" IEEE Transactions on Nuclear Science, Vol. 50, No. 6, pp. 1791-1796, December, 2003.

[5] Umana-Membreno G.A., Dell J.M., Parish G., Nener B.D., Faraone L., Mishra U.K., "^{60}Co Gamma Iirradiation Effects on /n/-GaN Schottky Diodes", IEEE Transactions on Electron Dev., 50, 12, pp. 2326-2334 (Dec. 2003).

[6] R. Coffie, L. Shen, G. Parish, A. Chini, D. Buttari, S. Heikman, S. Keller and U. K. Mishra, "Unpassivated p-GaN/AlGaN/GaN HEMTs with 7.1W/mm at 10GHz," IEE Electronics Letters, vol. 39, no. 19, pp. 1419-1420, Sep. 2003.

[7] L. Shen, A. Chini, R. Coffie, D. Buttari, S. Heikman, S. Keller, and U. K. Mishra, "Temperature dependence of the Current-Voltage Characteristics of AlGaN/ GaN HEMT," Proceedings of the 61st Device Research Conference, pp.63-64, Jun. 2003.

[8] X. Hu, B. Choi, H. Barnaby, D. Fleetwood, R. Schrimpf, K. Galloway, R. Weller, K. McDonald, U. Mishra, and R. Dettmer, "Proton-Induced Degradation in AlGaAs/GaAs Heterojunction Bipolar Transistors" IEEE Transactions on Nuclear Science, Vol. 49, No. 6, pp. 3213-3216, December, 2002.

[9] R. Coffie, D. Buttari, S. Heikman, S. Keller, A. Chini, L. Shen, and U. K. Mishra, "p-capped GaN-AlGaN-GaN high-electron mobility transistors (HEMTs)," IEEE Electron Device Letters, vol. 23, no. 10, pp. 588-590, Oct. 2002.

[10] Umana-Membreno G.A., Dell J.M., Hessler T.P., Nener B.D., Parish G., Faraone L., Mishra U.K.,"^{60}Co gamma-irradiation induced defects in /n/-GaN", Appl. Phys. Lett., 80(23), 4354-6 (2002) .

[11] Umana-Membreno G.A., Dell J.M., Parish G., Faraone L., Mishra U.K., "^{60}Co gamma-irradiation induced defects in MOCVD GaN", Symp. on Microelectronics and Micro-Electro-Mechanical Systems (MICRO/MEMS2001), 17-19 Dec. 2001, Adelaide, Australia, SPIE Proc. 4593 (Design, Characterization, and Packaging for MEMS and Microelectronics II), pp.220-227 (2001)

[12] Umana-Membreno G.A., Nener B.D., Dell J.M., Faraone L., Parish G., Mishra U.K., "Charge trapping centres in -irradiated Gallium Nitride grown by MOCVD Conf. on Optoelectron. and Microelectron. Mat. and Dev. (COMMAD 2000), Melbourne, Australia, IEEE Proc., pp. 332-335 (2000)

[13] C. Zheng, "AlGaAs/GaAs/InGaAs pHEMT on Oxide" 2000 IEEE/Cornell conference on High Performance Devices, August 7 ~9, 2000 Ithaca, NY

[14] J. Champlain, "High-Speed HBTs with Oxide Apertures" 2000 IEEE/Cornell conference on High Performance Devices, August 7 ~9, 2000 Ithaca, NY

Appendix A

Charge trapping centers in GaN grown by MOCVD with relatively low dose of gamma irradiation

Charge trapping centres in γ-irradiated Gallium Nitride grown by MOCVD

G.A. Umana-Membreno, B.D. Nener, J.M. Dell, L. Faraone, G. Parish, U.K. Mishra[a)]
Dept. of Electrical and Electronic Engineering,
The University of Western Australia, Crawley 6009, Australia
[a)]*Dept. of Electrical and Computer Engineering,*
University of California Santa Barbara, CA 93106, USA

Abstract- Deep-level transient capacitance measurements (DLTS) were performed on Schottky diodes fabricated on undoped MOCVD-grown GaN epilayers before and after exposure to different doses of ^{60}Co gamma-irradiation. The DLTS measurements were performed from 77 to 300 K, and the samples exposed to accumulated doses of 200, 500 and 1000 krad(Si). Three deep-levels were found in the sample prior to irradiation with thermal activation energies of 241 ± 5, 294 ± 32 and 575 ± 2 meV. Our measurements indicate that for low doses (≤ 1Mrad(Si)) no new traps have been induced, and that the traps present in the unirradiated material do not experience any significant change in their characteristics. In contrast, a recent report on ^{60}Co γ–irradiated magnetron-sputtered GaN indicates an increase in the concentrations of deep-levels with thermal activation energies of 590 and 820 meV for accumulated doses of 1 Mrad and above [4].

A. Introduction

III-nitride semiconductors are currently of great interest due to their unique optical and electronic properties. Epitaxial growth breakthroughs have made possible the commercial success of GaN-based light-emitting diodes, lasers and UV detectors, and the development of ultraviolet detectors and heterostructure field-effect transistors. Moreover, the low thermal generation rates and high breakdown fields of the III-nitride alloys make them attractive for the development of radiation-hard electronic devices capable of operating at high temperatures and high power/voltage [1].

It is of great interest to determine the susceptibility of GaN to ionising radiation because of it inherent implications to device reliability. This is particularly important for space electronics and ionising radiation environments. Radiation-induced defects may significantly affect the electrical and optical properties of semiconductor materials, and may provide important indicators to the nature of radiation induced and intrinsic defects. It is therefore essential to study the effect of different radiation sources on III-nitride materials, and determine their effect in producing new defects or increasing the concentration of defects present in un-irradiated material.

For MOCVD-grown GaN epilayers, electron irradiation appears to introduce two donor-like centres with thermal activation energies of 60 and 110 meV. The latter has a thermally activated capture barrier of 55 meV. The 60 meV trap has been attributed to the nitrogen vacancy (V_N), whereas the 110 meV is thought to arise from a more complex defect, but also related to V_N [2]. Goodman *et al.* found that irradiation with He-ions introduced three different levels with thermal activation energies of 200, 780 and 950 meV, whereas irradiation with high-energy protons introduced levels at 130, 160 and 200 meV [3]. A recent work on ^{60}Co γ-irradiated radio-frequency magnetron-sputtered (RFMS) GaN epilayers indicate an increase in the concentrations of deep-levels with thermal activation energies of 590 and 820 meV for accumulated doses of 1 Mrad and above [4].

In this work, we present a study of capacitance deep-level transient spectroscopy (DLTS) measurements of n-type MOCVD-grown GaN Schottky diodes exposed to ^{60}Co γ-

0-7803-6698-0/00/$10.00 ©2000 IEEE

radiation. The diodes were exposed to total doses ranging from 200 to 1000 krad(Si) at room temperature. The irradiated devices were characterised using transient capacitance measurements from 77 to 300 K. Our measurements indicate that for these radiation doses no detectable new traps have been induced, and that the traps present in the unirradiated material do not experience any significant change in their characteristics. This is in contrast to the results of Wang *et al.* on RFMS deposited GaN [4].

B. Experimental Details

Schottky barrier diodes were fabricated on 2 μm thick n-type nominally undoped GaN epilayers grown by MOCVD on sapphire substrates at the University of California Santa Barbara (USA). Prior to contact fabrication, the samples were degreased by boiling in trichloroethylene, acetone and methanol followed by rinsing in de-ionised water. The samples were then dipped in buffered HF and rinsed in de-ionised water. Large-area ohmic contacts were patterned using standard lift-off techniques and formed by depositing Al/Cr/Au. The contacts were then annealed in nitrogen atmosphere at 800 °C for 60 seconds, yielding a contact resistance of $6x10^{-4}\,\Omega$-cm^2 from circular transmission line patterns. After patterning and dipping in buffered HF, coplanar circular geometry Ni/Au Schottky contacts were deposited with radii of 300 and 200 μm. All metals were thermally evaporated at pressures better than $8x10^{-7}$ mbar. Room temperature capacitance-voltage (C-V) measurements indicate a Schottky barrier height of 1.08 ± 0.05 eV and a uniform n-type carrier density of $3.2x10^{16}$ cm^{-3}.

Transient capacitance measurements were performed using a HP 4280A 1 MHz C-V meter with a 30 mV_{rms} AC signal, a HP 3245A source for the quiescent reverse bias and a HP 8116A pulse generator. The measurements were performed from 77 to 300 K, with the temperature stabilised for at least 15 minutes at each temperature point to achieve stability better than ±0.1 K. The full capacitance transients were recorded with sampling intervals ranging from 50 ms to 1 s, up to a maximum of 200 seconds total transient time. Averaging was used to improve signal to noise ratio. The measurements were performed at quiescent reverse bias of $V_r = 2$ V with 10 ms and filling pulses of $V_p = 0$ V. Under these conditions, the AC series resistance was less than 150 Ω, while the AC parallel conductance was less than 20 μS, for all temperatures.

The samples were irradiated at room temperature in a ^{60}Co AECL Gammacell 220 irradiator, yielding a dose rate of 2 krad(Si)/min. The sample was exposed to accumulated total doses of 200, 500 and 1000 krad(Si), while maintained in a nitrogen atmosphere. After each irradiation exposure, the samples were loaded in a cryostat and held at room temperature for 3 hours prior to sample cooling. The full capacitance transients were simultaneously fitted as a function of temperature using a Levenberg-Marquardt least squares routine based on a discrete trap model. This procedure avoids the uncertainties and errors associated with the estimation of trap parameters from Arrhenius plots and allows and accurate analysis of traps with overlapping transients [2].

C. Experimental Results and Discussion

The trap parameters of all traps prior and after irradiation are presented in Table I. A simulated DLTS spectrum from the full transient data is shown in Fig. 1. Three different traps were detectable in the 77 to 300K temperature range, with no significant change in either apparent thermal activation energy, capture cross-section or trap concentration. As indicated by the relatively low concentration of traps prior to irradiation, the sample is suitable for studying the effects of ionising radiation. Of the trapping centres detected, the dominant trap with a

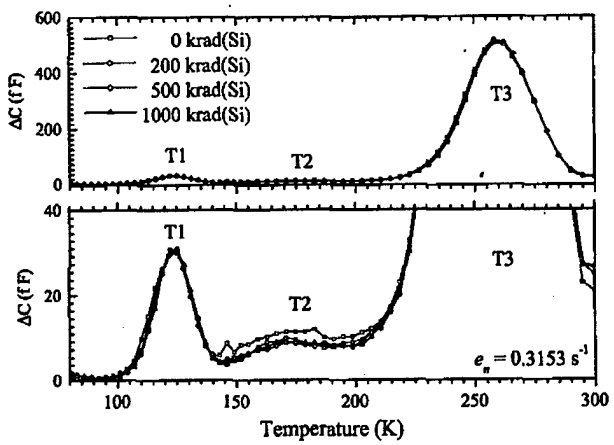

Fig. 1. DLTS spectrum obtained from full transient measurements as a function of γ-radiation dose. There is no significant change in trap parameters of trap concentrations

thermal activation energy of about 580 meV, labelled T3, is present with a concentration corresponding to about of 1.6% of the free carrier concentration. The parameters for this defect are in agreement with those reported for 580 meV trap reported by Hacke *et al.* and the 598 meV level reported by Haase *et al* [5,6]. This trap has been consistently detected in GaN epilayers grown by HVPE, MOCVD, MBE and magnetron sputtering. The trap labelled T2 has an activation energy of about 240 meV, and corresponds to a intrinsic defect present in GaN grown by different techniques, and observed at 270 meV by Goodman *et al.*, 264 meV by Hacke *et al.* and 250 meV by Gotz *et al.* [3,5,7]. Although the origin of these traps is yet to be determined, Haase *et al.* have suggested that the dominant trap at about 600 meV is related to nitrogen antisite based on their study of nitrogen-implanted GaN.

The very low concentration level labelled T2 has a relatively small apparent capture cross-section and thermal activation energy of 292 meV is also present. Its presence is not detectable for filling pulses less than 5 ms, in agreement with the extracted small capture cross-section. Since the signal from this level, even with a 10ms filling pulse is near the resolution edge of our system, the extracted trap parameters should be regarded as estimates only. As can be seen in Fig. 1 and Table I, there is no significant change in trap concentrations. Although there is an apparent small decrease in the concentration of trap T2, we regard this change as negligible as it lies within the calculated experimental and model fit error bars. However, our observations for trap T3 are in disagreement with the observations of Wang *et al.* in γ-irradiated magnetron-sputtered GaN[4]. Wang *et al.* report a significant increase in the concentration of the level at 590 ± 20 meV for doses of, and above, 1Mrad. In order to explain the behaviour of this defect, and based on the report of Huang *et al.*[9], they attribute the origin of this defect to a V_N related defect. This assumption contradicts the findings of Haase *et al.* and the absence of any significant changes in the concentration of this level with exposure other sources of ionising radiation[2,3,8]. However, due to the difference growth process, its is difficult to establish an adequate comparison. This difference, however, may be correlated to aspects unique to RFMS deposited GaN technology, not present in MOCVD-grown epilayers. Furthermore, the apparent contradiction between our results and those of Wang *et al.* could indicate that susceptibility to ionising radiation is correlated to GaN thin films growth technology. Further irradiations are

Table I. Extracted defect level parameters as a function of ^{60}Co γ-irradiation dose.

Trap T1			
Dose krad(Si)	N_T (x10^{13} cm^{-3})	E_a (meV)	σ_∞ (x10^{-16} cm^2)
0	3.4 ± 0.1	241 ± 5	2.5 ± 0.3
200	3.4 ± 0.1	244 ± 2	3.0 ± 0.2
500	3.4 ± 0.1	238 ± 3	1.7 ± 0.8
1000	3.4 ± 0.1	238 ± 3	1.7 ± 1.0
Trap T2			
Dose krad(Si)	N_T (x10^{13} cm^{-3})	E_a (meV)	σ_∞ (x10^{-18} cm^2)
0	1.18 ± 0.2	294 ± 32	6.0 ± 0.3
200	1.02 ± 0.1	289 ± 35	5.8 ± 0.1
500	0.96 ± 0.1	295 ± 26	5.6 ± 0.4
1000	0.89 ± 0.1	277 ± 35	4.6 ± 1.0
Trap T3			
Dose krad(Si)	N_T (x10^{14} cm^{-3})	E_a (meV)	σ_∞ (x10^{-15} cm^2)
0	5.6 ±0.2	575 ± 2	1.1 ± 0.1
200	5.6 ± 0.5	577 ± 2	1.2 ± 0.1
500	5.6 ± 0.1	583 ± 3	1.4 ± 0.1
1000	5.5 ± 0.1	578 ± 2	1.2 ± 0.1

currently being undertaken to determine the γ-radiation damage threshold of MOCVD-grown epilayers.

D. Conclusions

We have presented deep-level transient spectroscopy results of MOCVD-grown GaN epilayers exposed to relatively low doses of γ-radiation from a ^{60}Co source. The measurements were performed from 77 to 300 K, after the sample was a sample exposed to accumulated doses of 200, 500 and 1000 krad(Si). Three deep-levels were found to be present in low concentrations in the sample prior to irradiation with activation energies of 241 ± 5, 294 ± 32 and 575 ± 2 meV. No significant changes were observed in trap parameters or concentrations up to doses of 1Mrad(Si). Although the parameters of the traps detected are in agreement with those observed by others, our results are in apparent disagreement with a recent report of γ-irradiation effects indicating an increase in trap concentration for a level at 590 meV level in RFMS deposited GaN thin films. This difference, however, could be related to aspects unique to RFMS GaN growth technology, not present in MOCVD-grown epilayers.

Acknowledgements

The work presented here is financially supported by the Australian Research Council (ARC).

References

[1] S.J. Pearton, J.C. Zolper, R.J. Shul and F. Ren, J. Appl. Phys. 86 (1999) 1.
[2] L. Polenta L, Z.Q. Fang, D.C. Look, Appl. Phys. Lett. 76 (2000) 2086.
[3] S.A. Goodman, F.D. Auret, F.K. Koschnick, J.-M. Spaeth, B. Beaumont, P.Gibart, MRS Internet J. Nitride Semicond. Res. 4S1 (1999), G6.12.
[4] C.-W. Wang, B.-S. Soong, J.-Y. Chen, C.-L. Chen, Y.-K. Su, J. of App.l Phys. 88 (2000) 6355.
[5] P. Hacke, T. Detchprohm, K. Hiramatsu, N. Sawaki, K. Tadatomo, and K. Miyake, J. Appl. Phys. 76 (1994) 304.
[6] Haase, M. Schmid, W. Kurner, A. Dornen, V. Harle, F. Scholz, M. Burkard, and H. Scheizer, Appl. Phys. Lett. 69 (1996) 2525.
[7] W. K. Gotz, J. Walker, L. T. Romano, N. M. Johnson, and R. J. Molnar, Mater. Res. Soc. Symp. Proc. 449 (1997) 525.
[8] Z-Q. Fang, J. W. Hemsky, D. C. Look, and M. P. Mack, Appl. Phys. Lett. 72 (1998) 448.
[9] Z.C. Huang, J.C. Chen, D. Wickenden, J. Cryst. Growth, 170 (1997) 362.

Appendix B

^{60}Co gamma irradiation effects on n-GaN Schottky diodes

^{60}Co Gamma Irradiation Effects on n-GaN Schottky Diodes

G. A. Umana-Membreno, *Student Member, IEEE*, J. M. Dell, G. Parish, *Member, IEEE*, B. D. Nener, *Senior Member, IEEE*, L. Faraone, *Senior Member, IEEE*, and U. K. Mishra, *Fellow, IEEE*

***Abstract*—The effect of γ-ray exposure on the electrical characteristics of Nickel/n-GaN Schottky barrier diodes has been investigated using current–voltage (*I–V*), capacitance–voltage (*C–V*), and deep-level transient spectroscopy (DLTS) measurements. The results indicate that γ-irradiation induces an increase in the effective Schottky barrier height extracted from *C–V* measurements. Increasing radiation dose was found to degrade the reverse leakage current, whereas its effect on the forward *I–V* characteristics was negligible. Low temperature ($\leq$50°) post-irradiation annealing after a cumulative irradiation dose of 21 Mrad(Si) was found to restore the reverse *I–V* characteristics to pre-irradiation levels without significantly affecting the radiation-induced changes in *C–V* and forward *I–V* characteristics. Three shallow radiation-induced defect centers with thermal activation energies of 88 104 and 144 meV were detected by DLTS with a combined production rate of 2.12×10^{-3} cm^{-1}. These centers are likely to be related to nitrogen–vacancies. The effect of high-energy radiation exposure on device characteristics is discussed taking into account possible contact inhomogeneities arising from dislocations and interfacial defects. The DLTS results indicate that GaN has an intrinsically low susceptibility to radiation-induced material degradation, yet the effects observed in the Schottky diode *I–V* and *C–V* characteristics indicate that the total-dose radiation hardness of GaN devices may be limited by susceptibility of the metal-GaN interface to radiation-induced damage.**

***Index Terms*—Gallium compounds, gamma-ray effects, Schottky barriers, Schottky diodes, semiconductor defects, semiconductor device radiation effects, semiconductor diodes, semiconductor–metal interfaces.**

I. Introduction

THE III-NITRIDE wide-bandgap semiconductors continue to attract considerable research effort due to their unique electronic and optical properties. Low thermal carrier generation rates and large breakdown fields make them attractive for the development of electronic devices capable of reliable operation under extreme conditions, such as high power/voltage levels, high temperatures, and in radiation harsh environments [1], [2].

Recently, several groups have investigated the effect of high-energy radiation on the material properties of GaN [3]–[18]. In many of these studies, exposure to energetic radiation has been employed as a tool to controllably introduce point defects and gain insight into the nature of intrinsic defects, such as vacancies and interstitials, and their effect on optical and transport properties [3]–[7]. Exposure of n-GaN to energetic radiation has been found to degrade electron mobility due to the introduction of defects that act as scattering centers, while the effect on carrier concentration has been noted to be sensitive to the presence of intentional and unintentional impurities and existing defects [3], [8]. The charge trapping characteristics of irradiation induced defects have been reported by several groups using deep-level transient spectroscopy (DLTS) studies. Two distinct radiation-induced defects have been consistently reported, with thermal activation energies within the ranges of 130–200 meV and 790–900 meV [9]–[13]. There is increasing evidence that the broadened DLTS emission signals exhibited by these defects arise from the convolution of several emission signals [12]–[14].

However, there are relatively few reports on the effects of high-energy irradiation on the electrical characteristics of GaN-based devices, even though most reported DLTS studies of radiation-induced defects have been realized using Schottky barrier diodes. An indication of radiation-induced degradation is found in the report of Fang *et al.* [19], where it was briefly noted that the reverse leakage current increased significantly after exposure to a 10^{15} cm^{-2} dose of 1 MeV electrons. A more recent study indicates that exposure to a 10^{13} cm^{-2} neutron dose improved the current–voltage (*I–V*) characteristics of Au/GaN diodes fabricated on magnetron-sputtered *n*-GaN; but subsequent irradiation caused device and material degradation [15]. Nonradiative recombination centers induced by exposure of GaN-based heterostructure light emitting diodes to 2 MeV protons have been shown to affect the optical characteristics more severely than the electrical characteristics [16], [17]. Proton irradiation has also been shown to affect two-dimensional electron gas transport in AlGaN/GaN field effect transistor structures [18]. Most of these studies have employed very large total-dose irradiation [>10 Mrad(Si)], thus indicating that GaN-based electronic and optoelectronic devices have superior radiation hardness compared to GaAs-based devices.

In this work, we present results of a study on the effect of ^{60}Co γ-ray irradiation on the electrical characteristics of a Ni/n-GaN Schottky barrier diode exposed to a maximum cumulative dose of 21 Mrad(Si). Diode characteristics, before and after irradiation, were investigated using capacitance–voltage (*C–V*) and *I–V* measurements, and the introduction of radiation-induced defects was monitored using capacitance deep-level transient spectroscopy (DLTS). Prior to irradiation, the Schottky barrier height extracted from *C–V* is found to be consistent with that

Manuscript received July 9, 2003. The review of this paper was arranged by Editor C.-P. Lee.

G. A. Umana-Membreno, J. M. Dell, G. Parish, B. D. Nener, and L. Faraone are with the School of Electrical, Electronic and Computer Engineering, Crawley, WA 6009 Australia (e-mail: umana-ga@ieee.org).

U. K. Mishra is with the Department of Electrical and Computer Engineering, University of California, Santa Barbara, CA 93106 USA.

Digital Object Identifier 10.1109/TED.2003.820122

obtained from forward *I–V*, however the barrier height extracted from *C–V* measurements manifests a large increase after exposure to 1 Mrad(Si) whereas the barrier height extracted from the forward *I–V* characteristics remained essentially constant. Significant degradation in reverse *I–V* characteristics was evident after a total-dose of 21 Mrad(Si). It was found that a low temperature ($\leq$50 °C) post-irradiation anneal restored the reverse leakage current to pre-irradiation levels without significantly affecting the radiation-induced changes in *C–V* and forward *I–V* characteristics. These effects cannot be explained using the conventional Schottky barrier diode models, which assume an intimate, homogeneous and defect-free metal-semiconductor junction, and are likely to be related to the presence of dislocations in the GaN epilayer and interfacial defects at the Ni/n-GaN junction. The analysis of the DLTS measurements indicates that exposure to a cumulative γ-ray dose of 21 Mrad(Si) introduced three shallow defects with activation energies of 88, 104 and 144 meV. The defect parameters of three deep-level defects detected prior to device irradiation, with activation energies of 265, 355 and 581 meV, were not affected by the high-energy irradiation exposure.

II. Experimental

Schottky-barrier diodes were fabricated on a 2-μm-thick nominally undoped GaN epilayer grown by metal-organic chemical vapor deposition (MOCVD) on a sapphire substrate at the University of California at Santa Barbara. Prior to ohmic contact metallization, the wafer was degreased in organic solvents and etched in hot aqua regia. Large-area ohmic contacts were patterned using standard lift-off techniques and formed by deposition of Al/Cr/Au followed by rapid thermal annealing in a N_2 ambient at 800°C for 60 s. The Schottky barrier regions were etched in a buffered hydrogen fluoride (HF) solution prior to metal deposition, and the coplanar Schottky contacts of 600 μm diameter were formed by thermal evaporation of Ni/Au. The separation between ohmic and Schottky contacts was 30 μm and the GaN surface between the contacts was not passivated.

Exposure to high-energy γ-rays, with an average photon energy of 1.25 MeV, was realized in an AECL Gammacell 220 ^{60}Co irradiator at an average dose rate of 2 krad(Si)/min. The irradiations were carried out at room temperature in a N_2 ambient with all ohmic and rectifying contacts electrically shorted. The sample was exposed to cumulative γ-ray doses of 1, 2, 5, 10 and 21 Mrad(Si). *C–V* and *I–V* measurements were carried out at room temperature under dark conditions using a HP 4280A 1 MHz *C–V* meter and a HP 4145B Semiconductor Parameter Analyzer, respectively. Isothermal DLTS measurements were performed in the 60–300 K temperature range by sampling the capacitance transients resulting from a 10 ms voltage pulse to $V_P = 0$ V from a quiescent reverse bias of $V_R = 2$ V, unless otherwise stated. To avoid possible transient short-term post-irradiation effects, the sample was held at room temperature for at least 3 hours after irradiation exposure prior to to performing any measurements. All measurements were undertaken within as short a time frame as practicable, with only minimal exposure to noncooled room temperature conditions. Two low temperature post-irradiation annealing steps were performed after 21 Mrad(Si): six days at room temperature followed by a 15 minute anneal at 50 °C (both performed in N_2 ambient).

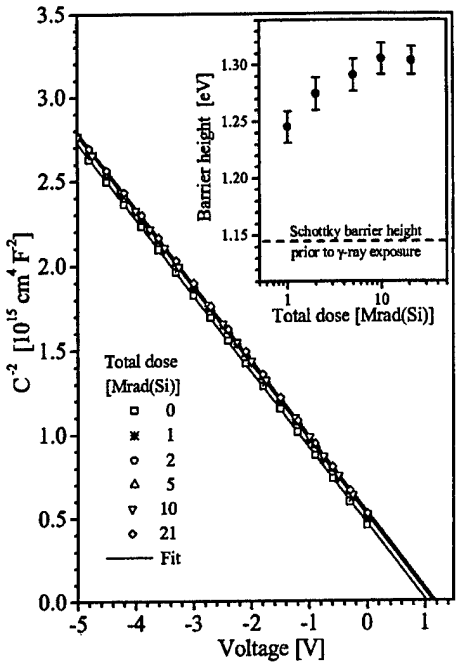

Fig. 1. C^{-2}–V diode characteristics before and after irradiation. For clarity, only 1 out of every 5 experimental points is shown. Inset: Extracted Schottky barrier height as a function of cumulative γ-ray dose. The dashed line in the inset indicates the pre-irradiation value.

III. Results and Discussion

A. C–V and I–V Characteristics

The analysis of the *C–V* characteristics was realized using the expression for the bias dependence of the depletion capacitance, C, of an ideal Schottky barrier diode

$$C^{-2} = (2/qA^2\epsilon_s N_d)(V_{d0} - V - k_B T/q) \quad (1)$$

$$V_{d0} = \phi_B^{cv} - (k_B T/q)\ln(N_c/N_d) \quad (2)$$

where A is the diode area, V is the applied bias, q is the electronic charge, k_B is Boltzmann's constant, T is the device temperature, ϵ_s is the permittivity of GaN ($9.5\epsilon_0$), V_{d0} is the built-in voltage, ϕ_B^{cv} is the flat-band Schottky barrier height, N_c is the effective density of states in the conduction band of GaN (2.6×10^{18} cm^{-3} at 300 K) and N_d is equivalent to the free electron concentration when all shallow donor levels are ionized. By plotting C^{-2} versus V, N_d is obtained from the gradient $(-2/qA^2\epsilon_s N_d)$ while ϕ_B^{cv} is obtained from the extrapolated intercept with the V-axis $(V_{d0} - k_B T/q)$ with the aid of (2).

Prior to sample irradiation, the *C–V* measurements revealed a Schottky barrier height of $\phi_B^{cv} = 1.14 \pm 0.02$ eV and a uniform n-type carrier concentration of 3.3×10^{16} cm^{-3}. The effect of γ-ray exposure on the *C–V* characteristics is shown in Fig. 1, where it is evident that the intercept of the C^{-2}–V characteristics shifts with increasing total dose toward more positive volt-

ages while the gradient remains constant. The negligible change in the slope of the C^{-2}–V characteristics indicates that the carrier concentration remains constant within $\pm 0.03 \times 10^{16}$ cm^{-3} for cumulative radiation doses up to 21 Mrad(Si). The lateral shift in the C^{-2}–V characteristics is due to an increase in V_{d0} which, according to (2), results from an increase in $\phi_B^{\rm cv}$. Thus, $\phi_B^{\rm cv}$ exhibited an increase of 0.13±0.03 eV after 2 Mrad(Si), and 0.16±0.03 eV after 21 Mrad(Si), as shown in the inset of Fig. 1. The zero-bias ac conductance exhibited a small decrease from a pre-irradiation level of 68 to 62 μS after 1 Mrad(Si) total-dose and remained constant within ±2 μS thereafter. The low temperature post-irradiation annealing treatment after 21 Mrad(Si) had no significant effect on the C–V characteristics.

The measured I–V characteristics were analyzed using the conventional Schottky barrier thermionic emission theory model [20]

$$I = I_s \exp(qV/nk_BT)[1 - \exp(-qV/k_BT)] \quad (3)$$

$$I_s = AA^{**}T^2 \exp\left(-\phi_{B0}^{\rm iv}/k_BT\right) \quad (4)$$

where I_s is the saturation current, A^{**} is the effective Richardson constant, $\phi_{B0}^{\rm iv}$ is the effective Schottky barrier height at zero bias, and n is the ideality factor. An effective Richardson constant of $A^{**} = 26.4$ cm^{-2}K^{-2}(m_e =0.22) was used to extract $\phi_{B0}^{\rm iv}$, and the effect of series resistance $R_{\rm s}$ was included by replacing V with $V - I\,R_s$ in (3).

The effective Schottky barrier height, $\phi_{B0}^{\rm iv}$, series resistance, $R_{\rm s}$, and ideality factor, n, extracted from the pre-irradiation forward I–V characteristics using the above model were 1.11±0.01 eV, 48.7 ± 0.7 Ω, and 1.17±0.01, respectively. The ideality factor was extracted for forward current I >2 nA, since a larger value of ideality factor n' = 1.53±0.02 was evident for forward currents below 2 nA. Nevertheless, the diode exhibited excellent rectification characteristics with a relatively low leakage current density of 0.1 μA/cm^2 at a reverse bias of $V_{\rm R}$ =5 V. In contrast to the C–V results, the effect of γ-irradiation on forward I–V characteristics was minimal, as indicated by the results in Fig. 2. A marginal reduction in n' was observed for all doses, and a similarly small improvement in n was noted for doses above 10 Mrad(Si). For all measurements, both $\phi_{B0}^{\rm iv}$ and $R_{\rm s}$ remained approximately constant within ±0.03 eV and ±3 Ω, respectively. The reverse I–V characteristics manifested gradual degradation for increasing radiation doses below 5 Mrad(Si), which worsened significantly for increasing accumulated dose, as indicated in Fig. 2. At a reverse bias of $V_{\rm R}$ = 5, the leakage current increased from the pre-irradiation level of 0.1 μA/cm^2 to 0.34 μA/cm^2 after 2 Mrad(Si) total-dose and to 14.9 μA/cm^2 for cumulative doses $\gtrsim$ 10 Mrad(Si). However, as shown in Fig. 3, the post-irradiation low-temperature anneal fully restored the reverse I–V characteristics to pre-irradiation levels (0.1 μA/cm^2 at V = −5 V). This is consistent with the diode degradation observed by Fang *et al.* and the subsequent recovery observed by Polenta *et al.* [14], [19]. It should be noted that while the anneal had no significant effect on the forward I–V characteristics for I > 2 nA, the low current (I <2 nA) ideality factor n degraded to a value of 1.78 ± 0.03 from 1.31 ± 0.02 before the anneal. The extracted diode parameters are summarized in Table I.

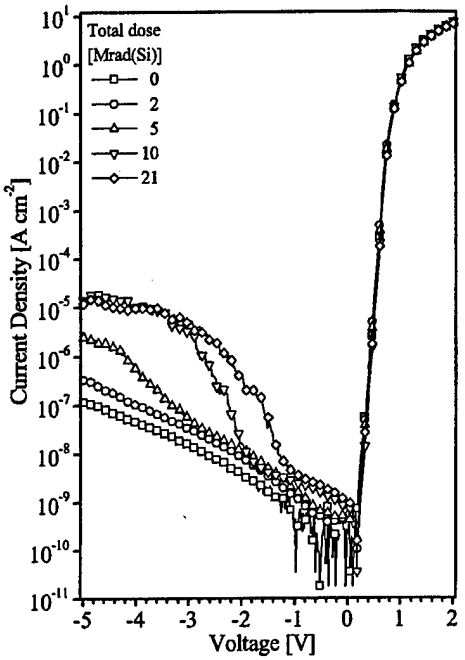

Fig. 2. I–V characteristics of an n-GaN Schottky diodes before and after exposure to accumulated ^{60}Co γ-ray doses up to 21 Mrad(Si).

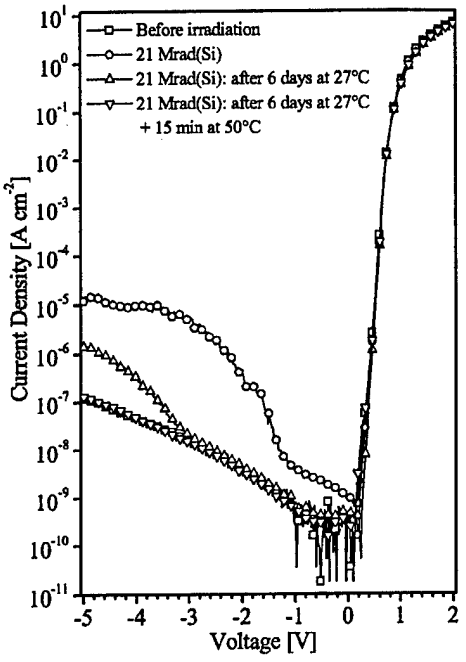

Fig. 3. Effect of two low temperature annealing steps on the I–V characteristics of Ni/n-GaN Schottky diodes exposed to 21 Mrad(Si) ^{60}Co γ-ray total-dose.

The change in barrier height and ideality factor due to image-force barrier lowering are given by [20]

$$\Delta\phi_{B,\rm if} = \left\{\frac{q^3N_d}{8\pi^2\epsilon_\infty^2\epsilon_s}\left(V_{d0}-V-\frac{k_BT}{q}\right)\right\}^{1/4} \quad (5)$$

$$n_{\rm if}^{-1} = 1 + \frac{1}{4}\left(\frac{q^3N_d}{8\pi^2\epsilon_\infty^2\epsilon_s}\right)^{1/4}\left(V_{d0}-V-\frac{k_BT}{q}\right)^{-3/4} \quad (6)$$

TABLE I
SUMMARY OF SCHOTTKY DIODE PARAMETERS EXTRACTED FROM THE *C–V* AND FORWARD *I–V* CHARACTERISTICS. A TWO-STEP LOW-TEMPERATURE ANNEAL (LT ANNEAL) WAS PERFORMED AFTER 21 Mrad(Si)

Dose [Mrad(Si)]	N_d [10^{16} cm^{-3}]	ϕ_B^{cv} [eV]	ϕ_{B0}^{iv} [eV]	n ($I > 2$ nA)	n' ($I < 2$ nA)	R_s [Ω]
0	3.29±0.01	1.14±0.02	1.11±0.01	1.17±0.01	1.52±0.03	48.7±1.2
1	3.29±0.01	1.25±0.01				
2	3.28±0.01	1.27±0.01	1.09±0.01	1.18±0.01	1.14±0.02	46.0±1.1
5	3.31±0.01	1.29±0.01	1.10±0.02	1.18±0.01	1.16±0.02	46.8±0.9
10	3.32±0.01	1.31±0.01	1.14±0.01	1.13±0.01	1.16±0.02	46.8±0.7
21	3.29±0.01	1.30±0.01	1.13±0.02	1.14±0.01	1.31±0.02	48.4±0.8
LT anneal	3.28±0.01	1.30±0.01	1.13±0.02	1.14±0.01	1.78±0.03	49.6±1.0

where ϵ_∞ is the high frequency dielectric permittivity of GaN ($5.2\epsilon_0$). Using the values of $\phi_B^{cv} = 1.14$ eV and $N_d = 3.3 \pm 16$ cm^{-3} obtained from *C–V* measurements, $\Delta\phi_{B,if} \simeq 0.052$ and $n_{if} \simeq 1.013$. Whereas the difference in the values of between ϕ_{B0}^{iv} and ϕ_B^{cv} extracted from the device characteristics prior to γ-irradiation is consistent with image-force barrier lowering, the value of $n = 1.19$ is found to be greater than n_{if} and the reverse leakage current is larger than expected from image-force barrier lowering alone. Furthermore, the difference in ϕ_{B0}^{iv} and ϕ_B^{cv} becomes more significant with increasing total dose. Although ϕ_B^{cv} increased significantly, tending to approximately 1.30 eV, ϕ_{B0}^{iv} remained essentially constant for all doses. Evidently, the effect of irradiation on diode characteristics cannot be explained using the simple models described by (1)–(6), which presume an intimate, homogeneous and defect-free metal-semiconductor interface. These discrepancies are not surprising in view of the nonidealities in device characteristics reported in most studies of metal/n-GaN Schottky barrier diodes [21]–[24].

The nonideal electrical characteristics of as-fabricated GaN Schottky diodes and, in particular, the scatter in reported Schottky barrier height of Ni/GaN contacts, have been thought to arise from effects associated with metal-induced gap states, dislocation-related leakage paths, interfacial defects induced during metal deposition, thin-interfacial layers due to metal/GaN chemical reactions and surface preparation, and epilayer uniformity and quality [21], [25]–[33]. Of these, two are of particular relevance to this work because their effects can be qualitatively correlated with our results.

Firstly, the effect of the ubiquitously high density of dislocations in epitaxial GaN on the electrical characteristics of Schottky barrier diodes needs to be taken into account. There is increasing evidence that dislocations act as efficient current leakage paths [28]–[30]. For the case of Au/GaN contacts, the Schottky barrier height of the regions corresponding to the surface termination of dislocations has been reported to be lower than the barrier height of dislocation-free areas. Undoubtedly, these will affect the *I–V* characteristics because carrier transport across the interface will preferentially occur through these dislocation-related paths. According to the model proposed by Tung [34], [35], the analysis of the forward *I–V* characteristics of diodes with a high density of low Schottky barrier regions yields an ϕ_{B0}^{iv} which underestimates the true effective Schottky barrier height and results in an ideality factor greater than n_{if} [34]–[36]. Since the regions corresponding to the surface termination of dislocations exhibit a width of $\lesssim$50 nm [28], [29], which is small relative to the depth into the GaN epilayer probed by the *C–V* measurement (180 nm at zero bias), fluctuations in interface potential are screened out at the edge of the depletion region, and ϕ_B^{cv} values extracted using (1) and (2) represent an average barrier height over the entire Schottky diode gate [34]–[36]. Thus, the values of ϕ_B^{cv} and ϕ_{B0}^{iv} extracted using the conventional models for Schottky diode *C–V* and *I–V* characteristics may differ significantly. This is particularly true in diodes with a high density of dislocations which are exposed to increasing doses of energetic irradiation, because any radiation-induced changes within the dislocation-free area of the metal-GaN interface may not be manifest in the forward *I–V* characteristics, yet may significantly affect the *C–V* characteristics, in agreement with our observations.

Additionally, the introduction of radiation-induced defects near the metal-GaN interface also needs to be taken into consideration. Even though radiation-induced improvements in diode characteristics have been reported in both GaAs and GaN devices for relatively low irradiation doses [15], [37], the high cumulative doses employed in this study are likely to lead to device degradation due to radiation-induced introduction of interfacial defects via displacement damage. This is supported by reports indicating that exposure to γ-rays, and low energy electrons, causes desorption of N and Ga near the surface of GaN. In terms of the model employed thus far to extract ϕ_B^{cv}, it is important to note that implicit in (1) and (2) is the assumption of a uniform charge density in the depletion region. This assumption is unlikely to be valid in the presence of a high density interfacial defects. Although detailed information regarding the existence and nature of these radiation-induced interfacial defects is needed for a complete analysis, the apparent increase in ϕ_B^{cv} can be phenomenologically attributed to the formation of a negatively-charged thin-layer near the Ni/n-GaN interface. A simple depletion approximation approach can be employed to model a uniformly doped GaN epilayer containing a sheet of negative charge of areal-density qD_{ss} located at δ_s below the metal/GaN interface. In this case, the apparent ϕ_B^{cv} can be shown to be correlated to the true flatband Schottky barrier height ϕ_B^{fb}:

$$\phi_B^{cv} = \phi_B^{fb} + \frac{qD_{ss}\delta_s}{\epsilon_s} \tag{7}$$

Thus, using the above model, the apparent increase in ϕ_B^{cv} of 0.16 eV after 21 Mrad(Si) corresponds to an increase in $D_{ss}\delta_s$ of 8.4×10^5 cm^{-1}, provided that ϕ_B^{fb} and ϵ_s remain constant. It should be noted that while the this negative charge could be attributed to radiation-induced acceptor-like defects below the Fermi level, radiation-induced lattice defects could also induce changes in uniaxial strain near the metal-GaN junction which, in turn, would induce a change in polarization charges that may lead to an apparent increase in ϕ_B^{cv}. Such effects, which are similar to those observed in GaAs barrier diodes under externally applied uniaxial stress, may be of significance given the very large piezoelectric constants of GaN [40], [41].

The radiation-induced degradation observed in reverse *I–V* characteristics could be attributed to an increase in interfacial defect density. However, our observation that the low temperature anneal restores the leakage current to pre-irradiation levels without affecting the *C–V* characteristics indicates that the inter-

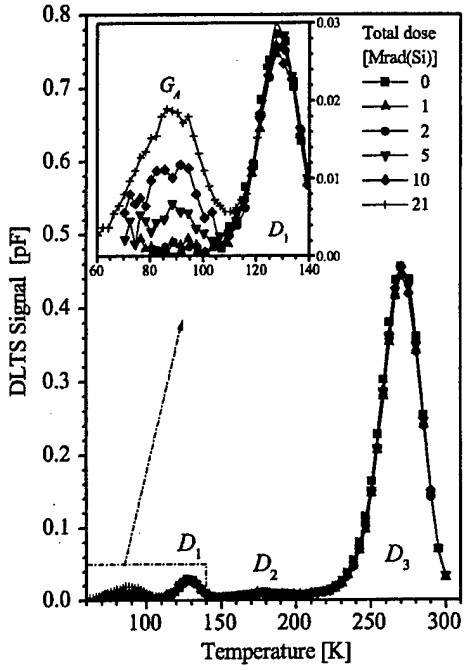

Fig. 4. DLTS spectra showing defects $D_{1,2,3}$, detected prior to irradiation, as a function of cumulative γ-radiation dose, with $e_n = 1.02\ s^{-1}$ and $t_p = 10$ ms. Inset: Expanded view of D_1 and the evolution of radiation-induced level G_A with γ-ray total-dose.

facial defects responsible for the degradation in reverse leakage current are unlikely to be associated with the apparent shift in ϕ_B^{cv}. It is unclear whether dislocation related leakage-paths are the dominant mechanisms associated with the reverse leakage current degradation and recovery. Nevertheless, these results together with the low density of radiation-induced defects in the bulk of the sample, as will be shown in the next section, indicate that the susceptibility to radiation induced degradation in GaN based devices is likely to be dominated by interfacial and surface related effects rather than by the intrinsic radiation hardness of the underlying GaN epilayer.

B. Deep-Level Transient Spectroscopy

The analysis of the DLTS spectra was facilitated by transforming the digitally recorded isothermal capacitance transients into rate-windows with a constant gating time ratio of $t_2/t_1 = 10$. The thermal activation energies E_T and apparent capture cross-sections σ_∞ were extracted using the traditional Arrhenius plot of $\ln(e_n/T_m^2)$ versus $1000/T_m$, where e_n is the emission rate and T_m is the temperature at which the DLTS maximum occurs.

Three deep-level defects, labeled D_1, D_2, and D_3, were detected in the sample before irradiation. Their defect parameters and thermal emission characteristics are summarized in Table II and Fig. 7. Deep-level centers D_1 and D_3 are the most common defects detected by DLTS in n-GaN grown by various methods [11], [42]. The D_2 level is similar to the magnesium-related defect reported in n-GaN by Hacke *et al.* [42], possibly indicating background Mg contamination in the growth chamber. For accumulated γ-ray doses up to 21 Mrad(Si), the effect of irradiation on the characteristics of these three defects is negligible,

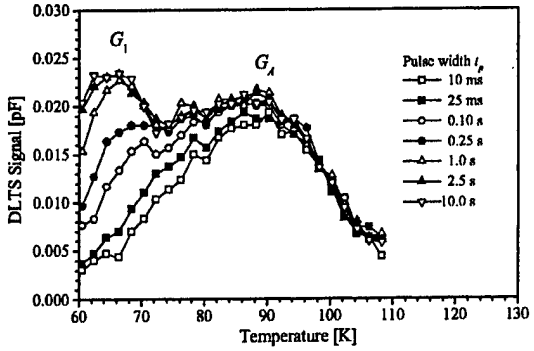

Fig. 5. DLTS spectra as a function of filling pulse, after 21 Mrad(Si) with $e_n = 1.02\ s^{-1}$ and reverse quiescent bias of 2 V.

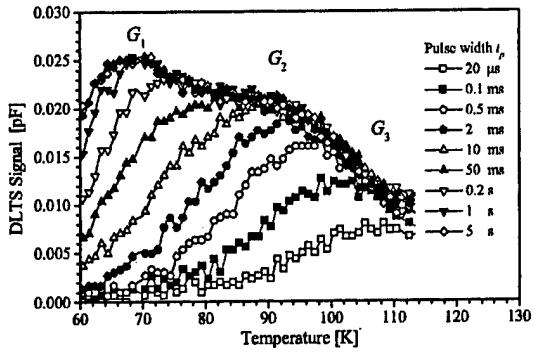

Fig. 6. DLTS spectra as a function of filling pulse, after 21 Mrad(Si) with $e_n = 1.02\ s^{-1}$ and reverse quiescent bias of 5 V.

TABLE II
DEFECT PARAMETERS FOR THE DEEP-LEVELS DETECTED IN THE GaN SAMPLE PRIOR TO γ-RAY EXPOSURE. THE EFFECT OF IRRADIATION AND POST-IRRADIATION LOW-TEMPERATURE ANNEALING ON DEFECT PARAMETERS WAS NEGLIGIBLE

Label	N_T (10^{13} cm^{-3})	σ_∞ (cm^2)	E_T (meV)
D_1	4.3	2.5×10^{-15}	265± 7
D_2	1.7	6.5×10^{-16}	355±30
D_3	61.0	1.4×10^{-15}	581± 9

as shown in Fig. 4, and is consistent with studies employing high-energy electron irradiation [11].

No significant changes in the DLTS spectra were observed for cumulative doses below 2 Mrad(Si). The introduction of radiation-induced defects is only noticeable for cumulative doses greater than 5 Mrad(Si), primarily as as a broad emission signal at temperatures below 110 K, with a magnitude that increases with γ-ray dose (see inset of Fig. 4). In order to determine whether the breadth of this radiation-induced emission signal was due to more than one defect, further measurements were performed after exposure to 21 Mrad(Si) using trap-filling pulse widths t_p ranging from 10 ms to 10 s at $V_R = 2$ V, and from 10 μs to 10 s at $V_R = 5$ V. The DLTS spectra thus obtained, shown in Figs. 5 and 6, indicate the presence of at least two well-defined but broad emission lines labeled G_1 and G_A in Fig. 5. These defects are characterized by E_T and σ_∞ of (G_1) 89±6 meV and 3.1×10^-18 cm^{-2}, and

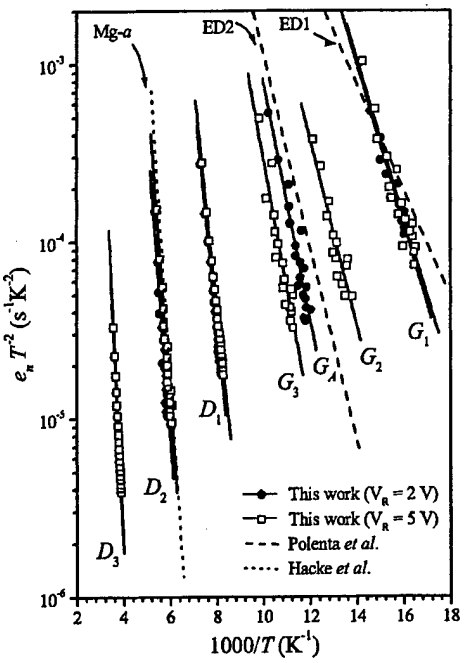

Fig. 7. Arrhenius plot of defects identified by DLTS, for quiescent reverse bias of (•) 2 V and (□) 5 V. Defects $D_{1,2,3}$ are present prior to ^{60}Co γ-ray exposure. $G_{1,2,3}$ are radiation-induced defects, with the signature labeled G_A being formed by the convolution of the DLTS signals of G_1 and G_2. Also shown: 1 MeV electron irradiation-induced defects (ED1) 60 meV and (ED2) 110 meV in [14]; and (Mg-*a*) 400 meV magnesium-related defect in [42].

(G_A) 132±11 meV and 4.9×10^{-18} cm^{-2}. However, more detailed probing into the characteristics of the G_A carrier emission, using shorter t_p at $V_R = 5$ V (see Fig. 6), indicates that its DLTS signal is formed by the convolution of two defects. By subtracting spectra at different trap-filling pulse widths, and employing only DLTS signals that are almost saturated, we obtained Arrhenius plots for 3 different levels, labeled G_1, G_2 and G_3, with E_T and σ_∞ of (G_1) 88 ± 7 meV and 2.6×10^{-18} cm^2, (G_2)104±12 meV and 1.2×10^{-18} cm^2, and (G_3)144±13 meV and 7.6×10^{-18} cm^2. The characteristics of the G_3 level are consistent with the 155 meV radiation-induced defect observed by Schimdt and coworkers using $t_p = 1$ ms and $V_R = 7$ in n-GaN exposed to a ^{60}Co γ-ray fluence equivalent to $\sim 1.5 \times 10^4$ Mrad(Si) [10]. The defect parameters and Arrhenius plots for the radiation-induced levels are presented in Table III and Fig. 7, respectively. The parameters obtained at $V_R = 5$ V are expected to be more accurate due to the increased observation volume during emission. It should be noted that the extracted parameters of irradiation-induced levels describe adequately the evolution of the saturated DLTS peaks with temperature, but they are insufficient to account for the observed filling-pulse behavior since we have neglected the possible presence of any barriers for carrier capture. The trap-filling pulse widths required to saturate the G_1 signal are of the same magnitude as the emission time constants, indicating that the true capture cross-section may be significantly smaller than the apparent cross-section and/or that a barrier for carrier capture is present. The extensive overlap in the emission signals does not allow for extraction of unique values of the barrier for carrier capture, or of the true capture cross-section, from the trap-filling characteristics.

TABLE III
RADIATION-INDUCED DEFECT PARAMETERS IN n-GaN AFTER EXPOSURE TO 21 Mrad(Si) CUMULATIVE γ-RAY DOSE. THE EFFECT OF POST-IRRADIATION LOW-TEMPERATURE ANNEALING ON DEFECT PARAMETERS WAS NEGLIGIBLE

Label	V_R (V)	Production rate (10^{-4} cm^{-1})	N_T (10^{13} cm^{-3})	σ_∞ (cm^2)	E_T (meV)
G_1	2	6.7	2.8	3.1×10^{-18}	89± 6
G_A	2	5.9	2.5	4.9×10^{-18}	132±11
G_1	5	9.1	3.8	2.6×10^{-18}	88± 7
G_2	5	7.3	3.0	1.2×10^{-18}	104±12
G_3	5	4.8	2.0	7.6×10^{-18}	144±13

The defect production rates obtained after 21 Mrad(Si) cumulative dose, included in Table III, were calculated from the equivalent 1.25 MeV photon fluence obtained using the relation [43]: 1 rad(Si) = 2.0×10^9 photons/cm^{-2}. The combined production rate for all radiation induced defects, using the parameters obtained at $V_R = 5$ V, is 2.12×10^{-3} cm^{-1}. From the DLTS spectra at $V_R = 2$ V as a function of total γ-ray dose, the production rate for the G_A center (G_2 and G_3 combined) is 5.9×10^{-4} cm^{-1} and is approximately constant within $\pm 1 \times 10^{-4}$ cm^{-1}, for cumulative doses greater than 2 Mrad(Si). The production rate for the G_3 center is 4.8×10^{-4} cm^{-1}, in close agreement with the 3.3×10^{-4} cm^{-1} production rate of the 155 meV γ-ray-induced defect reported by Schimdt *et al.* [10]. This suggests that the defect production rates are quite low and not significantly dependent on total γ-ray dose.

The charge-trapping parameters of the radiation induced defects in GaN detected in this study are consistent with previously reported nitrogen-related defects. It is likely, however, that more complex defects may arise near the metal-GaN interface since the radiation-induced defect production rates are influenced by the presence of lattice flaws and impurities [8], [44]. The low defect production rates are clear evidence of the low susceptibility of GaN to ionizing radiation induced damage.

IV. CONCLUSION

The effect of γ-irradiation on the electrical characteristics of Ni/n-GaN Schottky diodes has been studied using *C–V*, *I–V*, and DLTS measurements. Exposure to increasing cumulative γ-ray doses was found to have the following effects: a) an apparent increase in the Schottky barrier height extracted from *C–V* measurements; b) the effective barrier height extracted from forward *I–V* measurements remains essentially constant with a marginal improvement in ideality factor; and c) significant degradation in reverse *I–V* characteristics for total doses above 2 Mrad(Si). Low temperature post-irradiation annealing (six days at room temperature plus 15 min at 50 °C) was found to restore the reverse *I–V* characteristics to pre-irradiation levels without having any significant effect on the forward *I–V* characteristics or on the radiation-induced changes in the *C–V* characteristics. These effects have been discussed taking into consideration possible effects due to the high density of dislocations common in GaN epilayers and radiation-induced defects at the metal-semiconductor

interface. It is postulated that the apparent increase in flatband Schottky barrier height is due to the formation of a sheet of negative charge arising from radiation-induced defects or piezoelectric effects near the metal-GaN interface. The negligible change in forward *I–V* characteristics, which tends to indicate a nearly constant barrier height with irradiation dose, is attributed to the low Schottky barrier height in regions associated with the surface termination of dislocations. Even though the degradation observed in the reverse *I–V* characteristics is undoubtedly due to an increase in radiation-induced defects, the recovery after annealing indicates that these defects are not responsible for the changes in *C–V* characteristics.

The introduction of radiation-induced defects was monitored using isothermal DLTS measurements. Three radiation-induced defects were detected after a radiation dose of 21 Mrad(Si) with activation energies of 88 104 and 144 meV, and produced at a combined rate of 2.12×10^{-3} cm^{-1}. Given the general agreement of our results with those obtained by other authors for 1 MeV electron irradiated GaN, we attribute these defects to nitrogen–vacancy-related defects. Three deep-level defects detected in the sample before irradiation exposure, with activation energies of 265, 355, and 581 meV, did not manifest any significant changes in their parameters or concentrations after cumulative γ-ray doses up to 21 Mrad(Si).

Our results indicate that epitaxial GaN has an intrinsically low susceptibility to radiation-induced material degradation. However, radiation hardness of GaN devices is more likely to be limited by susceptibility of the metal-GaN interface to radiation-induced damage and by the deleterious effect of a high density dislocations. These effects are likely to have a negative impact on the reverse-bias characteristics of Schottky gates and, hence, the performance and reliability of GaN-based high power rectifiers, MESFETs and HFETs operating in high-energy radiation environments.

ACKNOWLEDGMENT

The authors wish to acknowledge the support of this project by the Australian Research Council (ARC) and the AFOSR MURI on Radiation Physics (monitored by Dr. G. Witt).

REFERENCES

[1] U. K. Mishra, Y.-F. Wu, B. P. Keller, S. Keller, and S. P. DenBaars, "GaN microwave electronics," *IEEE Trans. Microwave Theory Tech.*, vol. 46, pp. 756–761, June 1998.

[2] S. J. Pearton, F. Ren, A. P. Zhang, and K. P. Lee, "Fabrication and performance of GaN electronic devices," *Mater. Sci. Eng.*, vol. R30, pp. 55–212, 2000.

[3] D. C. Look, D. C. Reynolds, J. W. Hemsky, J. L. Sizelove, R. L. Jones, and R. J. Molnar, "Defect donor and acceptor in GaN," *Phys. Rev. Lett.*, vol. 79, no. 12, pp. 2273–2276, 1997.

[4] M. Linde, S. J. Uftring, and G. D. Watkins, "Optical detection of magnetic resonance in electron-irradiated GaN," *Phys. Rev. B*, vol. 55, no. 16, pp. R10177–R10180, 1997.

[5] I. A. Buyanova, Mt. Wagner, W. M. Chen, B. Monemar, J. L. Lindström, H. Amano, and I. Akasaki, "Photoluminescence of GaN: Effect of electron irradiation," *Appl. Phys. Lett.*, vol. 73, no. 20, pp. 2968–2970, 1998.

[6] K. H. Chow, G. D. Watkins, A. Usui, and M. Mizuta, "Detection of interstitial Ga in GaN," *Phys. Rev. Lett.*, vol. 85, no. 13, pp. 2761–2764, 2000.

[7] S. M. Khanna, J. Webb, A. J. Houdayer, and C. Carlone, "2 MeV proton radiation damage studies of Gallium Nitride films through low temperature photoluminescence spectroscopy measurements," *IEEE Trans. Nucl. Sci.*, vol. 47, pp. 2322–2328, June 2000.

[8] V. V. Emtsev, V. Y. Davydov, V. V. Kozlovskii, V. V. Lundin, D. S. Poloskin, A. N. Smirnov, N. M. Schmidt, A. S. Usikov, J. Aderhold, H. Klausing, D. Mistele, T. Rotter, J. Stemmer, O. Semchinova, and J. Graul, "Point defects in γ-irradiated n-GaN," *Semicond. Sci. Technol.*, vol. 15, no. 1, pp. 73–78, 2000.

[9] S. A. Goodman, F. D. Auret, F. K. Koschnick, J.-M. Spaeth, B. Beaumont, and P. Gibart, "Electrical characterization of defects introduced in n-GaN during high energy proton and He-ion irradiation," *MRS Internet J. Nitride Semicond. Res.*, vol. 4S1, p. G6.12, 1999.

[10] N. M. Schmidt, D. V. Davydov, V. V. Emtsev, I. L. Krestnikov, A. A. Lebedev, W. V. Lundin, D. S. Poloskin, A. V. Sakharov, A. S. Usikov, and A. V. Osinsky, "Effect of annealing on defects in as-grown and γ-ray irradiated n-GaN layers," *Phys. Stat. Sol. (b)*, vol. 216, pp. 533–536, 1999.

[11] Z.-Q. Fang, L. Polenta, J. W. Hemsky, and D. C. Look, "Deep centers in as-grown and electron-irradiated n-GaN," in *Proc. SIMC-IX* , 2000, pp. 35–42.

[12] S. A. Goodman, F. D. Auret, M. J. Legodi, G. Myburg, B. Beaumont, and P. Gibart, "Electron irradiation induced defects in n-GaN," in *Proc. SIMC-IX*, 2000, pp. 43–46.

[13] G. A. Umana-Membreno, J. M. Dell, T. P. Hessler, B. D. Nener, G. Parish, L. Faraone, and U. K. Mishra, "^{60}Co gamma-irradiation-induced defects in n-GaN," *Appl. Phys. Lett.*, vol. 80, no. 23, pp. 4354–4356, 2002.

[14] L. Polenta, Z.-Q. Fang, and D. C. Look, "On the main irradiation-induced defect in GaN," *Appl. Phys. Lett.*, vol. 76, no. 15, pp. 2086–2088, 2000.

[15] C.-W. Wang, "Neutron-irradiation effect on radio-frequency magnetron-sputtered GaN thin films and Au/GaN Schottky diodes," *J. Vac. Sci. Technol. B*, vol. 20, no. 5, pp. 1821–1826, 2002.

[16] M. Osiński, P. Perlin, H. Schöne, A. H. Paxton, and E. W. Taylor, "Effects of proton irradiation on AlGaN/InGaN/GaN green light emitting diodes," *Electron. Lett.*, vol. 33, no. 14, pp. 1252–1253, 1997.

[17] F. Gaudreau, C. Carlone, A. Houdayer, and S. M. Khanna, "Spectral properties of proton irradiated Gallium Nitride blue diodes," *IEEE Trans. Nucl. Sci.*, vol. 48, pp. 1778–1784, June 2001.

[18] S. J. Cai, Y. S. Tang, R. Li, Y. Y. Wei, L. Wong, Y. L. Chen, K. L. Wang, M. Chen, Y. F. Zhao, R. D. Schrimpf, J. C. Keay, and K. F. Galloway, "Annealing behavior of a proton irradiated $Al_xGa_{1-x}N$/GaN high electron mobility transistor grown by MBE," *IEEE Trans. Electron. Devices*, vol. 47, pp. 304–307, Feb. 2000.

[19] Z.-Q. Fang, J. W. Hemsky, D. C. Look, and M. P. Mack, "Electron-irradiation-induced deep level in GaN," *Appl. Phys. Lett.*, vol. 72, no. 4, pp. 448–449, 1998.

[20] E. H. Rhoderick and R. H. Williams, *Metal-Semiconductor Contacts*: Clarendon, 1988, ch. 4.

[21] L. S. Yu, Q. Z. Liu, Q. J. Qiao, S. S. Lau, and J. Redwing, "The role of the tunneling component in the current-coltage characrteristics of metal-GaN Schottky diodes," *J. Appl. Phys.*, vol. 84, no. 4, pp. 2099–2104, 1998.

[22] J. C. Carrano, T. Li, P. A. Grudowski, C. J. Eiting, R. D. Dupuis, and J. C. Campbell, "Comprehensive characterization of metal-semiconductor-metal ultraviolet photodetectors fabricated on single-crystal GaN," *J. Appl. Phys.*, vol. 83, no. 11, pp. 6148–6160, 1998.

[23] T. Sawada, Y. Ito, K. Imai, K. Suzuki, H. Tomozawa, and S. Sakai, "Electrical properties of metal/GaN and SiO_2/GaN interfaces and effects of thermal annealing," *Appl. Surf. Sci.*, vol. 159/160, pp. 449–455, 2000.

[24] H. Hasegawa and S. Oyama, "Mechanism of anomalous current transport in n-type GaN Schottky contacts," *J. Vac. Sci. Technol. B*, vol. 20, no. 4, pp. 1647–1655, 2000.

[25] V. M. Bermudez, R. Kaplan, M. A. Khan, and J. N. Kuznia, "Growth of thin Ni films on GaN(0001)-(1 × 1)," *Phys. Rev. B*, vol. 48, no. 4, pp. 2436–2444, 1993.

[26] M. H. Kim, S. N. Lee, C. Huh, S. Y. Park, J. Y. Han, J. M. Seo, and S. J. Park, "Interfacial reaction and Fermi level movement induced by sequentially deposited metal on GaN: Au/Ni/GaN," *Phys. Rev. B*, vol. 61, no. 16, pp. 10 966–10 971, 2000.

[27] A. Barinov, L. Gregoriatti, B. Kaulich, M. Kiskinova, and A. Rizzi, "Defect induced lateral chemical heterogeneity at Ni/GaN interfaces and its effect on the electronic properties of the interface," *Appl. Phys. Lett.*, vol. 79, no. 17, pp. 2752–2754, 2001.
[28] E. G. Brazel, M. A. Chin, and V. Narayamurti, "Direct observation of localized high current densities in GaN films," *Appl. Phys. Lett.*, vol. 74, no. 16, pp. 2367–2369, 1999.
[29] J. W. P Hsu, M. J. Manfra, D. V. Lang, S. Richter, S. N. G. Chu, A. M. Sergent, R. N. Kleinman, L. N Pfeiffer, and R. J. Molnar, "Inhomogeneous spatial distribution of reverse leakage in GaN Schottky diodes," *Appl. Phys. Lett.*, vol. 78, no. 12, pp. 1685–1681, 2001.
[30] J. W. P. Hsu, M. J. Manfra, R. J. Molnar, B. Heying, and J. S. Speck, "Direct imaging of reverse-bias leakage through pure screw dislocations in GaN films grown by molecular beam epitaxy on GaN templates," *Appl. Phys. Lett.*, vol. 81, no. 1, pp. 79–81, 2002.
[31] J. D. Guo, F. M. Pan, M. S. Feng, R. J. Guo, P. F. Chou, and C. Y. Chang, "Schottky contact and the thermal stability of Ni on n-type GaN," *J. Appl. Phys.*, vol. 80, no. 3, pp. 1624–1627, 1996.
[32] Q. Z. Liu and S. S. Lau, "Ni and Ni silicide Schottky contacts on n-GaN," *J. Appl. Phys.*, vol. 84, no. 2, pp. 881–886, 1998.
[33] K. Shiojima, J. M. Woodall, C. J. Eiting, P. A. Grudowski, and R. D. Dupuis, "Effect of defect density on the electrical characteristics of n-type GaN Schottky contacts," *J. Vac. Sci. Technol. B*, vol. 17, no. 5, pp. 2030–2033, 1999.
[34] R. T. Tung, "Electron transport at metal-semiconductor interfaces: General theory," *Phys. Rev. B*, vol. 45, no. 23, pp. 13 509–13 523, 1992.
[35] ——, "Recent advancements in Schottky barrier concepts," *Mater. Sci. Eng.*, vol. R35, pp. 1–138, 2001.
[36] J. H. Werner and H. H. Güntler, "Barrier inhomogeneities at Schottky contacts," *J. Appl. Phys.*, vol. 69, no. 3, pp. 1522–1533, 1991.
[37] O. Yu. Borkovskaya, N. L. Dmitruk, R. V. Konakova, V. G. Litovchenko, and O. I. Maeva, "Influence of gamma radiation on surface generation and recombination in semiconductor structures based on GaAs," *Sov. Phys. Semicond.*, vol. 20, no. 9, pp. 1028–1031, 1986.
[38] S. Yoshida, M. Sasaki, and T. Ishikawa, "The effect of EB irradiation with and without hot-jet Cl_2 on an ultra-thin GaN layer for selective etching," *Appl. Surf. Sci.*, vol. 100/101, pp. 184–188, 1996.
[39] C.-W. Wang, B.-S. Soong, J.-Y. Chen, C.-L. Chen, and Y.-K. Su, "Effect of gamma-ray irradiation on the microstructural and luminescent properties of radio-frequency magnetron-sputtered GaN thin films," *J. Appl. Phys.*, vol. 88, no. 11, pp. 6355–6358, 2000.
[40] K.-W. Chung, Z. Wang, J. C. Costa, F. Williamson, P. P. Ruden, and M. I. Nathan, "Barrier height change in GaAs Schottky diodes induced by piezoelectric effect," *Appl. Phys. Lett.*, vol. 59, no. 10, pp. 1191–1193, 1991.
[41] R. P. Strittmatter, R. A. Beach, J. Brooke, E. J. Preisler, G. S. Picus, and T. C. McGill, "GaN Schottky diodes for piezoelectric strain sensing," *J. Appl. Phys.*, vol. 93, no. 9, pp. 5679–5681, 2003.
[42] P. Hacke, H. Nakayama, T. Detchprohm, K. Hiramatsu, and N. Sawaki, "Deep levels in the upper band-gap region of lightly Mg-doped GaN," *Appl. Phys. Lett.*, vol. 68, no. 10, pp. 1362–1364, 1996.
[43] G. C. Messenger and M. S. Ash, *The Effects of Radiation on Electronic Systems*: Van Nostrand Reinhold, 1992, ch. 10, pp. 542–583.
[44] B. T. Kelly, *Irradiation Damage to Solids*. New York: Pergamon Press, 1966, ch. 2, pp. 72–117.

G. A. Umana-Membreno (S'93) received the B.E. degree (with honors) in electrical and electronic engineering from The University of Western Australia, Crawley, in 1996, where he is currently pursuing the Ph.D. degree.

His main research interests are in characterization of III-nitride semiconductor materials and devices. Specific research interests include high-energy irradiation effects and device reliability, and carrier transport and charge-trapping effects in electronic devices.

J. M. Dell was born in Australia on September 22, 1957. He received the B.E. (with honors), and Ph.D. degrees in electronic engineering from The University of Western Australia (UWA), Crawley, in 1980 and 1989, respectively.

From 1984 to 1990 he was a Senior Research Engineer with Telecom Australia Research Laboratories, (now Telstra Research Laboratories), Melbourne, where he was involved with photonics, OEIC development, and characterization of III-V semiconductors. From 1989 to 1991, he was a Research Scientist with Matra Marconi Space Systems, France, working in the area of space radiation effects. From 1992 to 1993 he was a Principal Research Scientist with Telecom Australia Research Laboratories leading the semiconductor photonics research. Since joining UWA in 1995 as a Member of the Academic Staff, his research interests have been in the general areas of photonics, semiconductor materials, radiation effects, and recently MEMS. In particular he is interested in HgCdTe infrared detector devices and GaN electronics.

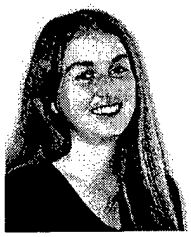

G. Parish (S'98–M'01) received the B.S. degree in chemistry in 1995, and the B.E. and M.Eng.Sc degrees in electronic engineering in 1995 and 1997, respectively, all from The University of Western Australia (UWA), Crawley, and the Ph.D. degree in electrical engineering from the University of California, Santa Barbara, in 2001. She is currently an Australian Research Council Postdoctoral Fellow at UWA.

Her main research interests are the growth and characterization of the III-V nitride material system. Specific interests within this area currently include development of processing technology, measurement of minority carrier properties, and transport and defect studies in electronic devices.

B. D. Nener (S'79–M'89–SM'93) received the B.E. (with honors) and Ph.D. degrees from The University of Western Australia (UWA), Crawley, in 1977 and 1987, respectively, and the M.Eng.Sc. degree in electronic engineering in 1980 from the University of Tokyo, Japan.

From 1985 to 1986, he was a Wyn-Spence Medical Research Fellow at UWA investigating the effect of diabetes on the retina. From 1986 to 1987 he was a Senior Research Engineer at ACET Ltd., Perth, designing and installing data acquisition and control systems for the iron-ore industry. From 1987 to 1989, he was an ARC Post-doctoral Fellow investigating GaAs deep-level defects. He was with the School of Electrical, Electronic and Computer Engineering, UWA, as Lecturer in 1989, Senior Lecturer in 1994, Associate Professor from 1999 to the present, and as Director of the Centre for Electro-Optic Propagation and Sensing. From 1996 to 1997, he was a Visiting Professor to the U.S. Navy's Space and Naval Warfare Center, San Diego, CA, and the University of California at Santa Barbara. His current research interests are atmospheric propagation of light (particularly UV and IR), IR and UV optical detectors, measurement of electronic transport properties and electronic deep level traps in the AlGaN semiconductors.

L. Faraone (SM'03) was born in Italy on October 26, 1951. He received the Ph.D. degree from the University of Western Australia (UWA), Crawley, in 1979.

He worked as a Research Scientist in the Sherman Fairchild Laboratory, Lehigh University, Bethlehem, PA, from 1979 to 1980, where he was involved in studies on MOS devices. From 1980 to 1986, he was a Member of Technical Staff at RCA Laboratories, David Sarnoff Research Center, Princeton, NJ, including time as a Project Leader in the area of VLSI CMOS technologies, and as Principal Investigator of a research team studying space radiation effects in silicon-on-sapphire MOS integrated circuits. He joined the School of Electrical, Electronic and Computer Engineering at UWA as a Senior Lecturer in 1987, and was promoted to Associate Professor in 1993 and Professor in 1998. He held the position of Head of Department/School from 1999 to 2003. Since his arrival at UWA, his research interests have been in the area of non-volatile memory technology, compound semiconductor materials and devices, and micro-electro-mechanical systems (MEMS). In particular, his interests include mercury cadmium telluride materials and device technologies for infrared detector arrays, gallium nitride technology for ultraviolet detectors and high-speed/high-power electronics, and MEMS technologies for tuneable optical cavity detectors. He currently holds more than ten U.S. patents, has supervised more than 15 Ph.D. student completions, and published more than 200 refereed technical papers.

Dr. Faraone was awarded the RCA Laboratories Individual Outstanding Achievement Award in 1983 and 1986, and the John de Laeter Innovation Award in 1997.

U. K. Mishra (S'80–M'83–SM'90–F'95) received the B.Tech. from the Indian Institute of Technology (IIT) Kanpur, India in 1979, the M.S. degree from Lehigh University, Bethlehem, PA in 1980, and the Ph.D. degree from Cornell University, Ithaca, NY, in 1984, all in electrical engineering.

He has worked in various laboratory and academic institutions, including Hughes Research Laboratories, Malibu, CA, The University of Michigan, Ann Arbor, and General Electric, Syracuse, NY, where he has made major contributions to the development of AlInAs-GaInAs HEMTs and HBTs. He is now the Department Chair and a Professor at the Department of Electrical and Computer Engineering, University of California at Santa Barbara. His current research interests are in oxide based III-V electronics and III-V nitride electronics and opto-electronics. He has authored or co-authored over 400 papers in technical journals and conferences and holds eight patents.

Dr. Mishra was a co-recipient of the Hyland Patent Award given by Hughes Aircraft, and the Young Scientist Award presented at the International Symposium on GaAs and Related Compounds.

Appendix C

Annealing behavior of ^{60}Co Gamma radiation-induced damage in Ni/n-GaN Schottky diodes

Annealing behavior of ^{60}Co Gamma radiation-induced damage in Ni/n-GaN Schottky diodes

G. A. Umana-Membreno, J. M. Dell, G. Parish, B. D. Nener, L. Faraone and U. K. Mishra

Abstract

The effect of isochronal thermal annealing on ^{60}Co gamma-irradiated Ni/n-GaN Schottky barrier diodes, which had previously been exposed to 21 Mrad(Si) total dose, has been investigated using capacitance-voltage (C–V) and current-voltage (I–V) measurements, whereas capacitance deep-level transient spectroscopy (DLTS) has been employed to monitor the evolution and annihilation of radiation-induced defects during thermal annealing. While a relatively low temperature anneal at 50 °C has been shown to restore the reverse bias I–V characteristics to pre-irradiation levels without any significant effect on the C–V and forward I–V characteristics, subsequent thermal annealing up to 160 °C is shown to further improve device characteristics. However, annealing above 250 °C is found to degrade both forward and reverse I–V characteristics and induce a reduction in the free carrier concentration obtained from C–V characteristics. Detailed analysis of the forward current and C–V characteristics indicate that the apparent reduction in Schottky barrier height after annealing above 250 °C, is associated with dislocation-related to annealing effects. Annealing at temperatures above 250 °Cwere found to result in the annihilation of radiation-induced defects, as evidenced by DLTS measurements. From the detailed analysis of the radiation-induced defect concentrations, the dominant annealing process is characterized by an activation energy in the range of 1.77 eV to 1.92 eV. The physical origin of radiation-induced defects, and of defects involved in their annihilation process, is discussed in the perspective of recent theoretical calculations of native defect diffusion mechanisms in GaN.

G. A. Umana-Membreno, J.M. Dell, G. Parish, B. D. Nener and L. Faraone are with the School of Electrical, Electronic and Computer Engineering, Crawley WA 6009 Australia

U.K Mishra is with the Department of Electrical and Computer Engineering, University of California, Santa Barbara, CA 93106

I. INTRODUCTION

Gallium nitride and related wide bandgap semiconductor alloys are of increasing importance for the fabrication of short-wavelength light emitters and detectors. The low thermal carrier generation rates and high breakdown fields, which are both a consequence of the wide energy gap of GaN, render the material an attractive candidate for the fabrication of microelectronic devices capable of reliable operation at high power/voltage levels, at high temperatures, and in high-energy radiation environments [1, 2]. For applications in high-energy radiation environments, such as those prevailing in aerospace, medicine, military and nuclear applications, the study of high-energy irradiation effects on device performance is essential in order to assess the long-term device reliability and in the development radiation-tolerant circuits and systems.

Exposure of GaN semiconducting films to energetic particle irradiation invariably results in the introduction of vacancy and interstitial point-defects by displacement of N and Ga species from their respective sublattices. However, the isolated character of these defects may be compromised by defect migration and interactions with native defects at temperatures near or above 300 K. The evolution from isolated point defects, as introduced by irradiation at cryogenic temperatures, to more complex defect structures has been clearly evidenced by electron paramagnetic resonance studies of electron-irradiated GaN films [2–5]. Furthermore, these studies have also allowed unambiguous identification of Ga interstitials (Ga_I), have established that this type of defect is mobile slightly below room temperature, and have produced evidence that the migration of Ga_I can be electronically stimulated at cryogenic temperatures [2, 5, 6]. For the case of isolated Ga vacancies (V_{Ga}) in n-GaN, as well as complexes associated with the N vacancy (V_N) in p-type GaN, these have been detected by positron annihilation spectroscopy and have been shown to become mobile at 200–350 and 500-800 °C, respectively [7, 8].

Similar to other semiconductor materials, the introduction of radiation-induced defects in GaN films invariably results in the creation of levels in the forbidden energy gap that may act simultaneously as scattering centers as well as donors, acceptors, traps or recombination centers, thereby affecting the electronic and optical material properties and device performance [9–16]. At sufficiently high concentrations, radiation-induced defects have been shown to result in mobility degradation and induce changes in free carrier concentration which vary with material doping level, a possible indication that irradiation-induced point defects interact with impurities and other native defects [17–19]. From the observed changes in the magnetotransport properties of electron-irradiated n-GaN films, Look and co-workers identified V_N as a radiation-induced shallow donor with a thermal activation energy of 0.07 eV, and observed that thermal annealing at 200–400 °C induced a complete recovery of the radiation-induced mobility degradation which was attributed to recombination of radiation-induced V_N and N interstitial (N_I) pairs [17]. Emtsev *et al.* observed a more complex post-irradiation thermal annealing behavior in both doped and undoped n-GaN layers, which was interpreted as an indication that the process of defect annihilation occurs via interactions with native defects and/or impurities and the consequent formation of complex defect aggregates [18]. This view appears to be supported by the complex emission characteristics of radiation-induced defects in n-GaN as detected by deep-level transient spectroscopy (DLTS) techniques [15, 20–23].

It is important to note that the relatively high irradiation doses employed in most published studies, which has

been found to be necessary in order to induce sufficiently high defect concentrations, are indicative of the low defect production rates and the high energy thresholds for displacement damage in GaN. Such studies confirm the potential of GaN-related materials and devices for circuit and system applications requiring radiation-hardness. However, even though low material susceptibility to radiation damage is fundamental for radiation-hard devices, the radiation tolerance of electronic devices and circuits can be limited by radiation-induced effects associated with electrical contacts, surfaces and interfaces, and the presence of extended defects such as dislocations and grain boundaries [24]. For the case of GaN, there are still relatively few published reports on the effects of post-irradiation annealing on metal-GaN rectifying Schottky contacts, which constitute a critical element of metal-semiconductor field effect transistors and heterostructure-based high electron-mobility field effect transistors, even though most DLTS studies of radiation-induced defects in n-GaN have been realized using Schottky barrier diodes. Perhaps one of the earliest indications of radiation-induced degradation of Schottky contacts on GaN can be found in the reports of Fang *et al.* and Polenta *et al.*, where it was noted that device degradation induced by exposure to 1 MeV electrons was annealed by prolonged storage at room temperature, which resulted in a recovery of device characteristics and reduction in the concentration of radiation-induced defects [21, 25]. Irradiation with various energetic particles has been noted to produce similar defects to electron-irradiation in n-GaN, and their annealing behaviour has been found to coincide with a recovery in forward bias current-voltage (I–V) device characteritics [26]. More recently, we have reported on the ^{60}Co gamma-irradiation induced effects on the characteristics of Ni/GaN Schottky diodes. In summary, device irradiation was found to cause increases in Schottky barrier height as extracted from capacitance-voltage C–V measurements and resulted in significant degradation in reverse bias I–V characteristics. However, the barrier height extracted from forward bias I–V characteristics remained essentially approximately constant for doses up to 21 Mrad(Si). Post-irradiation storage at room temperature and subsequent thermal annealing at 50 °C was found to fully recover reverse bias I–V characteristics to pre-irradiation levels without having any significant effect on (i) the C–V characteristics, (ii) forward bias I–V characteristics, or (iii) the parameters associated with the three shallow radiation-induced defect levels detected by DLTS [15].

In this report, we present results of a study on the effect of isochronal thermal annealing on ^{60}Co gamma-irradiated Ni/n-GaN Schottky barrier diodes. The effect of thermal annealing on device characteristics has been investigated using C–V and I–V measurements, while transient capacitance DLTS has been employed to monitor the evolution and/or annihilation of radiation-induced defects.

II. Experimental techniques and Analysis

Schottky-barrier diodes were fabricated on a 2-μm thick nominally undoped GaN epitaxial layer grown at the University of California at Santa Barbara by metal-organic chemical vapor deposition on sapphire. The devices were defined by alloyed Al/Cr/Au ohmic contacts and subsequently-formed coplanar Ni/Au Schottky contacts of 600 μm diameter, with a separation of 30 μm over which the GaN surface was not passivated. The devices were exposed to a maximum total dose of 21 Mrad(Si) total dose ^{60}Co gamma-rays at an average dose rate of 2 krad(Si)/min. As previously reported [15], measurements performed following the maximum total dose of 21 Mrad(Si) and after sample storage at room temperature for six days followed by thermal annealing for 15

minutes at 50 °C indicated a complete recovery of reverse *I–V* characteristics to pre-irradiation levels, whereas the post-irradiation *C–V* characteristics and DLTS parameters of the radiation-induced levels were unaffected.

A series of consecutive post-irradiation thermal anneals were performed isochronally for 30 minutes in a N_2 ambient at temperatures ranging from 80 to 350 °C. Measurements of *C–V* and *I–V* device characteristics were undertaken at room temperature under dark conditions using a HP 4280A 1 MHz *C–V* meter and a HP 4145B Semiconductor Parameter Analyzer, respectively. Since signals associated with carriers emission from the radiation-induced defects were only detectable from 60 to 150 K, DLTS measurements were limited to this temperature range and were performed isothermally by sampling the capacitance transients resulting from a 10 s voltage pulse (V_P) to zero volts from a quiescent reverse bias (V_R) of 5 V; such a long trap-priming pulse was necessary in order to enable observation of the combined emission signal resulting from the various radiation-induced levels.

III. Experimental Results and Discussion

A. C–V and I–V Characteristics

Analysis of experimental diode *C–V* characteristics was performed using the usual expression for the bias dependent depletion capacitance per unit area C of an ideal Schottky barrier diode:

$$C^{-2} = \frac{2}{q\epsilon_s N}(V_{d0} - V) \quad (1)$$

$$V_{d0} = \phi_B^{cv} - (k_B T/q)\ln(N_c/N) - k_B T/q \quad (2)$$

where V and T are the applied bias and device temperature, q is the electronic charge, k_B is Boltzmann's constant, ϵ_s is the permittivity of GaN ($9.5\epsilon_0$), V_{d0} is the zero-bias diffusion potential, ϕ_B^{cv} is the flat-band Schottky barrier height, N_c is the effective density of states in the conduction band (for of GaN N_c=2.6×10^{18} cm^{-3} at 300 K) and N is the free electron concentration. For a uniform carrier concentration, C^{-2} is a linear function of V with a gradient of $-2/(q\epsilon_s N)$ and an intercept with the V-axis of $V_{d0} - k_B T/q$, wherefrom ϕ_B^{cv} can be extracted with the aid of (2).

As indicated by the data plotted in Fig.1, the dominant effect of thermal annealing of the post-irradiation *C–V* characteristics is an increase in the gradient of C^{-2}–V for annealing temperatures above 250 °C, which translates to a decrease of 7±3% in carrier concentration after a 350 °C anneal (see inset in Fig.1). As shown in Fig. 2, a marginal decrease in the *C–V* Schottky barrier height (ϕ_B^{cv}) is also observed after annealing in this temperature range, however this may not be of significance since it falls within the error bounds of the extracted parameter ϕ_B^{cv}. Thus, ϕ_B^{cv} should be considered as remaining approximately unchanged from its post-irradiation value of 1.30±0.03 eV for all annealing temperatures. This is also evident from the nearly-constant Voltage-axis intercept of C^{-2} shown in Fig. 1.

The effective zero-bias Schottky barrier height , ϕ_{B0}^{iv}, and diode ideality factor, n, were extracted from forward bias *I–V* measurements using the conventional thermionic-emission model [27]:

$$I = AJ_s \exp\left(\frac{qV}{nk_B T}\right)\left[1 - \exp\left(-\frac{qV}{k_B T}\right)\right] \quad (3)$$

$$J_s = A^{**}T^2 \exp\left(-\frac{\phi_{B0}^{iv}}{k_B T}\right) \quad (4)$$

where A is the device active area, J_s is the saturation current density and A^{**} is the effective Richardson constant. The effect of series resistance, R_s, can be incorporated in (3) by replacing V with $V - IR_s$. The curve-fitting was performed numerically, and ϕ_{B0}^{iv} was obtained assuming $A^{**} = 26.4$ cm^{-2}K^{-2}.

From the forward post-irradiation *I–V* characteristics, consecutive isochronal anneals up to about 250 °C were found to induce a marginal increase in effective Schottky barrier height ϕ_{B0}^{iv} from 1.13±0.01, after 21 Mrad(Si) accumulated gamma-ray dose, to 1.16±0.02 eV after consecutive annealing at 250°C. Over the same annealing temperature range n and R_s were noted to remain approximately constant at 1.14±0.01 and 49±2 Ω,respectively. As evident from the *I–V* curves in Fig.3, further thermal annealing at temperatures ≥250 °C treatment induced significant degradation in the forward *I–V* characteristics. This degradation is evident as increase in current levels at low values of forward bias and is characterized by ϕ_{B0}^{iv} decreasing from 1.16±0.02 eV to 0.97±0.02 eV after consecutive anneals from 250 °C to 350 °C, with n increasing from 1.14±0.01 to 1.50±0.02 (see inset in Fig.3) and R_s increasing marginally from 49±2 Ω to 52±2 Ω over the same annealing temperature range. In contrast to the above behavior, the reverse *I–V* characteristics were found to be virtually unaffected by thermal anneals up to 160 °C as shown in Fig. 4. Subsequent higher temperature annealing resulted in significant reverse leakage degradation which was more severe at higher reverse biases. However, this degradation appears to level off with increasing annealing temperature, and even recover slightly for reverse bias voltages < -3 V at annealing temperatures above 250 °C.

Of particular note is that the degradation in the measured *I–V* characteristics that occurs for annealing temperatures above 250 °C coincides with the temperature range over which *C–V* measurements indicate a decreasing carrier concentration and no significant change in barrier height. The observed decrease in carrier concentration of approximately 7% is unlikely to have significant influence on the forward *I–V* characteristics, since in the present samples R_s is dominated by contact resistance rather than by the sheet resistance of the GaN epitaxial layer. On the other hand, the differences between the extracted ϕ_{B0}^{iv} and ϕ_B^{cv} combined with the large values of ideality factor for annealing above 250 °C cannot be solely attributed to image-force barrier lowering since the maximum corrections to ϕ_{B0}^{iv} and n are estimated to be $\Delta\phi_B < 0.06$ and $\Delta n < 0.02$. While such discrepancies are not surprising in view of the non-idealities reported in most studies of metal/n-GaN Schottky barrier diodes [28–31], in the present study the difference in *I–V* and *C–V* extracted barrier heights is primarily due to radiation-induced changes. For example, and as shown in Fig.2, ϕ_B^{cv} was found to increase from 1.14±0.02 to 1.30±0.01 eV after a cumulative gamma-ray dose of 21 Mrad(Si), whereas ϕ_{B0}^{iv} remained essentially constant with irradiation exposure [15].

In previous studies, the non-ideal electrical characteristics of as-fabricated GaN Schottky diodes and, in particular, the scatter in the reported barrier height of Ni/GaN contacts, have been are proposed to be attributable to surface-states and interfacial defects, dislocation-related current paths, interfacial layers induced by metal/GaN reactions or surface preparation, and material non-uniformity and quality [28, 32–40]. While a combination of the above is also likely to have an effect on the present samples, effects associated with dislocations and interfacial defect states are of particular relevance to this study because irradiation and/or post-irradiation annealing are likely to have a significant influence on device characteristics.

Electrically-active dislocations are known to affect the characteristics of Schottky barrier diodes mainly by

acting as efficient current leakage paths across the depletion layer and metal-GaN interface [35–37, 41, 42]. There is evidence for previous studies suggesting that the electrical activity at dislocation is correlated to defects and impurities trapped in their stress field [43, 44], and that the Schottky barrier height in localized regions near or at the surface termination of dislocations is lower than in dislocation-free areas [35]. It has also been reported that while the surface termination of active dislocations tends to be dimensionally small with diameters of $47 - -105$ nm, their electrically active cross-sectional area can be much larger with current conduction characteristics that vary with biasing conditions [35, 36]. Since carrier transport across the metal-semiconductor interface will occur preferentially through localized low-barrier-height regions, the overall *I–V* characteristics manifest a ϕ_{B0}^{iv} which underestimates the true barrier height of the dislocation-free area and exhibits an ideality factor greater than expected from thermionic-emission and image-force barrier-lowering [45, 46]. For devices in which interface potential fluctuations are small relative to the depletion depth probed during *C–V* measurements (that is, screened out at the edge of the depletion region), the extracted ϕ_B^{cv} represents an average barrier height over the entire diode area which may differ significantly from ϕ_{B0}^{iv} [45, 46].

In order to further investigate this issue, the measured *I–V* characteristics have been analyzed assuming that dislocations act as localized non-interacting Schottky barrier diodes in parallel with the ideal dislocation-free Ni/n-GaN interface. Thus, the total current can be expressed as an extension of equation (3):

$$I_{total} = \left\{ \hat{A}_{ideal}\, J_{s,ideal} \exp\left(\frac{qV}{k_B T}\right) + \hat{A}_{disl}\, J_{s,disl} \exp\left(\frac{qV}{n_{disl} k_B T}\right) \right\} \times \left[1 - \exp\left(\frac{qV}{k_B T}\right)\right] \qquad (5)$$

where $\hat{A}$ and J represent the effective electrically-active surface area and saturation current density of dislocation-free regions and dislocation-related, respectively denoted by the subscripts *ideal* and *disl*. The saturation densities are simply defined by expressions of the form of equation (4), with zero-bias barrier heights of $\phi_{B0,ideal}^{iv}$ and $\phi_{B0,disl}^{iv}$. In equation (5), carrier transport at the metal-GaN interface of the dislocation-free regions has been assumed to be dominated by thermionic-emission ($n_{ideal} \approx 1$), whereas in dislocation-affected regions the ideality factor has been taken to be $n_{disl} > 1$. It is noted that the form of equation (5) is consistent with *I–V* models for inhomogeneous Schottky barrier diodes proposed by R. T. Tung [47]. Additionally, and although not explicitly indicated in equation (5), the current flow is assumed to be limited by series resistance in both regions: (i) a spreading-resistance-related $R_{s,disl}$ at regions associated with dislocations and, (ii) a contact-related series resistance $R_{s,ideal}$ in the dislocation-free regions. As shown in Fig.5, this simple model provides an excellent fit to the experimental forward *I–V* characteristics and, while the analysis yields only the current components associated with dislocation-related and ideal regions, an estimate of the barrier heights can be obtained by using published values of dislocation density and surface-termination areas undoped n-GaN films [35, 37, 41, 42]. Alternatively, an estimate of the aggregate effective area of ideal and dislocation-affected regions can be obtained by correlating the barrier heights to ϕ_B^{cv} which must effectively be the average of $\phi_{B0,ideal}^{iv}$ and $\phi_{B0,disl}^{iv}$ [46, 48]. Formally, the equilibrium average barrier height must be obtained from the solution of Poisson's equation in cylindrical coordinates [47], thus detailed knowledge of the carrier accumulation/depletion and of the fixed charge state and distribution of defects in the vicinity of threading dislocations would be required. An alternative approach is to estimate the average barrier height from the average fixed charge in the depletion region as an extension of the one-dimensional solution of Poisson's equation. Thus, and in the spirit

of the depletion approximation, charge density per unit volume in the space-charge layer of a homogeneous metal/n-GaN Schottky barrier diode at zero-bias is given by [27]:

$$Q_{sc} = A(2q\epsilon_s N_d V_{d0})^{1/2}$$

with N denoting the uniform ionized donor density and V_{d0} being define by equation (2). The average space-charge density $\langle Q_{sc}\rangle$ in a diode with two distinct n-type regions, formed by the aggregate ideal and dislocation-related regions, can be expressed as:

$$\begin{aligned}\langle Q_{sc}\rangle =& A_{disl}(2q\epsilon_s N_{d,disl}V_{d0,disl})^{1/2} + A_{ideal}(2q\epsilon_s N_{d,ideal}V_{d0,ideal})^{1/2} \\ =& A(2q\epsilon_s\langle N_d\rangle\langle V_{d0}\rangle)^{1/2}\end{aligned} \tag{6}$$

where brackets denote a statistical average over the entire device area A, and A_{disl} and A_{ideal} are geometrical areas ($A = A_{disl} + A_{ideal}$). It can be shown that from equation (6) the average barrier height $\langle\phi^{iv}_{B0}\rangle$ in terms of the barrier heights of the dislocation-free and dislocation-related regions can be expressed as:

$$\begin{aligned}\langle\phi^{iv}_{B0}\rangle =& \left(\frac{\hat{A}_{ideal}}{A}\right)^2\phi^{iv}_{B0,ideal} + \left(\frac{\hat{A}_{disl}}{A}\right)^2\phi^{iv}_{B0,disl} \\ &+ 2\frac{\hat{A}_{ideal}\hat{A}_{disl}}{A^2}\left\{(V_{n,ideal}V_{n,disl})^{1/2} + \left(\phi^{iv}_{B0,ideal} - V_{n,ideal}\right)^{1/2}\left(\phi^{iv}_{B0,ideal} - V_{n,disl}\right)^{1/2}\right\}\end{aligned} \tag{7}$$

with

$$\langle V_n\rangle = \xi_n + \frac{k_BT}{q} = \frac{k_BT}{q}\left\{\ln\left(\frac{N_C}{\langle N_d\rangle}\right) + 1\right\}$$

$$V_{n,(ideal|disl)} = \xi_{n,(ideal|disl)} + \frac{k_BT}{q} = \frac{k_BT}{q}\left\{1 + \ln\left(\frac{N_C}{N_{d,(ideal|disl)}}\right)\right\}$$

$$\hat{A}_{(ideal|disl)} = A_{(ideal|disl)}\sqrt{\frac{N_{d,(ideal|disl)}}{\langle N_d\rangle}} \tag{8}$$

$$A\sqrt{\langle V_n\rangle} = \hat{A}_{ideal}\sqrt{V_{n,ideal}} + \hat{A}_{disl}\sqrt{V_{n,disl}} \tag{9}$$

where ξ_n and $\xi_{n,(ideal|disl)}$ are the global and local energy difference between the Fermi level and the bottom of the conduction band. Equations (8) and (9) correlate the effective area of the dislocation-related and ideal interfacial surface regions to their respective geometrical surface areas and to the local fixed-charge density $N_{d,(ideal|disl)}$ and $\xi_{n,(ideal|disl)}$ at the edge of the depletion layer. Devices fabricated on high-quality hetero-epitaxial films, $\xi_{n,ideal} \rightarrow \xi_n$ under equilibrium conditions in the dislocation-free neutral region. For regions in the vicinity of a threading dislocations three limiting cases are considered: (i) carrier depletion $\xi_{n,disl} \rightarrow \phi^{iv}_{B0,disl}$, (ii) carrier accumulation $\xi_{n,disl} \rightarrow 0$, and (iii) $\xi_{n,disl} \rightarrow \xi_{n,ideal}$ and the effect of dislocations is effectively screened at the edge of the zero-bias depletion region. It should be noted that the effects of dislocations, as considered in the above three limiting cases, depend on their detailed nature and charge-state and on the presence of shallow donor defects such as V_N and O_N and/or acceptor states, such as V_{Ga} and V_{Ga}-O_N [43, 49, 50]. Using the above models, the barrier heights were obtained from the analysis of the various device characteristics. While for $\xi_{n,disl} \rightarrow 0$ and $\xi_{n,disl} \rightarrow \phi^{iv}_{B0,disl}$ the extracted values average barrier height $\langle\phi^{iv}_{B0}\rangle$ consistent with ϕ^{cv}_B were obtained, the best fit to ϕ^{cv}_B was obtained for $\xi_{n,disl} \rightarrow \xi_{n,ideal}$, as shown in Fig. 2. To obtain $\langle\phi^{iv}_{B0}\rangle$ from *I–V* characteristics consistent with those obtained from measured *C–V*

characteristics, as shown in Fig.2, the only fitting parameter employed has been the aggregated electrically-active surface area of the ideal and dislocation-related regions as the saturation currents for the two regions were extracted independently. For the case of $\xi_{n,disl} \rightarrow \phi^{iv}_{B0,disl}$, $\phi^{iv}_{B0,disl} \approx 0.74$ eV and $\phi^{iv}_{B0,ideal} \approx 1.4$ from the pre-irradiated characteristics requiring a ratio of dislocation-affected area to total Schottky diode area A_{disl}/A of 0.06 ± 0.005; that is, for a dislocation with a circular surface area with radius 50 nm the areal dislocation density must be 7.6 ± 8 cm^{-2}. For $\xi_{n,disl} \rightarrow 0$, a relatively good fit could be only be obtained for $\xi_n \rightarrow \xi_{n,disl}$ and $A_{disl}/A < 3\times10^{-4}$, even for a single 100 nm diameter dislocation with a $\phi^{iv}_{B0,disl} \approx 0.7$ for $\phi^{iv}_{B0,ideal} \approx 1.32$. For the case of $\xi_{n,disl} \rightarrow \xi_{n,ideal}$, the required A_{disl}/A is 0.39 ± 0.01 corresponding to a 100 nm diameter dislocation density of 5 ± 9 cm^{-2}. Although no assessment of dislocation density in the GaN epilayer was undertaken, the above estimates of dislocation areal density and electrically-active surface area in consistent with reported dislocation-related reverse-bias leakage spots with radii of 40–150 nm and areal densities of 10^8–10^9 [35, 37, 41, 42]. Since it is possible to obtain a good fit to the various characteristics using different assumptions, it is likely that the regions characterized by a low-barrier-height are the aggregated effect of different types of dislocations (edge threading dislocations are likely to be charged but depleted of carriers and screw-type dislocations have been correlated to localized reverse-bias leakage spots [35, 37, 41–43, 49, 50]). In the preceding analysis the total area of dislocation-dominated regions refer to the area in immediate vicinity of the metal-GaN interface and do not imply that dislocations exhibit a similar degree of electrical activity or influence deeper into underlying epitaxial film. Nonetheless, it is important to note that the parameters obtained in the preceding analysis provide a clear indication that the degradation in device most significant observation that can be arising from the preceding analysis is that the observed degradation in device *I–V* characteristics is dominated by dislocation related effects. It is interesting to note that the value of extracted barrier height for the dislocation-free area ranges from 1.32–1.45 eV is in excellent agrement with the experimental value of 1.4 ± 0.1 eV for Ni/n-GaN obtained X-ray and synchrotron photoemission spectroscopies [33, 51]. While it can be argued that the models proposed by R. T. Tung are perhaps more appropriate for the interfacial inhomogeneities herein considered [46], the simple models herein employed include effects related to charge accumulation and/or depletion along the dislocation-axis which are absent in other models. Nevertheless, and for the sake of completeness, analysis of the device characteristics using R. T. Tung's models were also undertaken. However, neither of these models were able to yield fits as good as those obtained for the various $\xi_{n,disl}$ herein considered. It is noted that while the same value for A^{**} has been used for both dislocation-related and dislocation-related regions, its effect on the barrier height of the dislocation-related regions is negligible ($\phi^{iv}_{B0,disl}$ decreasing by 0.06 eV per order of magnitude reduction in A^{**}).

While the agreement between $\langle\phi^{iv}_{B0}\rangle$ and ϕ^{cv}_{B} shown in Fig.2 is remarkable given that a unique value of dislocation-related active area has been employed throughout, the increase of 0.08 eV in ϕ^{cv}_{B} after 1 Mrad(Si) irradiation exposure cannot be associated with dislocation-related effects and is likely to be due to either radiation-induced re-ordering at the metal-GaN interface or to introduction of a thin layer of acceptor-like interfacial defects. Firstly, deposition of Ni on GaN has been reported to introduce V_N-related defects at the metal-GaN interface [33], which are likely to appear as a thin-interfacial n-layer since these defects are donor-like V_N [17]. The modification of the potential thus induced results in a reduction of the reverse bias depletion

capacitance and in an extracted value of barrier height from C^{-2}–V characteristics which underestimates the true ϕ_B^{cv}. In this case, irradiation could induce re-incorporation of N desorbed during metal deposition or from nearby N_I produced by irradiation [33]. This argument is supported by the observation of improved GaAs and GaN diode characteristics after relatively low irradiation doses [11, 52], and by the observation improvement in I–V characteristics up to 160 °C — a temperature range over which N_I is expected to be sufficiently mobile [53]. On the other hand, since it is also likely that the doses employed could induce interfacial defect-states via displacement of N and Ga species from their sublattice sites. A net accumulation of acceptor-like defects, such as N_I and V_{Ga} and possibly in N antisites (N_{Ga}), at the interface would induce the appearance of a negatively charged region in the vicinity of the Ni/GaN interface resulting in an apparent increase in Schottky barrier height with irradiation dose. Of these two mechanisms, the case of radiation-induced reordering is perhaps the most likely since it takes into account N-vacancies introduced during Ni deposition [33] and it does not require a significant concentration of N_I and/or V_{Ga} at the metal-GaN interface. It should be noted that during thermal annealing N_I and V_{Ga} will have finite probability of migration and will tend to move into the bulk due to the electric field gradient in the space charge region [54].

Recent calculations of defect migration barriers indicate that both N_I and V_{Ga} are mobile at the annealing temperatures here employed, as indicated by the activation energies of the defect migration processes involved in the annihilation of the radiation induced defects as obtained from DLTS measurements and presented in the following section [53]. Migration of isolated N_I and V_{Ga} towards the bulk would result a reduction of carrier concentration. Furthermore, mobile isolated Ga vacancies can become trapped by oxygen substitutional on N sites (O_N), which is most likely donor in the undoped epitaxial GaN, and results in the formation of V_{Ga}–O_N acceptor defect complexes [7]. The latter are known to be immobile in the annealing temperature range herein employed. Thermal annealing would then result in an increase in background acceptor concentration and a net reduction in free carrier concentration which is consistent with our observations. Given that V_{Ga}–O_N are double acceptors, a decrease of $2.4\pm1.0\times10^{15}$ cm^{-3} requires approximately $7.7\pm3.0\times10^{14}$ cm^{-3} V_{Ga}–O_N centers and the introduction of an equivalent concentration of isolated V_{Ga} defects during irradiation. This concentration is an order of magnitude greater than that of the V_N-related defects detected by DLTS. It is important to note that V_N defect introduction rates are expected to be higher that those of V_{Ga} for Compton electrons with a mean energy of ~0.7 MeV [17]. The relatively low defect production rates observed for V_N-related defects may be a consequence of spontaneous recombination of N_I–V_N pairs during irradiation resulting from the relatively high energy barriers for defect migration of V_N and N_I [53]. In contrast, radiation-induced Ga_I–V_{Ga} pairs are likely to be separated during irradiation due to the relatively high mobility of Ga_I at room temperature and its susceptibility to electronically enhanced migration [2, 5, 6, 53]. Given that the reduction in carrier concentration with annealing temperature is likely to be due to a significant concentration of radiation-induced V_{Ga}-related acceptors, a significant concentration of is consequently produced during irradiation. On the other hand, and taking into account that Ga_I is the only radiation-induced lattice point defect known to be mobile at room temperature [2, 5, 6, 53], it is likely that Ga_I plays a dominant role in the post-irradiation recovery of reverse I–V characteristics observed after prolonged storage at room temperature and after annealing temperatures up to 160 °C. Further, the dislocation-related decrease in barrier height observed in the I–V characteristics, evidenced

in Fig. 2, is likely to be attributable to the interaction of Ga_I segregated from the bulk with Ni at the interface between metal and dislocation surface terminations [33].

****

NOTE: - Possible alternative explanation: Hydrogen

H is an amphoteric defect which has a relatively low migration barrier (0.9-1.4 eV) when in the (+) state but its formation is favorable under p-type growth conditions. Under the thermodynamic equilibrium conditions of n-type growth, the (+) state has a high formation energy and the (-) charge state is favored... but H^- has a high barrier for migration (2-2.2 eV). Note that what this essentially means is that the charge state and defect mobility depends on Fermi level position. Since as-grown n-GaN has a high concentration of relatively immobile H^-, the change in Fermi level induced during irradiation can induce a change in the (-) state to (-) by emission of two electrons (only during irradiation) these then can efficiently passivate acceptor defects: isolated $V_{Ga}{}^{-3}$ and $(V_N\text{-}O_N)^{-2}$ and isolated $N_I{}^-$. Particularly because high concentrations of H are likely in as grown GaN, it is likely that H plays a significant role in the reduction in carrier concentration, BUT BUT BUT the dissociation energies of these defects are not known and it is thus difficult to justify the carrier reduction and defect annihilation process on the grounds of H-related effects. Particularly in the context of recently published theoretical calculations which indicate defect migration barriers for N_I and V_{Ga} in the 1.4–2.0 eV range. (the binding energies of H-defect complexes would have to be in this range to justify such this alternative view)...

End of note

****

B. Deep-level Transient Spectroscopy

To further investigate the characteristics of the radiation induced defects, the sample exposed to 21 Mrad(Si) cumulative gamma-ray dose was isochronally annealed for 30 min at temperatures ranging from 80 to 350 °C. The evolution of the defect characteristics was monitored by DLTS measurements over the 60 to 150 K temperature range. The results, presented in Figs. 7 and 6, indicate that these defects are stable at temperatures below 100 °C and confirm that the broad emission initially labeled as G_A is indeed formed by the convolution of the G_2 and G_3 defects.

For the extraction of the activation energy of the defect annihilation process we have assumed that the carrier emission activation energies and capture cross-sections of the three radiation-induced defects did not shift with annealing temperature. The isochronal thermal annealing characteristics were fitted using a first order of reaction model:

$$N_T(T_{i+1}) = N_T(T_i) \times \exp\left\{-\nu\,\Delta t\,\exp\left(-\frac{qE_{TA}}{k_B T_i}\right)\right\} \tag{10}$$

where $N_T(T)$ is the fraction of annealed defects after annealing at a temperature T_i, with i indicates the isochronal step, Δt is the annealing time, ν is a frequency factor ($\nu = 10^{13}$ s^{-1}, commonly assumed), and E_{TA} is the activation energy of the process that leads to defect annihilation [53, 55].

The annealing characteristics of the three defects followed a similar trend, as evidenced in Figs. 6 and 7, manifesting typically sharp defect annihilation transitions between 250 and 350 °C with the annihilation temperature of G_3 slightly higher than that of G_1 and G_2. A relatively slow stepwise decrease in defect concentration below 250 °C affects the annealing curve of the three defects.

To obtain an adequate fit to the experimental characteristics, three different defect recombination processes were necessary for each irradiation induced level. Interestingly, the activation energies obtained by independently fitting the defect annealing characteristics below 250 °C are nearly identical and are likely to arise from V_N-N_I pair recombination as these activation energies are consistent with the 1.6 eV barrier energy for migration of $N_I$as calculated by S. Limpijumnong and C.G. Van de Walle [53]. On the other hand, the activation energy of 1.77–1.92 extracted above 250 °C, is in excellent agreement

with the activation energy for migration of V_{Ga} [53]. Aside from defect complexing induced by interaction with native O_N donors, V_{Ga} migration may result in annihilation of V_N by formation of V_{Ga}–V_N di-vacancies, double acceptor defects, resulting also in a decrease of carrier concentration [5, 7].

IV. Conclusions

Hmmm... too many... I may have to break this paper into two.

V. Acknowledgements

The authors wish to acknowledge the support of this project by the Australian Research Council (ARC) and the AFOSR MURI on Radiation Physics (monitored by Dr. G. Witt).

References

[1] U. K. Mishra, Y.-F. Wu, B. P. Keller, S. Keller, and S. P. DenBaars, "GaN microwave electronics", *IEEE Trans. Microwave Theory Tech.*, vol. 46, no. 6, pp. 756–761, 1998.

[2] K. H. Chow, G. D. Watkins, A. Usui, and M. Mizuta, "Detection of interstitial Ga in GaN", *Phys. Rev. Lett.*, vol. 85, no. 13, pp. 2761–2764, 2000.

[3] M. Linde, S. J. Uftring, and G. D. Watkins, "Optical detection of magnetic resonance in electron-irradiated GaN", *Phys. Rev. B*, vol. 55, no. 16, pp. R10177–R10180, 1997.

[4] C. Bozdog, H. Przybylinska, G. D. Watkins, V. Härle, F. Scholz, M. Mayer, M. Kamp, R. J. Molnar, A. E. Wickenden, D. D. Koleske, and R. L. Henry, "Optical detection of electron paramagnetic resonance in electron-irradiated GaN", *Phys. Rev. B*, vol. 59, no. 19, pp. 12479–12486, May 1999.

[5] K. H. Chow, L. S. Vlasenko, P. Johannesen, C. Bozdog, G. D. Watkins, H. Sunakawa A. Usui, C. Sasaoka, and M. Mizuta, "Intrinsic defects in gan. i. ga sublattice defects observed by optical detection of electron paramagnetic resonance", *Phys. Rev. B*, vol. 69, pp. 045207, 2004.

[6] P. Johannesen, A. Zakrzewski, L. S. Vlasenko, G. D. Watkins, A Usui, H. Sunakawa, and M. Mizuta, "Intrinsic defects in GaN. II. Electronically enhanced migration of interstitial Ga observed by optical detection of electron paramagnetic resonance", *Phys. Rev. B*, vol. 69, pp. 045208, 2004.

[7] K. Saarinen, T. Suski, I. Grzegoryba, and D. C. Look, "Ga vacancies in electron irradiated GaN: introduction, stability and temperature dependence of positron trapping", *Physica B*, vol. 308–310, pp. 77–80, December 2001.

[8] S. Hautakangas, J. Oila, M. Alatalo, K. Saarinen, L. Liszkay, D. Seghier, and H.P. Gislason, "Vacancy Defects as Compensating Centers in Mg-Doped GaN", *Phys. Rev. Lett.*, vol. 90, no. 13, pp. 137402, April 2003.

[9] I. A. Buyanova, Mt. Wagner, W. M. Chen, B. Monemar, J. L. Lindström, H. Amano, and I. Akasaki, "Photoluminescence of GaN: Effect of electron irradiation", *Appl. Phys. Lett.*, vol. 73, no. 20, pp. 2968–2970, 1998.

[10] A. Ionascut-Nedelcescu, C. Carlone, A. Houdayer, H. J. von Bardeleben, J.-L. Cantin, and S. Raymond, "Radiation Hardness of Gallium Nitride", *IEEE Trans. Nucl. Sci.*, vol. 49, no. 6, pp. 2733–2738, 2002.

[11] C.-W. Wang, "Neutron-irradiation effect on radio-frequency magnetron-sputtered GaN thin films and Au/GaN Schottky diodes", *J. Vac. Sci. Technol. B*, vol. 20, no. 5, pp. 1821–1826, 2002.

[12] S. J. Cai, Y. S. Tang, R. Li, Y. Y. Wei, L. Wong, Y. L. Chen, K. L. Wang, M. Chen, Y. F. Zhao, R. D. Schrimpf, J. C. Keay, and K. F. Galloway, "Annealing behavior of a proton irradiated $Al_xGa_{1-x}N$/GaN High Electron Mobility Transistor grown by MBE", *IEEE Trans. Electron. Devices*, vol. 47, no. 2, pp. 304–7, 2000.

[13] S. M. Khanna, J. Webb, A. J. Houdayer, and C. Carlone, "2 MeV proton radiation damage studies of Gallium Nitride films through low temperature photoluminescence spectroscopy measurements", *IEEE Trans. Nucl. Sci.*, vol. 47, no. 6, pp. 2322–2328, 2000.

[14] F. Gaudreau, C. Carlone, A. Houdayer, and S. M. Khanna, "Spectral properties of proton irradiated Gallium Nitride blue diodes", *IEEE Trans. Nucl. Sci.*, vol. 48, no. 6, pp. 1778–1784, 2001.

[15] G. A. Umana-Membreno, J. M. Dell, B. D. Nener, G. Parish, L. Faraone, and U. K. Mishra, "^{60}Co gamma radiation effects on n-GaN Schottky diodes", *IEEE Trans. Electron. Devices*, vol. 50, no. 12, pp. 2326, 2003.

[16] S. A Vitusevich, N. Klein, A. E. Belyaev, S. V. Danylyuk, M. V. Petrychuk, R. V. Konakova, A. M. Kurakin, A. E. Rengevich, A. Yu. Avksentyev, B. A. Danilchenko, V. Tilak, J. Smart, A. Vertiatchikh, and L. F. Eastman, "Effects of γ-irradiation on AlGaN/GaN HEMTs", *Phys. Stat. Sol. (a)*, vol. 195, no. 1, pp. 101–105, 2003.

[17] D. C. Look, D. C. Reynolds, J. W. Hemsky, J. L. Sizelove, R. L. Jones, and R. J. Molnar, "Defect donor and acceptor in GaN", *Phys. Rev. Lett.*, vol. 79, no. 12, pp. 2273–2276, 1997.

[18] V. V. Emtsev, V. Y. Davydov, V. V. Kozlovskii, V. V. Lundin, D. S. Poloskin, A. N. Smirnov, N. M. Schmidt, A. S. Usikov, J. Aderhold, H. Klausing, D. Mistele, T. Rotter, J. Stemmer, O. Semchinova, and J. Graul, "Point defects in γ-irradiated n-GaN", *Semicond. Sci. Technol.*, vol. 15, no. 1, pp. 73–78, 2000.

[19] D. C. Look, G. C. Farlow, P. J. Drevinsky, D. F. Bliss, and J. L. Sizelove, "On the nitrogen vacancy in GaN", *Appl. Phys. Lett.*, vol. 83, no. 17, pp. 3525–3527, 2003.

[20] Z-Q. Fang, L. Polenta, J. W. Hemsky, and D. C. Look, "Deep centers in as-grown and electron-irradiated n-GaN", in *SIMC-IX Proceedings*, 2000, pp. 35–42.

[21] L. Polenta, Z-Q. Fang, and D. C. Look, "On the main irradiation-induced defect in GaN", *Appl. Phys. Lett.*, vol. 76, no. 15, pp. 2086–2088, 2000.

[22] S. A. Goodman, F. D. Auret, M. J. Legodi, G. Myburg, B. Beaumont, and P. Gibart, "Electron irradiation induced defects in n-GaN", in *SIMC-IX Proceedings*, 2000, pp. 43–46.

[23] G. A. Umana-Membreno, J. M. Dell, T. P. Hessler, B. D. Nener, G. Parish, L. Faraone, and U. K. Mishra, "^{60}Co gamma-irradiation-induced defects in n-GaN", *Appl. Phys. Lett.*, vol. 80, no. 23, pp. 4354–6, 2002.

[24] T. P. Ma and P. V. Dressendorfer, Eds., *Radiation Hardening Technology*, chapter 6, pp. 333–400, John Wiley & Sons, 1989.

[25] Z-Q. Fang, J. W. Hemsky, D. C. Look, and M. P. Mack, "Electron-irradiation-induced deep level in GaN", *Appl. Phys. Lett.*, vol. 72, no. 4, pp. 448–449, 1998.

[26] S.A. Goodman, F.D. Auret, F.K. Koschnick, J.-M. Spaeth, B. Beaumont, and P. Gibart, "Radiation induced defects in MOVPE grown n-GaN", *Material Sci. Eng. B*, vol. 71, pp. 100–103, 2000.

[27] E. H. Rhoderick and R. H. Williams, *Metal-Semiconductor Contacts*, chapter 4, Clarendon Press, 1988.

[28] L. S. Yu, Q. Z. Liu, Q. J. Qiao, S. S. Lau, and J. Redwing, "The role of the tunneling component in the current-voltage characrteristics of metal-GaN Schottky diodes", *J. Appl. Phys.*, vol. 84, no. 4, pp. 2099–2104, 1998.

[29] J. C. Carrano, T. Li, P. A. Grudowski, C. J. Eiting, R. D. Dupuis, and J. C. Campbell, "Comprehensive characterization of metal-semiconductor-metal ultraviolet photodetectors fabricated on single-crystal GaN", *J. Appl. Phys.*, vol. 83, no. 11, pp. 6148–6160, 1998.

[30] T. Sawada, Y. Ito, K. Imai, K. Suzuki, H. Tomozawa, and S. Sakai, "Electrical properties of metal/GaN and SiO_2/GaN interfaces and effects of thermal annealing", *Appl. Surf. Sci.*, vol. 159/160, pp. 449–455, 2000.

[31] H. Hasegawa and S. Oyama, "Mechanism of anomalous current transport in n-type GaN Schottky contacts", *J. Vac. Sci. Technol. B*, vol. 20, no. 4, pp. 1647–1655, 2000.

[32] V. M. Bermudez, R. Kaplan, M. A. Khan, and J. N. Kuznia, "Growth of thin Ni films on GaN(0001)-(1×1)", *Phys. Rev. B*, vol. 48, no. 4, pp. 2436–2444, 1993.

[33] M. H. Kim, S. N. Lee, C. Huh, S. Y. Park, J. Y. Han, J. M. Seo, and S. J. Park, "Interfacial reaction and Fermi level movement induced by sequentially deposited metal on GaN: Au/Ni/GaN", *Phys. Rev. B*, vol. 61, no. 16, pp. 10966–10971, 2000.

[34] A. Barinov, L. Gregoriatti, B. Kaulich, M. Kiskinova, and A. Rizzi, "Defect induced lateral chemical heterogeneity at Ni/GaN interfaces and its effect on the electronic properties of the interface", *Appl. Phys. Lett.*, vol. 79, no. 17, pp. 2752–2754, 2001.

[35] E. G. Brazel, M. A. Chin, and V. Narayamurti, "Direct observation of localized high current densities in GaN films", *Appl. Phys. Lett.*, vol. 74, no. 16, pp. 2367–2369, 1999.

[36] J. W. P Hsu, M. J. Manfra, D. V. Lang, S. Richter, S. N. G. Chu, A. M. Sergent, R. N. Kleinman, L. N Pfeiffer, and R. J. Molnar, "Inhomogeneous spatial distribution of reverse leakage in GaN Schottky diodes", *Appl. Phys. Lett.*, vol. 78, no. 12, pp. 1685–1681, 2001.

[37] J. W. P Hsu, M. J. Manfra, R. J. Molnar, B. Heying, and J. S. Speck, "Direct imaging of reverse-bias leakage through pure screw dislocations in GaN films grown by molecular beam epitaxy on GaN templates", *Appl. Phys. Lett.*, vol. 81, no. 1, pp. 79–81, 2002.

[38] J. D. Guo, F. M. Pan, M. S. Feng, R. J. Guo, P. F. Chou, and C. Y. Chang, "Schottky contact and the thermal stability of Ni on n-type GaN", *J. Appl. Phys.*, vol. 80, no. 3, pp. 1624–1627, 1996.

[39] Q. Z. Liu and S. S. Lau, "Ni and Ni silicide Schottky contacts on n-GaN", *J. Appl. Phys.*, vol. 84, no. 2, pp. 881–886, 1998.

[40] K. Shiojima, J. M. Woodall, C. J. Eiting, P. A. Grudowski, and R. D. Dupuis, "Effect of defect density on the electrical characteristics of n-type GaN Schottky contacts", *J. Vac. Sci. Technol. B*, vol. 17, no. 5, pp. 2030–2033, 1999.

[41] J. Spradlin, S. Dogan, J. Xie, R. Molnar, A. A. Baski, and H. Morkoc, "Investigation of forward and reverse current conduction in GaN films", *Appl. Phys. Lett.*, vol. 84, no. 21, pp. 4150–4152, May 2004.

[42] B. S. Simpkins, E. T. Yu, P. Waltereit, and J. S. Speck, "Correlated scanning Kelvin probe and conductive atomic force microscopy studies of dislocations in gallium nitride", *Appl. Phys. Lett.*, vol. 94, no. 3, pp. 1448–1453, August 2003.

[43] R. Jones, J. Elsner, M. Haugk, R. Gutierrez, Th. Frauenheim, M.I. Heggie, S. Öberg, and P.R. Briddon, "Interaction of Oxygen with Threading Dislocations in GaN", *Phys. Stat. Sol. (a)*, vol. 171, no. 1, pp. 167–173, Jan 1999.

[44] I. Arslan and N. D. Browning, "Role of Oxygen at Screw Dislocations in GaN", *Phys. Rev. Lett.*, vol. 91, no. 16, pp. 165501, October 2003.

[45] J. H. Werner and H. H. Güntler, "Barrier inhomogeneities at Schottky contacts", *J. Appl. Phys.*, vol. 69, no. 3, pp. 1522–1533, 1991.

[46] R. T. Tung, "Recent advancements in Schottky barrier concepts", *Material Sci. Eng.*, vol. R35, pp. 1–138, 2001.

[47] R. T. Tung, "Electron transport at metal-semiconductor interfaces: General theory", *Phys. Rev. B*, vol. 45, no. 23, pp. 13509–13523, 1992.

[48] J. H. Werner, "Schottky Barrier and pn-Junction I/V Plots - Small Signal Evaluation", *Appl. Phys. A*, vol. 47, pp. 291–300, 1988.

[49] J. Elsner, R. Jones, M. I. Heggie, P. K. Sitch, M. Haugk, Th. Frauenheim, S. Öberg, and P. R. Briddon, "Deep acceptors trapped at threading-edge dislocations in GaN", *Phys. Rev. B*, vol. 58, no. 19, pp. 12571–12574, November 1998.

[50] k. Leung, A. F. Wright, and E. B. Stechel, "Charge accumulation at a threding edge dislocation", *Appl. Phys. Lett.*, vol. 74, no. 17, pp. 2495–2497, April 1999.

[51] K. A Rickert, A. B. Ellis, J. Y. Kim, J.-L. Lee, F. J. Himpsel, F. Dwikusuma, and T. F. Kuech, "X-ray photoemission determination of the Schottky barrier height of metal contacts to n-GaN and p-GaN", *J. Appl. Phys.*, vol. 92, no. 11, pp. 6671–6678, December 2002.

[52] O. Yu. Borkovskaya, N. L. Dmitruk, R. V. Konakova, V. G. Litovchenko, and O. I. Maeva, "Influence of gamma radiation on surface generation and recombination in semiconductor structures based on GaAs", *Sov. Phys. Semicond.*, vol. 20, no. 9, pp. 1028–1031, 1986.

[53] S. Limpijumnong and C. G. Van de Walle, "Diffusivity of native defects in GaN", *Phys. Rev. B*, vol. 69, pp. 035207, 2004.

[54] W. Walukiewicz, "Mechanisms of Fermi-level stabilization in semiconductors", *Phys. Rev. B*, vol. 37, no. 9, pp. 4760–4763, 1988.

[55] B. T. Kelly, *Irradiation Damage to Solids*, chapter 4, pp. 179–209, Pergamon Press, 1966.

LIST OF TABLES

LIST OF FIGURES

TABLE I

SUMMARY OF ACTIVATION ENERGIES, E_A, EXTRACTED FROM CONSECUTIVE ISOCHRONAL THERMAL ANNEALING CHARACTERISTICS OF THREE SHALLOW RADIATION-INDUCED DEFECTS. THE INDICATED RATIOS CORRESPOND TO THE RELATIVE INFLUENCE OF DIFFERENT THERMALLY ACTIVATED DEFECT ANNIHILATION MECHANISMS AFFECTING ALL DEFECTS.

Defect Label	E_{TA} (eV)	Ratio (%)	Defect Label	E_{TA} (eV)	Ratio (%)	Defect Label	E_{TA} (eV)	Ratio (%)
G_1	1.77±0.01[a]	82±4	G_2	1.80±0.01[a]	66±3	G_3	1.92±0.01[a]	70±4
	1.52±0.05	5±2		1.56±0.04	17±5		1.57±0.02	13±4
	1.35±0.10	12±3		1.35±0.04	18±4		1.36±0.02	17±4

[a]process inducing complete defect annihilation

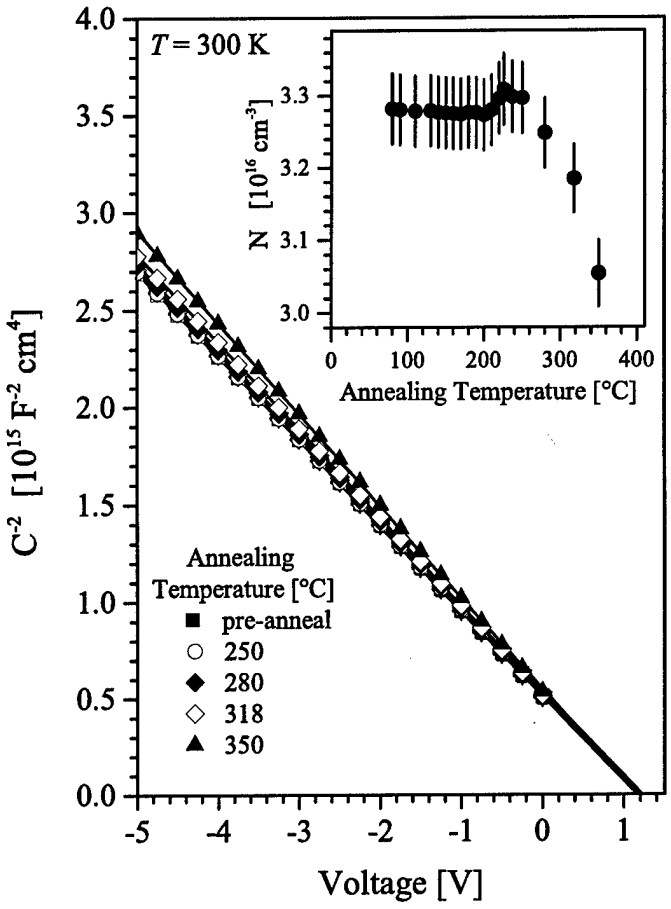

Fig. 1. Effect of isochronal thermal annealing on C^{-2}–V diode characteristics (showing only one of every 5 experimental data points); note the nearly constant intercept with the Voltage-axis and the increased gradient for annealing temperatures $\gtrsim$ 250 °C. Inset: Free electron concentration as a function of annealing temperature.

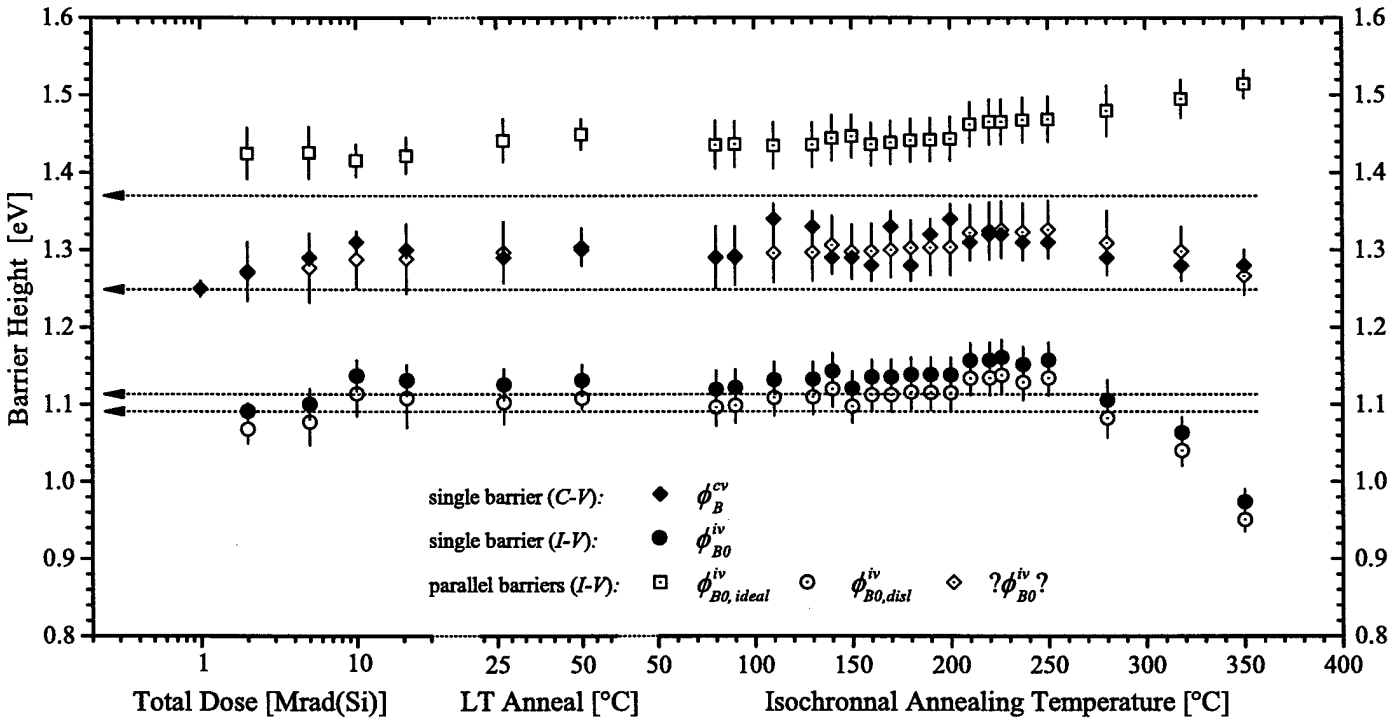

Fig. 2. Summary of extracted Schottky barrier height from *I–V* and *C–V* measurements during ^{60}Co gamma-irradiation and after post-irradiation thermal treatment. Open symbols denote parameters extracted by modeling the forward *I–V* characteristics as two Schottky barrier diodes (2SBH) in parallel in which dislocation-related current paths are assumed to be a non-interacting collection of diodes with a unique yet low barrier height. Solid symbols correspond to parameters the convectional analysis of *C–V* and *I–V* characteristics. Extracted parameters from *I–V* measurements before irradiation are indicated by dashed and ϕ_B^{cv} was 1.14 eV before irradiation. LT anneal denotes storage at 27 °C for 6 days, and thermal annealing in N_2 ambient for 15 minutes at 50 °C. The isochronal annealing time was 30 minutes and was performed in N_2 ambient

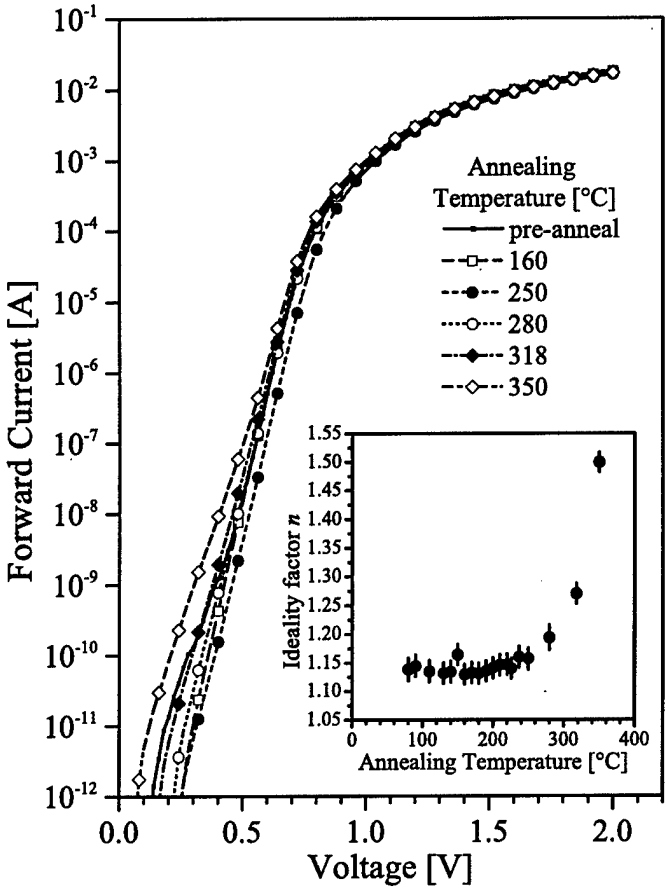

Fig. 3. Effect of isochronal thermal annealing on *I–V* characteristics. For the sake of clarity, the characteristics shown are for annealing steps from 250 °C. Note that the significant influence of annealing on current levels near 1 V. The inset shows extracted ideality factor for all annealing temperatures.

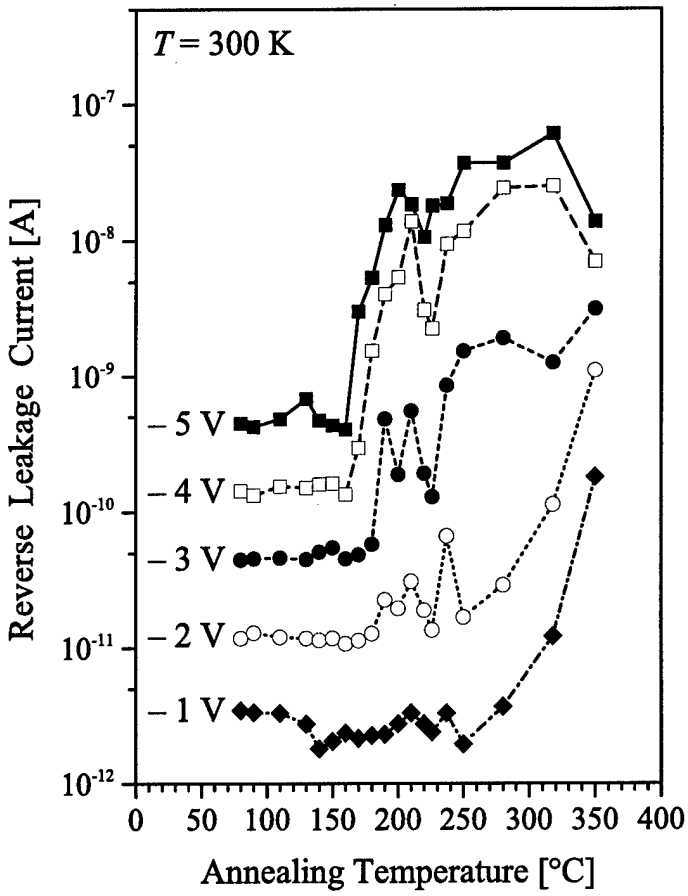

Fig. 4. Degradation of reverse *I–V* characteristics with isochronal thermal treatment for different biasing levels (bias is indicated next to each curve).

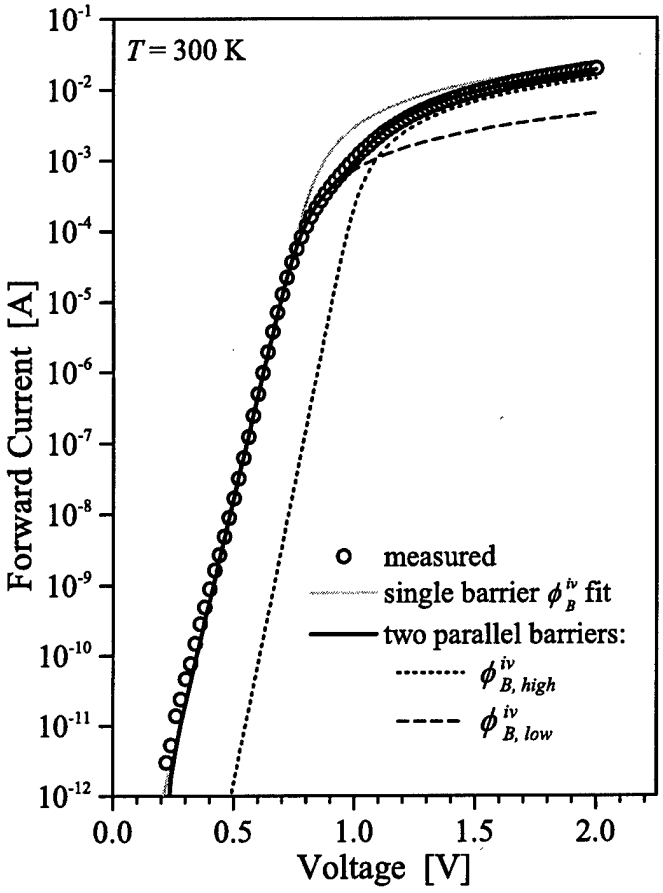

Fig. 5. Experimental and modeled forward *I–V* characteristics of an Ni/GaN diode exposed to 21 Mrad(Si) after room-temperature annealing for six day plus a 15 minutes at 50 °C.

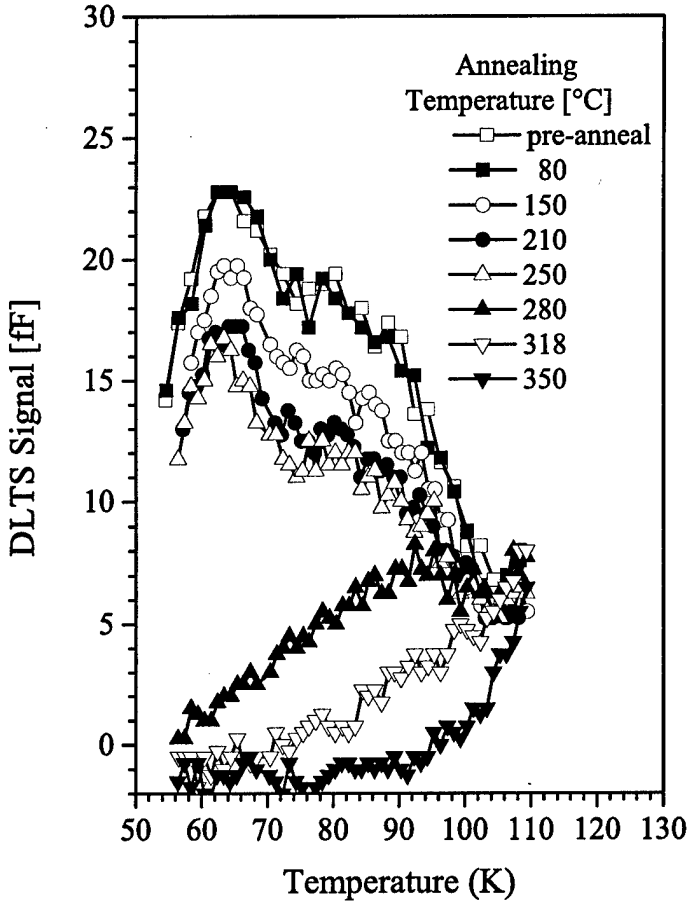

Fig. 6. DLTS spectra after each 30 min isochronal annealing step. The accumulated gamma ray dose was 21 Mrad(Si), the rate window is $e_n = 1.02\ s^{-1}$ with t_p = 10 s.

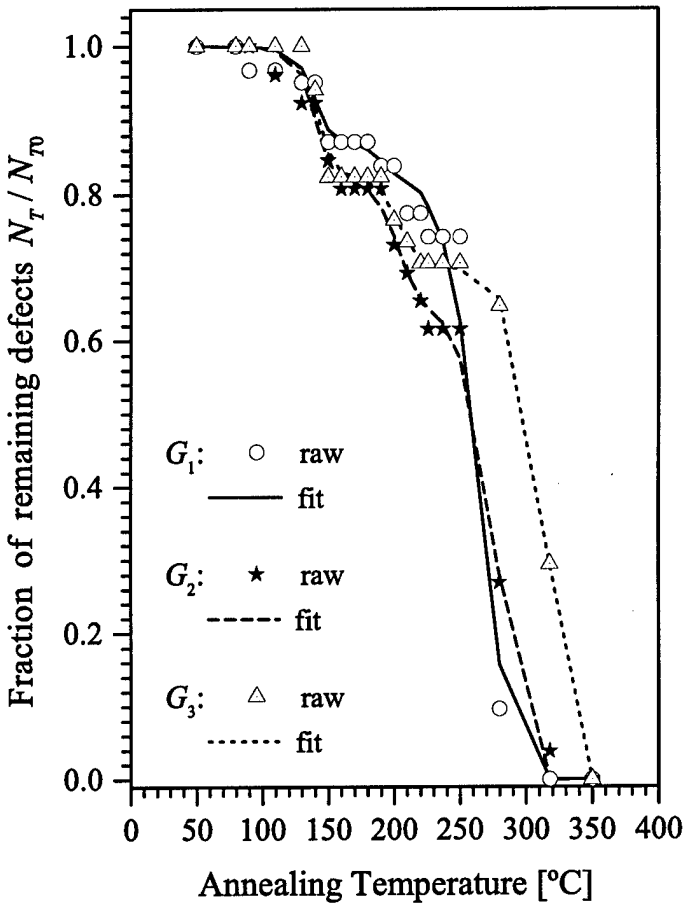

Fig. 7. Fractional change in radiation-induced defect concentration with consecutive post-irradiation isochronal thermal annealing of Ni/*n*-GaN Schottky diodes exposed to 21 Mrad(Si) ^{60}Co gamma-ray total-dose.

Appendix D

Magnetoresistance characteristics of gamma-irradiated $Al_{0.35}Ga_{0.65}N/GaN$ HEMTs

Magnetoresistance characteristics of gamma-irradiated $Al_{0.35}Ga_{0.65}N/GaN$ HFETs

Gilberto A. Umana-Membreno, John M. Dell, Giacinta Parish, Brett D. Nener, Lorenzo Faraone, Ramakhrishna Ventury†, Umesh K. Mishra†

School of Electrical, Electronic and Computer Engineering
The University of Western Australia, Crawley WA 6009, Australia

†Department of Electrical and Computer Engineering
University of California, Santa Barbara, CA 93106, U.S.A.

ABSTRACT

The effect of ^{60}Co gamma-irradiation on the device characteristics of $Al_{0.35}Ga_{0.65}N$-GaN heterojunction field effect transistors (HFET) has been investigated using DC and geometrical magnetoresistance measurements. Cumulative gamma-ray doses up to 20 Mrad(Si) are shown to induce drain current degradation, negative threshold voltage shifts and reverse gate leakage current degradation. Analysis of drain magneto-conductance characteristics measured at 80 K indicated an increase in two-dimensional electron gas (2DEG) sheet concentration with accumulated radiation dose. More importantly, the 2DEG mobility-concentration characteristics are noted to remain approximately constant for total gamma-radiation doses up to 20 Mrad(Si), indicating that the areal density of radiation-induced defects at the heterointerface is likely to be negligible. The threshold voltage shifts are therefore attributable to the introduction of relatively shallow radiation-induced defects in the AlGaN barrier region and/or to defects introduced at the gate-barrier interface. Although the drain conductance characteristics manifested similar degradation trends at 80 and 300 K, the 2DEG parameters obtained at 300 K exhibited significant scatter with increasing dose, possibly a manifestation of device instabilities induced by radiation-induced surface defects in the ungated access region near the edge of the gate. Device failure due to severe gate leakage and loss of gate control over the 2DEG charge, occurred after a total dose of 30 Mrad(Si).

Keywords: Gallium Nitride, Aluminum Gallium Nitride, Radiation-induced effects, Magnetoresistance, Heterostructures, Two-dimensional-electron-gas, Field-effect-transistor, HEMT, HFET

1. INTRODUCTION

Due to their low susceptibility to radiation-induced displacement damage, the III-nitride semiconductor alloys are attractive for the development of electronic devices capable of reliable operation in high-energy radiation environments.[1,2] In particular, AlGaN/GaN heterostructure field effect transistors are promising for satellite, military and nuclear applications requiring high speed, high output power and high tolerance to radiation-induced degradation.[3]

Over the past few years, exposure to various forms of high-energy radiation has been employed to study the effect of controllably introduced point defects on the optical and electrical properties of GaN-based materials.[2,4–9] The low defect production rates reported in these studies have demonstrated the low susceptibility of GaN to radiation induced damage. However, the reliability of electronic devices operating in high-energy radiation environments is not only determined by the vulnerability of the semiconductor material to radiation-induced degradation but is also dependent on the susceptibility of surfaces, interfaces, contacts and passivation layers to radiation-induced degradation.[10–12] Since the radiation hardness of GaN-based HFETs is likely to manifest similar dependence on device topology and fabrication technology, it is incorporate those elements in the investigation of radiation-induced effects on device performance and reliability.

Perhaps one of the earliest indications of radiation-induced device degradation in III-nitride-based devices can be found in the report of Fang *et al.*,[13] where it was briefly noted that exposure of Schottky diodes to 1 MeV electrons induced significant reverse leakage current degradation. In a recent report, we noted that while the defect production rates are very low, the tolerance of Ni/GaN Schottky diodes to radiation-induced damage was limited by degradation at the metal-GaN interface.[14] Exposure of GaN-based heterostructure light emitting

Microelectronics: Design, Technology, and Packaging, edited by Derek Abbott, Kamran Eshraghian, Charles A. Musca, Dimitris Pavlidis, Neil Weste, Proceedings of SPIE Vol. 5274 (SPIE, Bellingham, WA, 2004) · 0277-786X/04/$15 · doi: 10.1117/12.527255

diodes to high-energy proton irradiation has been reported to introduce non-radiative recombination centers which affect the device optical characteristics more severely than electrical characteristics.[15,16] Reports on the effect of irradiation on AlGaN/GaN HFETs are relatively few, with recent reports indicating that exposure to high energy protons and gamma-rays affect DC and RF performance.[17–20] The very high doses employed in these studies, and the relatively low level of degradation observed, indicate that III-nitride-based HFETs are indeed superior to their GaAs-based counterparts in terms of radiation hardness.

In this report, we present results of a magneto-transport study of AlGaN/GaN HFETs exposed to total ^{60}Co gamma-ray doses up to 20 Mrad(Si). Two-dimensional electron-gas transport (2DEG) parameters were extracted from geometrical magneto-resistance measurements of short gate-length HFETs at 80 and 300 K. Irradiation exposure is shown to induce drain current degradation, negative threshold voltage shifts and reverse gate leakage current degradation. Analysis of drain magneto-conductance characteristics at 80 K indicated increased two-dimensional electron gas sheet density with accumulated radiation dose, which resulted in shifts of the threshold voltage towards more negative gate biases. Importantly, the 2DEG mobility-concentration characteristics are noted to remain approximately constant for total gamma-radiation doses up to 20 Mrad(Si), indicating that the areal density of radiation-induced defects at the heterointerface is likely to be negligible. The threshold voltage shifts are therefore attributable to the introduction of, relatively shallow, radiation-induced defects centers in the AlGaN barrier region or to defects introduces at the interface between the gate Schottky contact and the AlGaN barrier layer. Although the drain conductance characteristics manifested similar degradation trend at 80 and 300 K, the 2DEG parameters obtained at 300 K exhibited significant scatter with increasing dose; which likely to be a manifestation of effects associated with radiation-induced surface defects in the ungated access region near the edge of the gate contact, and/or thermally activated device instabilities associated with radiation-induced defects. Device failure due to excessive gate leakage and loss of gate control over the 2DEG charge, occurred after a total dose of 30 Mrad(Si).

2. DEVICE AND EXPERIMENTAL DETAILS

Field-effect transistors were fabricated on heterostructures grown on *c*-plane sapphire by metal-organic chemical vapor deposition at the University of California, Santa Barbara. The epitaxial structure consisted of a low temperature grown GaN nucleation layer of 200 Å thickness followed by 3.4 μm of undoped GaN grown at high temperature. This was followed by the growth of 150 Å of nominally undoped $Al_{0.35}Ga_{0.65}N$ as the top layer. The device used in this study was a split source heterostructure field effect transistor with an active area defined by a 100 μm wide and 0.7 μm long Ni/Au gate. The source and drain contacts, formed using thermally annealed Ti/Al/Ni/Au metallization, had a separation of 2.4 μm. The source-gate separation was 0.7 μm.

The magnetoresistance characteristics were obtained from measurement of drain, source and gate currents for gate voltages of $-4.5 \leq V_{gs} \leq 0.5V$ at a drain-source voltage of $V_{ds} = 0.1V$. These measurements were performed for 26 magnetic fields in the range of 0 to 12 T, at device temperatures of 80 and 300 K. Exposure to ^{60}Co gamma-rays, with an average energy of 1.25 MeV, was realized in an AECL Gammacell 220 ^{60}Co-irradiator at an average dose rate of 2 krad(Si)/min. All irradiations, to cumulative gamma-ray doses from 1.5 to 20 Mrad(Si), were performed at room temperature in a nitrogen ambient with drain, source and gate contacts electrically shorted. The sample was held at room temperature for at least 3 hours before any measurements were taken to avoid possible short-term post-irradiation effects. Since a previous study of gamma-irradiated Ni/GaN Schottky diodes indicated that low temperature ($\leq 50°C$) annealing affects post-irradiation device characteristics,[14] the applied drain bias not allowed to exceeded 0.1 V to avoid device self-heating and possible unintentional annealing of radiation-induced defects.[21,22]

The as-fabricated HFET drain-current characteristics (I_{ds}–V_{gs}) manifested unusually lower drain current levels at 80 K than at 300 K, evident in Fig. 1, due to temperature dependent series resistance. High parasitic series resistances are known to affect the accuracy of transport parameters extracted using magnetoresistance measurements,[23] it was hence necessary to develop a procedure to extract the magnetic-field dependent channel conductance and parasitic resistances from the I_{ds}–V_{gs} characteristics measured at various magnetic field intensities. A brief outline of the analysis method is presented in the following section, a detailed description of the method has been published elsewhere.[24]

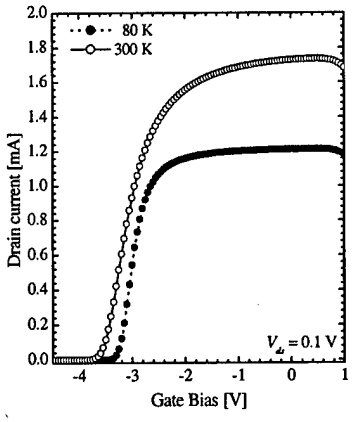

Figure 1. Drain current characteristics before sample exposure to gamma-radiation from a ^{60} source. The lower drain current at 80 K is caused by the temperature-dependent parasitic resistance of the drain/source ohmic contacts.

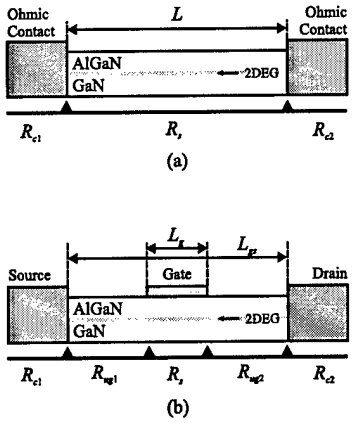

Figure 2. Schematic representations of: (a) Gateless AlGaN/GaN device structure. (b) AlGaN/GaN HFET.

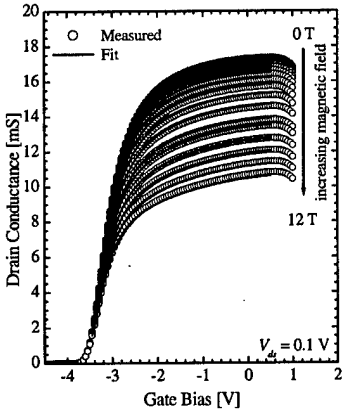

Figure 3. Effect of applied magnetic field on the drain conductance characteristics, before device irradiation. Solid lines represent the fit to the experimental data (open symbols) obtained using the analysis procedure described in this work.

3. ANALYSIS METHODOLOGY

The effect of parasitic resistances on 2DEG magneto-transport parameters is best illustrated by first considering the simple gateless AlGaN/GaN device structure of Fig.2(a). For a single dominant carrier, the magnetic-field dependent channel conductance $G_s(B)$ is given by

$$R_s{}^{-1}(B) = G_s(B) = \frac{qN_s\mu_s}{1+\mu_s{}^2B^2}\frac{W}{L} \tag{1}$$

where N_s and μ_s are the 2DEG sheet carrier concentration and mobility, respectively; W and L are the width and length of the device, and B is the magnetic field intensity perpendicular to the AlGaN/GaN interface. In the case of non negligible contact resistance $R_c = R_{c1} + R_{c2}$, the apparent 2DEG concentration N_m and mobility μ_m, obtained by neglecting R_c, is related to N_s and μ_s by:[23]

$$N_s = N_m(1 - R_c/R_T(0))^{-1/2}; \qquad \mu_s = \mu_m(1 - R_c/R_T(0))^{-1/2} \tag{2}$$

where R_c has been assumed to be independent of the magnetic field. The above corrections are particularly valuable to extract accurate 2DEG transport parameters when the contact resistance is known, or when the measurements are performed on structures with different inter-contact separation L

For case of gated structures, such as the AlGaN/GaN HFETs schematically depicted in Fig.2(b), the total device magnetoresistance $R_T(B)$ is affected by R_c and by the magnetoresistance of the ungated gate-to-source and gate-to-drain access regions $R_{ug}(B) = R_{ug1} + R_{ug2}$. It can be shown that the true N_s and μ_s are related to the apparent N_m and μ_m, obtained by neglecting R_c and $R_{ug}(B)$:[24]

$$\mu_s = \mu_m K_1 K_2; \qquad N_s = N_m K_1/K_2 \tag{3}$$

with

$$K_1 = \left[1 - \frac{R_{ug}(0) + R_c}{R_T(0)}\right]^{-1/2}; \qquad K_2 = \left[1 - \frac{R_{ug}(0)\mu_{ug}^2}{R_T(0)\mu_m^2}\right]^{1/2} = \left[1 - \frac{(R_{ug}(0) + R_c)\mu_{ug,m}^2}{R_T(0)\mu_m^2}\right]^{1/2} \tag{4}$$

where μ_{ug} and $\mu_{ug,m}$ are the true and apparent mobilities in the access regions (the latter assuming $R_c = 0$), respectively. R_c, R_{ug} and μ_{ug} are necessary for the extraction of accurate 2DEG channel transport parameters

but are generally unknown. Nevertheless, the above expressions are can be used to implement a computationally efficient algorithm to obtain N_s and μ_s from estimates of R_c, R_{ug} and μ_{ug}.

To obtain estimates of R_{ug} and μ_{ug}, we have employed the conventional HFET linear charge control model in which the 2DEG sheet carrier concentration in the channel is a linear function of applied gate bias:[25–27]

$$qN_s = C_{2D}(V_{gs} - V_T) \tag{5}$$

where V_T is the threshold voltage, and $C_{2D} = \epsilon_b/(d + \Delta d)$ is the parallel plate approximation to the gate-to-channel capacitance. The static dielectric permittivity of the barrier layer is ϵ_b, and $d + \Delta d$ denotes the effective location of the 2DEG from the gate electrode. The 2DEG concentration in the ungated access regions can also be modelled by a similar expression:

$$qN_{s,ug} = C_{2D}(-V_{T,ug}) \tag{6}$$

here $N_{s,ug}$ is the 2DEG concentration in the ungated access region and $V_{T,ug}$ is a *threshold voltage* that denotes the external surface "biasing" required to extinguish the 2DEG in the ungated access regions. In (6) the surface bias term has been omitted because we have assumed it to be negligible at low drain bias. Although this model for the 2DEG charge in the ungated region is quite simple, it is consistent with the localized modulation of the 2DEG induced by charge-injection into surface-states of the ungated access region reported in AlGaN/GaN HFETs subjected to bias stress.[28] Using (5) and (6), the threshold voltage in the ungated access region can be more conveniently expressed as:

$$V_{T,ug} = -(V_{cch} - V_T)$$

which allows (6) to be rewritten as:

$$qN_{s,ug} = C_{2D}(V_{cch} - V_T) \tag{7}$$

with V_{cch} denoting the continuous channel voltage, or gate bias required to induce the same 2DEG concentration in the gated channel and in the ungated access regions. It should be noted that in this context, C_{2D} represents the average capacitance of the 2DEG with respect to the surface of the ungated region and the gate electrode.

Using (7), the resistance of the gated and ungated channel access region can be expressed in terms of the total device resistance:

$$R_{ug}(B) = \frac{L_{ds} - L_G}{L_{ds}} [R_T(V_{cch}, B) - R_c] \tag{8}$$

$$R_s(V_{gs}, B) = R_T(V_{gs}, B) - R_T(V_{cch}, B) \left[\frac{L_{ds} - L_g}{L_{ds}}\right] - R_c \left[1 - \frac{L_{ds} - L_g}{L_{ds}}\right] \tag{9}$$

where the functional dependence on V_{gs} and B has been emphasized. A special case of (9) for $R_c = 0\ \Omega$ and $V_{cch} = 0$ V, was employed by to analyze the magnetoresistance of $Al_{0.25}Ga_{0.75}N$/GaN MODFETs.[29] While the main difficulty in the applicability of the above expressions is the need to know both V_{cch} and R_c, it can be partly circumvented by employing a non-linear least-squares fitting procedure to estimate at least one of these parameters if the other is known, or assumed. It should be noted that any algorithm using simultaneous fitting of V_{cch} and R_c leads non unique solutions. Fortunately, in practical HFET structures the assumption of $V_{cch} = 0$ V, as employed by Antoszewski *et al.*,[29] is an adequate approximation to the ungated channel conductance; R_c can then be obtained by fitting the experimental I_{ds}–V_{gs} characteristics as a function of magnetic field to 1, 4, 5, 8 and 9.

For the analysis of the experimental data presented herein, we have assumed $V_{cch} = 0$ V and treated R_c, C_{2D} and V_T as fitting parameters. The worst error in N_s and μ_s is estimated to be $\leq$15% if the true V_{cch} is in the range of -0.5 to 0.5 V. As illustrated in Fig. 3, the fitted characteristics adequately describe the measured magnetic-field-dependent drain conductance characteristics G_{ds}–V_{gs}.

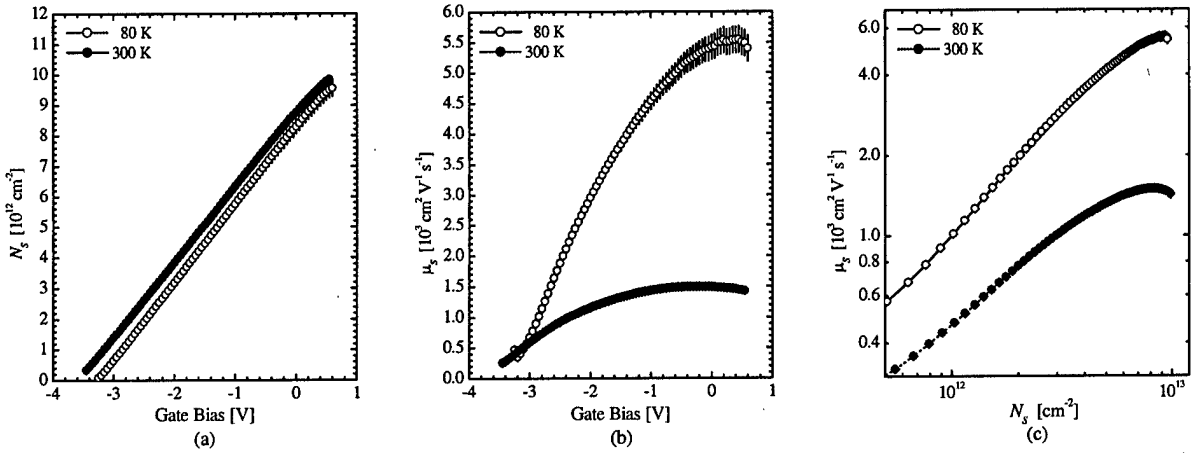

Figure 4. 2DEG carrier transport characteristics extracted from magnetoresistance measurements before device irradiation: (a) 2DEG sheet carrier concentration N_s with gate-bias, (b) 2DEG mobility μ_s with gate bias, and (c)Dependence of 2DEG mobility on 2DEG concentration.

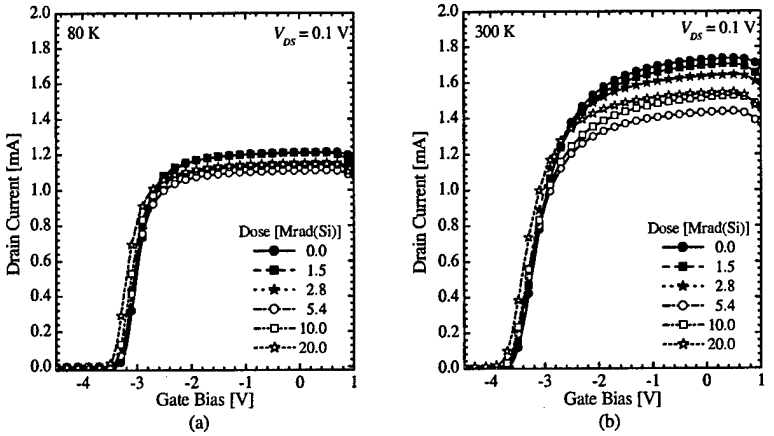

Figure 5. Effect of gamma-radiation exposure on the drain-current characteristics of an AlGaN/GaN HFET measured at: (a) 80 K, and (b) 300 K.

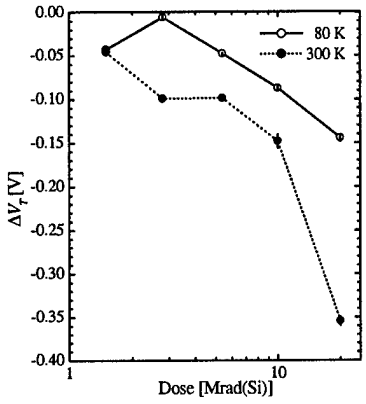

Figure 6. Threshold voltage shift induced by exposure to cumulative gamma-ray doses up to 20 Mrad(Si)

4. RESULTS AND DISCUSSION

As previously indicated, the I_{ds}–V_{gs} characteristics measured before device irradiation manifested lower drain currents at 80 K than at 300 K (Fig. 1) due to the presence of temperature-dependent high series resistance at the drain and source contacts. The series resistances, extracted using the analysis of the magnetoresistance, are 78.8±0.1 Ω and 45.3±0.1 Ω at 80 and 300 K, respectively. The transport characteristics of the gated 2DEG channel were extracted from the I_{ds}–V_{gs} characteristics measured at 26 magnetic fields in the 0 to 12 T range. The 2DEG concentration N_s and mobility μ_s thus extracted are shown in Fig. 4. The 2DEG mobility of the ungated region $\mu_{s,ug} = 1492\pm34$ cm^{2}V^{-1}s^{-1} at 300 K, is consistent with the 2DEG mobility of 1400 cm^{2}V^{-1}s^{-1} obtained from room-temperature Hall measurements on the as grown structure. As evident in Fig. 4(a), the gradient of the N_s–V_{gs} characteristics decreased at higher temperature, with C_{2D} of 4.05±0.01 and 3.90±0.01, at 80 and 300 K respectively, equivalent to an increase in the average distance of the 2DEG to the heterointerface of about 9 Å at 300 K. The relatively large shift in threshold voltage $\Delta V_T = 0.313\pm0.005$ V evident in the I_{ds}–V_{gs} and N_s–V_{gs} characteristics between 80 and 300 K (Figs. 1 and 4(a)) is generally assumed to indicate the presence of electrically active defects in the AlGaN barrier region, with an estimated upper-bound density of 1.4±18 cm^{-3}. Although an increase in 2DEG is expected to result a reduction in Δd, the decrease in Δd at

Table 1. Summary of parameters extracted from the fit to the magnetic field dependent I_{ds}–V_{gs} characteristics at 80 K

Dose (Mrad(Si))	C_{2D} (10^{-7} F cm^{-2})	V_T (V)	R_c (Ω)	N_{ug} (10^{12} cm^{-2})	μ_{ug} (10^3 cm^2 V^{-1}s^{-1})
0.0	4.05±0.01	−3.27±0.01	79.27±0.01	8.30±0.23	5.42±0.20
1.5	4.01±0.01	−3.31±0.00	79.44±0.01	8.32±0.23	5.43±0.20
2.8	4.16±0.01	−3.27±0.00	83.74±0.01	8.55±0.25	5.73±0.16
5.4	3.88±0.01	−3.31±0.00	86.93±0.01	8.07±0.21	5.58±0.19
10.0	4.04±0.01	−3.35±0.00	84.58±0.01	8.50±0.25	5.56±0.18
20.0	4.17±0.01	−3.41±0.00	84.41±0.01	8.96±0.31	5.68±0.20

Table 2. Summary of parameters extracted from the fit to the magnetic field dependent I_{ds}–V_{gs} characteristics at 300 K

Dose (Mrad(Si))	C_{2D} (10^{-7} F cm^{-2})	V_T (V)	R_c (Ω)	N_{ug} (10^{12} cm^{-2})	μ_{ug} (10^3 cm^2 V^{-1}s^{-1})
0.0	3.90±0.01	−3.58±0.01	46.42±0.06	8.76±0.11	1.49±0.03
1.5	3.58±0.02	−3.62±0.01	45.47±0.10	8.14±0.13	1.36±0.04
2.8	4.39±0.01	−3.68±0.01	52.23±0.02	10.10±0.14	1.66±0.02
5.4	3.47±0.01	−3.68±0.01	55.79±0.06	7.99±0.10	1.33±0.03
10.0	2.98±0.03	−3.73±0.01	46.66±0.27	6.93±0.16	1.12±0.05
20.0	3.72±0.01	−3.93±0.01	55.92±0.05	9.13±0.46	1.82±0.09

300 K is due to the de-confining effect of polar optical phonon scattering.[30]

The I_{ds}–V_{gs} characteristics measured after exposure to increasing total gamma-ray doses are shown in Fig. 5, where it is evident that irradiation affects both the drain current I_{ds} and induces negative threshold voltage shift. After 20 Mrad(Si), radiation-induced threshold voltage shifts of 0.14±0.02 V and 0.35±0.02 V were observed at 80 and 300 K, respectively. At both temperatures, the I_{ds}–V_{gs} characteristics manifested similar radiation-induced degradation, the magnitude of I_{ds} decreasing monotonically for cumulative doses up to 5.4 Mrad(Si) but exhibiting a modest recovery after subsequent device irradiation. This modest recovery in I_{ds} was accompanied by relatively larger shifts in V_T with dose as shown in Fig 6. For the characteristics measured at 80 K, the degradation in I_{ds} at gate bias near $V_{gs} = 0$ V appear to be strongly correlated to to the the effect of irradiation on total contact resistance R_c as shown in Fig. 7. This is not surprising because, as discussed earlier, the pre-irradiation I_{ds}–V_{gs} characteristics were noted to be dominated by a high contact resistance. In contrast, the degradation observed in the I_{ds}–V_{gs} at 300 K did not manifest such a good correlation with R_c, indicating that at 300 K the dominant mechanism responsible for device degradation with dose is dominated and/or measurements are affected by device instabilities. The extracted device parameters as a function of irradiation dose are summarised in Tables 1 and 2.

Exposure to gamma-rays was noted to significantly affect the reverse bias gate leakage current, as shown in Fig. 8. The degradation observed at 80 K was relatively worse: At a gate bias of $V_{gs} = -4.5$ V, the reverse leakage currents measured before irradiation of 46.41 μA and 83.14 μA increased to to 402.36 μA and 317.45 μA after 20 Mrad(Si) at 80 and 300 K, respectively. The radiation-induced gate leakage current increased almost monotonically with dose, but manifested a minor recovery after 5.4 Mrad(Si) that coincides with the dose at which the maximum degradation in R_c occurred. Interestingly, significant change in effect of gamma-irradiation has been noted to occur at doses between 4 and 5 Mrad in at n-GaN Schottky barrier diodes.[14,31]

From measurements performed 80 K, the 2DEG transport characteristics with accumulated gamma-ray dose evidenced an shift in N_s–V_{gs} toward more negative gate biases, as shown in (shown in Fig. 9(a)), indicating increases in 2DEG charge in the channel with increasing dose. Importantly, the mobility at a fixed 2DEG concentration remained approximately constant, or within the confidence bands of N_s and μ_s, for all irradiation doses employed in this study, as evidenced in Fig. 9(c). The combined effect of a negative shift in N_s and

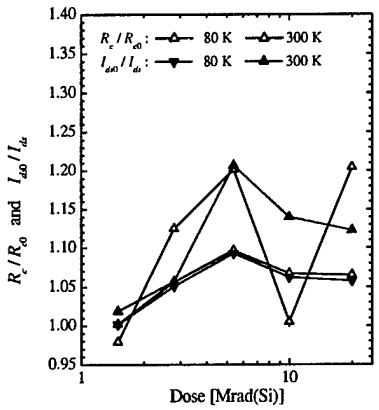

Figure 7. Effect of gamma-irradiation on contact resistance R_c and drain current at $V_{gs} = 0$. R_{c0} and I_{ds0} denote the pre-irradiation values of R_c and I_{ds}

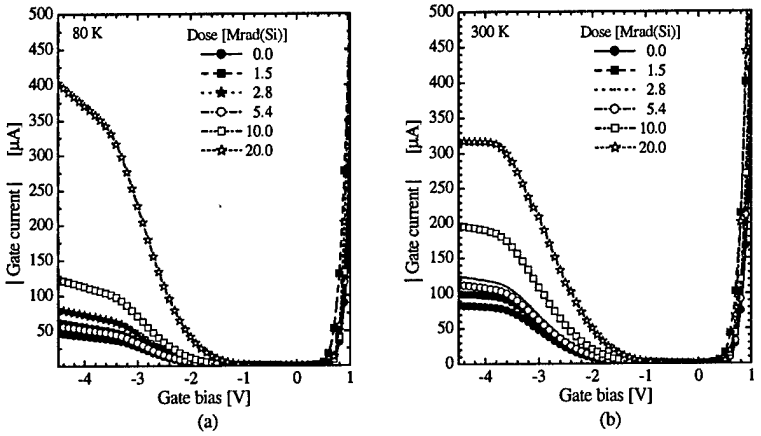

Figure 8. Effect of gamma-ray exposure on the gate current charcteristics at (a) 80 K, and (b) 300 K.

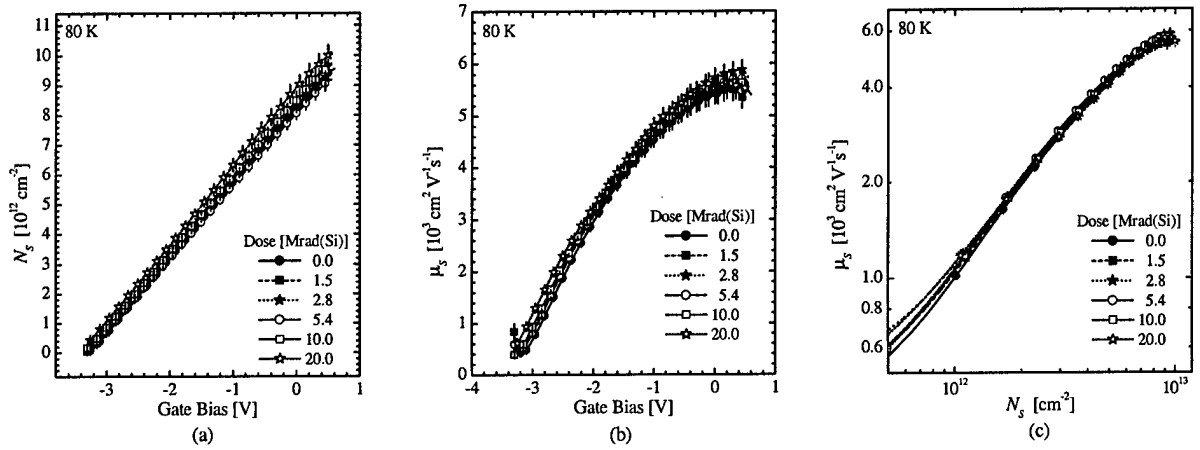

Figure 9. Effect of total gamma-irradiation dose on the 2DEG transport characteristics of an $Al_{0.35}GaN_{0.65}/GaN$ HFET extracted from magnetoresistance measurements at 80 K: (a) 2DEG concentration with gate bias, (b) 2DEG mobility with gate bias, and (c) 2DEG mobility-concentration profiles.

unchanged μ_s–N_{gs} characteristics cause an apparent increase in the mobility versus gate bias characteristics with dose , as shown in Fig. 9(b). The observed absence of 2DEG mobility degradation seems to indicates that the density of radiation-induced interfacial defects is negligible. The low production rates reported in gamma-irradiated GaN is expected to result in a radiation-induced defect concentration below 10^{14} cm^{-3} in the channel GaN epilayer,[9,14,32] thus their effect on the 2DEG mobility and the threshold voltage is likely to be negligible. The increase N_s and negative threshold voltage shifts with dose are hence likely to arise from the generation of relatively shallow radiation-induced defects in the AlGaN barrier region or to defects at the gate-barrier contact. If we assume the threshold voltage shift is due solely to defects in the AlGaN barrier, the estimated density of radiation induced defects is $7.3\pm0.2\times10^{17}$ cm^{-3}, after 20 Mrad(Si), corresponding to a defect 1.25 MeV photons defect production rate for 18.3 ± 0.6 cm^{-1} which is significantly greater than the reported production rate of 2.12×10^{-3} cm^{-1} for n-GaN exposed to ^{60} gamma-irradiation. Alternatively, interfacial defects at the gate-barrier interface, with a sheet density of approximately 1.1×10^{12} cm^2, could also be responsible for the observed threshold voltage shift through the influence of piezoelectric polarization in the strained AlGaN barrier. It is likely that both effects influence the observed device characteristics.

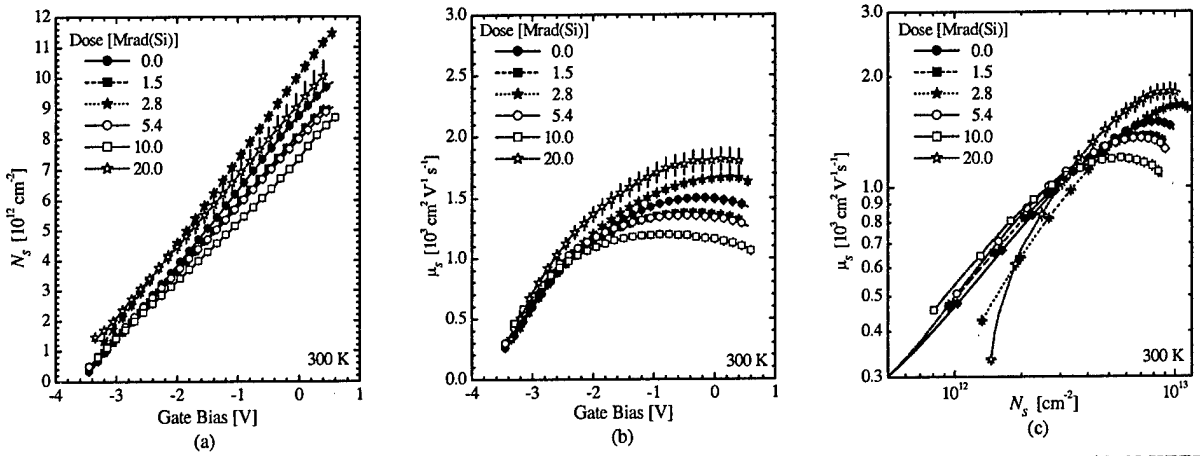

Figure 10. Effect of cumulative gamma-irradiation dose on the 2DEG transport characteristics of an $Al_{0.35}GaN_{0.65}/GaN$ HFET extracted from magnetoresistance measurements at 300 K: (a) 2DEG concentration with gate bias, (b) 2DEG mobility with gate bias, and (c) 2DEG mobility-concentration profiles.

In contrast with the results obtained from measurements performed at 80 K, the 2DEG parameters extracted from the 300 K magnetoresistance characteristics manifested significant scatter as evident in Fig. 10. This behavior is anomalous because the I_{ds}–V_{gs} and I_g–V_{gs} characteristics at 80 and 300 K manifested similar degradation trends with radiation dose. It is important to note that in the magneto-transport analysis model employed the following assumption are implicit: (a) The 2DEG channel dependence on gate bias remains linear for all doses; (b) the ungated channel magnetoresistance is approximated by $V_{cch} = 0$ V for all doses (i.e. irradiation effects on the barrier and channel regions are the same whether in the gated or ungated region). At 80 K these assumptions appear to be valid. However, it is possible that thermal activation of radiation-induced defects at 300 K may induced effects that invalidate the above assumptions: Radiation-induced surface states uniformly distributed over the ungated regions, causing the surface potential to be different from the assumed value of $V_{cch} = V_{gs} = 0$ V; surface-states localized near the gate periphery that interact with the gate electrode via a combination of thermal and tunnelling mechanisms; and other radiation-induced device instabilities. We have attempted to ascertain whether radiation-induced variations in V_{cch}, case (a), are responsible for observed scatter by assuming that constant μ_s remains constant for all irradiation doses, as observed at 80 K. However, it was not possible to obtain a satisfactory value of V_{chh} which could maintain the linear N_s–V_{gs} even when the 2DEG mobility and concentration in the ungated region are decoupled from V_{cch}. It is thus unlikely that uniform changes in the surface potential of the ungated regions would lead to the observed characteristics. For the case of localized charge-trapping states in the vicinity of the gate, modulation of their charge-state would lead to an apparent gate-bias dependent series resistance. This effect, that been previously reported in AlGaN/GaN HFETs at high applied drain bias,[28] is likely to become important as the density of irradiation-induced defects near the edge of the gate increases, and would also result in degraded reverse I_g–V_{gs} characteristics. Lastly, radiation-induced defects mobile at 300 K can cause a change in device characteristics with time. While we have attempted to avoid short-term port-irradiation effects by performing measurements at least 3 hour after irradiation, magnetic field measurements required at least 2 hours to be completed. It should be noted that defect migration would be significantly reduced, if not halted, during measurements at 80 K.

The degradation observed is significantly worse than that noted in previously reported irradiation studies of AlGaN/GaN HFETs,[17–20, 33, 34] particularly because device failure occurred after exposure to a relatively low total dose of 30 Mrad(Si) due to excessive gate leakage and loss of 2DEG charge control. In most reports, post-irradiation device characterisation was performed using I_{ds}–V_{ds} and I_{ds}–V_{gs} measurements which included the drain current saturation region. known to induce significant device self-heating.[21, 22] Since the characteristics of gamma-irradiated Schottky barrier diodes have been reported to recover to pre-irradiation levels after low temperature treatment, it is likely that device self-heating would induce unintentional thermal annealing of radiation-induced defects. However, and since AlGaN/GaN HFETs are most promising for high output power

applications, device self-heating may enhance radiation hardness by raising the dose at which the deleterious effect of irradiation exposure on device characteristic is evident. It should be noted that while the results herein presented are consistent with reported gamma-ray induced negative threshold voltage shifts and drain current degradation, the use of I_{ds}–V_{ds} and I_{ds}–V_{gs} characteristics alone has not been sufficient to unambiguously identify radiation effects on 2DEG parameter.

5. CONCLUSIONS

Low temperature magneto-transport measurements of AlGaN/GaN HFETs exposed to total ^{60}Co gamma-ray doses up to 20 Mrad(Si) indicate that irradiation causes an increase in 2DEG density yet has negligible effect on 2DEG mobility. Device irradiation was noted to also induce significant negative threshold voltage shift, increased parasitic drain/source resistance and degradation of the reverse bias characteristics of the gate. The increase in 2DEG density and the negative threshold voltage shift indicate the introduction of defects in the AlGaN barrier region or at the gate/barrier interface. While the degradation characteristics measured at 80 and 300 K were similar, the 2DEG parameters for 300 K manifested significant scatter. This anomaly is interpreted as arising from radiation-induced defects associated with surface-states and/or to device instabilities. The results herein reported indicate radiation-induce degradation in AlGaN/GaN HFETs results from effects associated with the barrier region, and the ohmic and rectifying contacts. Mechanisms influencing device susceptibility to radiation-induced device degradation.

ACKNOWLEDGMENTS

The authors acknowledge the financial support of this project by the Australian Research Council (ARC).

REFERENCES

1. U. K. Mishra, Y.-F. Wu, B. P. Keller, S. Keller, and S. P. DenBaars, "GaN microwave electronics," *IEEE Trans. Microwave Theory Tech.* **46**(6), pp. 756–761, 1998.
2. D. C. Look, D. C. Reynolds, J. W. Hemsky, J. L. Sizelove, R. L. Jones, and R. J. Molnar, "Defect donor and acceptor in GaN," *Phys. Rev. Lett.* **79**(12), pp. 2273–2276, 1997.
3. Y.-F. Wu, D. Kapolnek, J. P. Ibbetson, P. Parikh, B. P. Keller, and U. K. Mishra, "Very high power density AlGaN/GaN HEMTs," *IEEE Trans. Electron. Devices* **48**, pp. 586–590, 2001.
4. M. Linde, S. J. Uftring, and G. D. Watkins, "Optical detection of magnetic resonance in electron-irradiated GaN," *Phys. Rev. B* **55**(16), pp. R10177–R10180, 1997.
5. K. H. Chow, G. D. Watkins, A. Usui, and M. Mizuta, "Detection of interstitial Ga in GaN," *Phys. Rev. Lett.* **85**(13), pp. 2761–2764, 2000.
6. S. A. Goodman, F. D. Auret, F. K. Koschnick, J.-M. Spaeth, B. Beaumont, and P. Gibart, "Electrical characterization of defects introduced in n-GaN during high energy proton and He-ion irradiation," *MRS Internet J. Nitride Semicond. Res.* **4S1**, p. G6.12, 1999.
7. Z.-Q. Fang, L. Polenta, J. W. Hemsky, and D. C. Look, "Deep centers in as-grown and electron-irradiated n-GaN," in *SIMC-IX Proceedings*, pp. 35–42, 2000.
8. V. V. Emtsev, V. Y. Davydov, V. V. Kozlovskii, V. V. Lundin, D. S. Poloskin, A. N. Smirnov, N. M. Schmidt, A. S. Usikov, J. Aderhold, H. Klausing, D. Mistele, T. Rotter, J. Stemmer, O. Semchinova, and J. Graul, "Point defects in γ-irradiated n-GaN," *Semicond. Sci. Technol.* **15**(1), pp. 73–78, 2000.
9. G. A. Umana-Membreno, J. M. Dell, T. P. Hessler, B. D. Nener, G. Parish, L. Faraone, and U. K. Mishra, "^{60}Co gamma-irradiation-induced defects in *n*-GaN," *Appl. Phys. Lett.* **80**(23), pp. 4354–6, 2002.
10. T. P. Ma and P. V. Dressendorfer, eds., *Radiation Hardening Technology*, ch. 6, pp. 333–400. John Wiley & Sons, 1989.
11. N. Arpatzanis, G. J. P. M. Papastamatiou, Z. Hatzopoulos, and G. Konstandinides, "The gamma irradiation effects in high-electron-mobility transistors," *Semicond. Sci. Technol.* **10**, pp. 1445–1451, 1995.
12. S. Kayali, "Reliability of compound semiconductor devices for space applications," *Microelec. Reliab.* **39**, pp. 1723–1736, 1999.

13. Z.-Q. Fang, J. W. Hemsky, D. C. Look, and M. P. Mack, "Electron-irradiation-induced deep level in GaN," *Appl. Phys. Lett.* **72**(4), pp. 448–449, 1998.
14. G. A. Umana-Membreno, J. M. Dell, B. D. Nener, G. Parish, L. Faraone, and U. K. Mishra, "^{60}Co gamma radiation effects on n-GaN Schottky diodes," *IEEE Trans. Electron. Devices* . (accepted for publication).
15. M. Osiński, P. Perlin, H. Schöne, A. H. Paxton, and E. W. Taylor, "Effects of proton irradiation on AlGaN/InGaN/GaN green light emitting diodes," *Electron. Lett.* **33**(14), pp. 1252–1253, 1997.
16. F. Gaudreau, C. Carlone, A. Houdayer, and S. M. Khanna, "Spectral properties of proton irradiated Gallium Nitride blue diodes," *IEEE Trans. Nucl. Sci.* **48**(6), pp. 1778–1784, 2001.
17. S. J. Cai, Y. S. Tang, R. Li, Y. Y. Wei, L. Wong, Y. L. Chen, K. L. Wang, M. Chen, Y. F. Zhao, R. D. Schrimpf, J. C. Keay, and K. F. Galloway, "Annealing behavior of a proton irradiated $Al_xGa_{1-x}N$/GaN High Electron Mobility Transistor grown by MBE," *IEEE Trans. Electron. Devices* **47**(2), pp. 304–7, 2000.
18. B. Luo, J. Kim, F. Ren, A. G. Baca, R. D. Briggs, B. P. Gila, A. H. Onstine, K. K. Allums, C. R. Abernathy, S. J. Pearton, R. Dwivedi, T. N. Fogarty, and R. Wilkins, "dc and rf performance of proton-irradiated AlGaN/GaN high electron mobility transistors," *Appl. Phys. Lett.* **79**(14), pp. 2196–2198, 2001.
19. B. Luo, J. W. Johnson, F. Ren, K. K. Allums, C. R. Abernathy, S. J. Pearton, A. M. Dabiran, A. M. Wowchack, C. J. Polley, P. P. Chow, D. Schoenfeld, and A. G. Baca, "Influence of ^{60}Co γ-rays on dc performance of AlGaN/GaN high electron mobility transistors," *Appl. Phys. Lett.* **80**(4), pp. 604–606, 2002.
20. S. A. Vitusevich, N. Klein, A. E. Belyaev, S. V. Danylyuk, M. V. Petrychuk, R. V. Konakova, A. M. Kurakin, A. E. Rengevich, A. Y. Avksentyev, B. A. Danilchenko, V. Tilak, J. Smart, A. Vertiatchikh, and L. F. Eastman, "Effects of γ-irradiation on AlGaN/GaN HEMTs," *Phys. Stat. Sol. (a)* **195**(1), pp. 101–105, 2003.
21. R. Gaska, A. Osinsky, J. W. Yang, and M. S. Shur, "Self-heating in High-power AlGaN-GaN HFETs," *IEEE Trans. Electron. Devices* **19**(3), pp. 89–91, 1998.
22. J. Kuzmík and P. Javorka and A. Alam and M. Marso and M. Heuken and P. Kordoš, "Determination of Channel temperature in AlGaN/GaN HEMTs grown on sapphire and silicon substrates using DC Characterization method," *IEEE Trans. Electron. Devices* **49**(8), pp. 1496–1498, 2002.
23. P. Blood and J. W. Orton, *The Electrical Characterization of Semiconductors: Majority Carriers and Electron States*, ch. 3, pp. 94–180. No. 14 in Techniques of Physics, Academic Press, 1992.
24. G. A. Umana-Membreno, J. M. Dell, G. Parish, and L. Faraone, "Analysis of Geometrical Magneto-Resistance in $Al_{0.35}Ga_{0.65}N$/GaN MODFETs," in *Proceedings of the 2002 Conference on Optoelectronic and Microelectronic Materials and Devices (COMMAD 2002)*, 2002. to be published.
25. D. Delagebeaudeuf and N. T. Linh, "Metal-(n) AlGaAs-GaAs two-dimesional electron gas FET," *IEEE Trans. Electron. Devices* **ED-29**, pp. 955–960, 1982.
26. T. J. Drummond, H. Morkoć, K. Lee, and M. Shur, "Model for modulation-doped field effect transistors based on a two-dimensional numerical model," *IEEE Electron Dev. Lett.* **EDL-3**, pp. 338–341, 1982.
27. Rashmi, A. Kranti, S. Haldar, and R. S. Gupta, "An accurate charge-control model for spontanous and piezoelectric polarization dependent two-dimensional electron gas sheet charge density of lattice-mismatched AlGaN/GaN HEMTs," *Solid-State Electron.* **46**, pp. 621–630, 2002.
28. B. D. Weaver and E. M. Jackson, "Slow transients observed in AlGaN/GaN HFETs: Effect of SiN_x passivation and UV illumination," *IEEE Trans. Electron. Devices* **50**(4), pp. 886–893, 2003.
29. J. Antoszewski, M. Gracey, J. M. Dell, L. Faraone, T. A. Fisher, G. Parish, Y.-F. Wu, and U. K. Mishra, "Scattering mechanisms limiting two-dimensional electron gas mobility in $Al_{0.25}Ga_{0.75}N$/GaN modulation-doped field-effect transistors," *J. Appl. Phys.* **87**(8), pp. 3900–4, 2000.
30. L. Hsu and W. Walukiewicz, "Electron mobility in $Al_xGa_{1-x}N$/GaN heterostructures," *Phys. Rev. B* **56**(3), pp. 1520–1528, 1997.
31. C.-W. Wang, B.-S. Soong, J.-Y. Chen, C.-L. Chen, and Y.-K. Su, "Effect of gamma-ray irradiation on the microstructural and luminescent properties of radio-frequency magnetron-sputtered GaN thin films," *J. Appl. Phys.* **88**(11), pp. 6355–6358, 2000.

32. N. M. Schmidt, D. V. Davydov, V. V. Emtsev, I. L. Krestnikov, A. A. Lebedev, W. V. Lundin, D. S. Poloskin, A. V. Sakharov, A. S. Usikov, and A. V. Osinsky, "Effect of Annealing on Defects in As-Grown and γ-ray Irradiated n-GaN Layers," *Phys. Stat. Sol. (b)* **216**, pp. 533–536, 1999.
33. B. Luo, J. Kim, F. Ren, A. G. Baca, R. D. Briggs, B. P. Gila, A. H. Onstine, K. K. Allums, C. R. Abernathy, S. J. Pearton, R. Dwivedi, T. N. Fogarty, and R. Wilkins, "Effect of high-energy proton irradiation on the DC characteristics and current collapse of MgO and Sc_2O_3 passivated AlGaN/GaN HEMTs," *J. Appl. Phys.* **82**(9), pp. 1428–1430, 2003.
34. B. Luo, J. Kim, F. Ren, J. K. Gillespie, R. C. Fitch, J. Sewell, R. Dettmer, G. D. Via, A. Crespo, T. J. Jenkins, B. P. Gila, A. H. Onstine, K. K. Allums, C. R. Abernathy, S. J. Pearton, R. Dwivedi, T. N. Fogarty, and R. Wilkins, "Electrical characteristics of proton-irradiated Sc_2O_3 passivated AlGaN/GaN high electron mobility transistorts," *Electrochem. Solid-State Lett.* **6**(3), pp. G31–G33, 2003.

Appendix E

The energy dependence of proton-induced degradation in AlGaN/GaN high electron mobility transistors

The Energy Dependence of Proton-Induced Degradation in AlGaN/GaN High Electron Mobility Transistors

Xinwen Hu, *Member, IEEE*, Bo K. Choi, *Member, IEEE*, Hugh J. Barnaby, *Member, IEEE*, Daniel M. Fleetwood, *Fellow, IEEE*, Ronald D. Schrimpf, *Fellow, IEEE*, Sungchul Lee, S. Shojah-Ardalan, R. Wilkins, *Member, IEEE*, Umesh K. Mishra, *Fellow, IEEE*, and Ross W. Dettmer

***Abstract*—The effects of proton irradiation at various energies are reported for AlGaN/GaN high electron mobility transistors (HEMTs). The devices exhibit little degradation when irradiated with 15-, 40-, and 105-MeV protons at fluences up to 10^{13} cm^{-2}, and the damage completely recovers after annealing at room temperature. For 1.8-MeV proton irradiation, the drain saturation current decreases 10.6% and the maximum transconductance decreases 6.1% at a fluence of 10^{12} cm^{-2}. The greater degradation measured at the lowest proton energy considered here is caused by the much larger nonionizing energy loss of the 1.8-MeV protons.**

***Index Terms*—Displacement damage, GaN, high electron mobility transistors, nonioizing energy loss (NIEL), proton radiation effects.**

I. Introduction

AlGaN/GaN high electron mobility transistors (HEMTs) have been the subject of increasing interest since they were first demonstrated by Khan *et al.* in 1994 [1]. Great improvements in the performance of AlGaN/GaN HEMTs have been achieved since then [2], [3]. Since these devices are potentially useful as microwave devices in broadband satellite transmission for communications, television, and weather forecasting systems, it is important to understand the radiation response of these devices.

Luo *et al.* studied the influence of 40-MeV protons and ^{60}Co γ-rays on AlGaN/GaN HEMT performance [4], [5]. They observed significant degradation of the transconductance and drain current at the relatively low proton fluence of 5×10^9 cm^{-2}. The devices also degraded significantly after 600 Mrad γ-ray total dose. In both the proton and γ-ray cases, the degradation was attributed to the creation of deep traps in the bandgap that remove electrons from the channel.

Cai *et al.* [6] also examined the radiation-induced degradation and subsequent annealing of 1.8-MeV proton-irradiated AlGaN/GaN HEMTs. The transconductance degraded 65% after a fluence of 10^{14} cm^{-2}, but most of the damage was removed by rapid thermal annealing at 800 °C or higher.

To understand the radiation response and the energy dependence of proton-induced damage in AlGaN/GaN HEMTs more completely, this paper describes the results of 1.8-, 15-, 40-, and 105-MeV proton irradiations on devices from the same wafer. No significant degradation is observed at fluences of 10^{13} cm^{-2} or less for irradiation at the three higher proton energies. However, significant degradation occurred during 1.8-MeV proton irradiations.

TABLE I
TYPICAL VERTICAL STRUCTURE OF THE AlGaN/GaN HEMT

6 nm Al $_{0.36}$Ga$_{0.64}$N
16 nm Al$_{0.36}$Ga$_{0.64}$N: Si doped ~ 10^{18} cm^{-3}
2.8 nm Al$_{0.36}$Ga$_{0.64}$N
3.5 um GaN
Sapphire Substrate

II. Experimental Details

The AlGaN/GaN HEMT devices were fabricated at the University of California at Santa Barbara (UCSB) and packaged at the Air Force Research Laboratory (AFRL). The AlGaN/GaN heterostructures were prepared by metal-organic chemical vapor deposition (MOCVD) on a C-plane sapphire substrate. The gate length is 0.7 μm. The vertical structure of the device is described in Table I. The top and cross section views of the device are shown in Fig. 1.

Manuscript received October 31, 2002; revised March 27, 2003. This work was supported by the United States Air Force Office of Scientific Research MURI Program. The work at PVAMU was supported by NASA through Contract NCC 9-114. This work was originally presented at the RADECS 2003 Workshop.

X. Hu, B. K. Choi, D. M. Fleetwood, R. D. Schrimpf, and S. Lee are with the Department of Electrical Engineering and Computer Science, Vanderbilt University, Nashville, TN 37235 USA (e-mail: xhu@spang.com).

H. J. Barnaby is with the Electrical and Computer Engineering Department, University of Arizona, Tucson, AZ 85721 USA.

S. Shojah-Ardalan and R. Wilkins are with the NASA Center for Applied Radiation Research, Prairie View A&M University, Prairie View, TX 77446 USA.

U. K. Mishra is with the Electrical and Computer Engineering Department, University of California, Santa Barbara, CA 93106 USA.

R. W. Dettmer is with the Air Force Research Laboratory (AFRL), Wright-Patterson AFB, OH 45433 USA.

Digital Object Identifier 10.1109/TNS.2004.825077

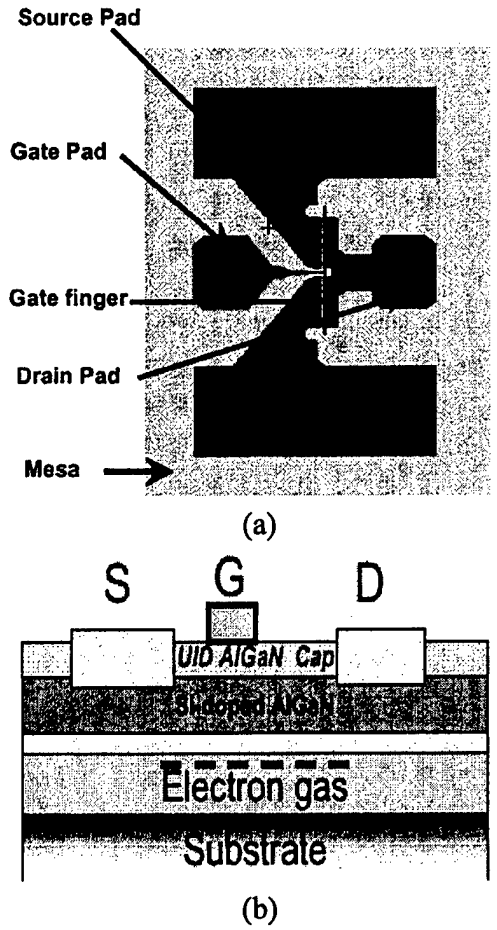

Fig. 1. (a) Top and (b) cross section view of the AlGaN/GaN HEMT device.

Samples were diced and mounted in 40 pin dual inline packages. 105-MeV proton irradiations were performed at the TRIUMF accelerator at the University of British Columbia, Vancouver, Canada. The proton flux was approximately 1.2×10^9 cm^{-2} s^{-1}, and devices were irradiated to fluences of 3×10^{11} cm^{-2}, 10^{12} cm^{-2}, 3×10^{12} cm^{-2}, and 10^{13} cm^{-2}, corresponding to radiation times of 4 min, 10 min, 30 min, and 2 h. 1.8-MeV proton experiments were performed at Vanderbilt University using a Van de Graaff accelerator with raster scanning for fluences of 5×10^{11} and 10^{12} cm^{-2}. 15- and 40-MeV proton irradiations were performed using the Texas A&M cyclotron with an average flux of 10^7 cm^{-2} s^{-1} and fluence of 5×10^{10} cm^{-2} and 10^{11} cm^{-2}, respectively. The details of the irradiation are summarized in Table II.

In all cases, the devices were irradiated at room temperature and all terminals were grounded during irradiation. After irradiation, the dc performance of the devices was measured immediately using an HP4156A semiconductor parameter analyzer. All of the measurements were performed at room temperature. For the 105-MeV proton experiments, the samples were measured again after 5 h to check for annealing effects. For the 15- and 40-MeV proton irradiations, the measurements were taken one day after irradiation. The devices were measured several times during characterization and no self-annealing effects occurred during the measurement.

TABLE II
SRIM [8] SIMULATION RESULTS FOR THE AlGaN/GaN HEMT DEVICE'S SENSITIVE THICKNESS (3.54 μm). IEL: IONIZING ENERGY LOSS; NIEL: NON-IONIZING ENERGY LOSS

Energy Loss	1.8 MeV	15 MeV	40 MeV	105 MeV
IEL (keV/Ion)	114	26.2	12.2	6.1
NIEL (eV/Ion)	3.1	0.27	0.1	0.05
Maximum Fluence (cm^{-2})	10^{12}	5×10^{10}	10^{11}	10^{13}
Total Ionizing Dose (rads)	1.1×10^6	1.7×10^4	1.6×10^4	8.0×10^5

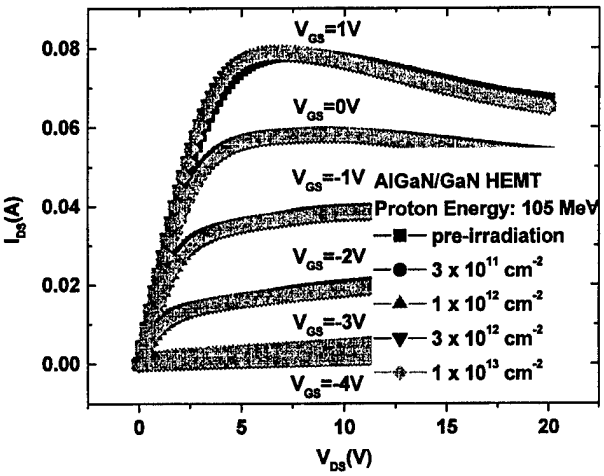

Fig. 2. $I_{DS} - V_{DS}$ characteristics for AlGaN/GaN HEMTs before and after 105-MeV proton irradiation at different fluences at room temperature.

III. RESULTS

Fig. 2 shows the drain-source current as a function of drain-source voltage ($I_{ds} - V_{ds}$) for an AlGaN/GaN HEMT before and after 105-MeV proton irradiation. The gate voltages range from +1 V to −4 V. Even at the highest fluence of 10^{13} cm^{-2}, the radiation-induced reduction of the drain-source current is small.

The transfer characteristics of a HEMT before and after 105-MeV proton irradiation are shown in Fig. 3. The device transconductance, g_m, is 214.4 mS/mm before irradiation. The maximum g_m decreases 11.3% after exposure to a proton fluence of 3×10^{11} cm^{-2} and 14% for a fluence of 3×10^{12} cm^{-2}. At the highest proton fluence of 10^{13} cm^{-2}, g_m has partially recovered to 5.7% below the initial value and after 5 h of room-temperature annealing, it is slightly higher than the pre-irradiation transconductance.

Fig. 4 shows the forward gate I-V characteristics of the HEMTs before and after 105-MeV proton irradiation. No significant degradation of the forward current occurred at the gate voltages examined here (between 0 and 2 V). At low voltage, recombination current plays an important role. As the voltage goes higher, it goes into the high-injection region. Finally, series resistance dominates at voltages greater than 1.25 V [7].

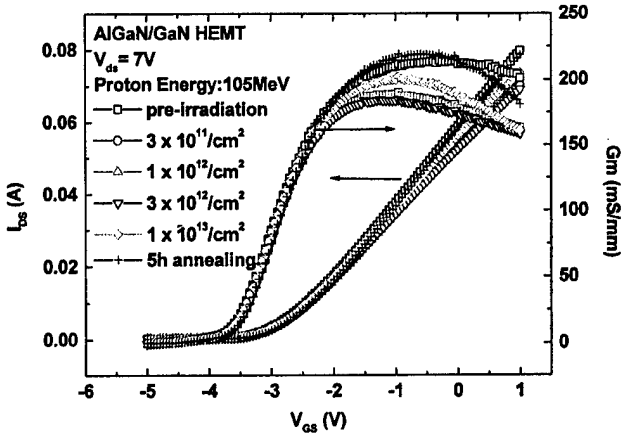

Fig. 3. Transfer characteristics for AlGaN/GaN HEMTs before and after 105-MeV proton irradiation at different fluences.

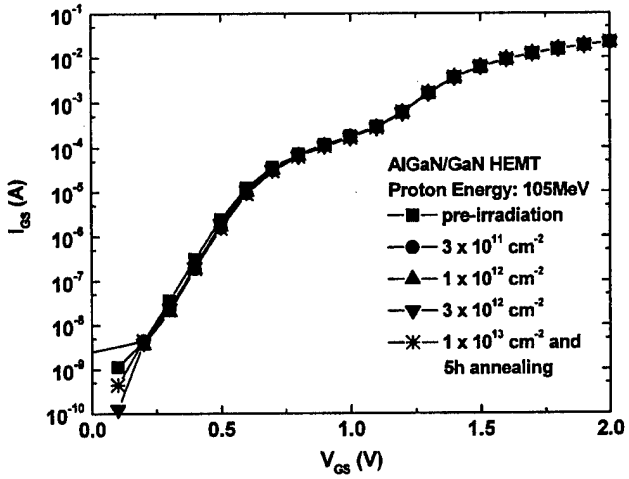

Fig. 4. Forward gate characteristics of AlGaN/GaN HEMTs before and after 105-MeV proton irradiation at different fluences.

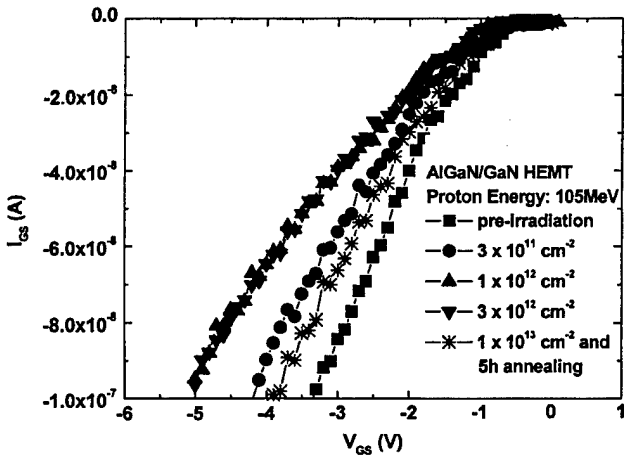

Fig. 5. Reverse gate characteristics of AlGaN/GaN HEMTs before and after 105-MeV proton irradiation at different fluences at room temperature.

The reverse I-V characteristics of the gate junction before and after proton irradiation are shown in Fig. 5. The magnitude of the breakdown voltage increases and the gate leakage current

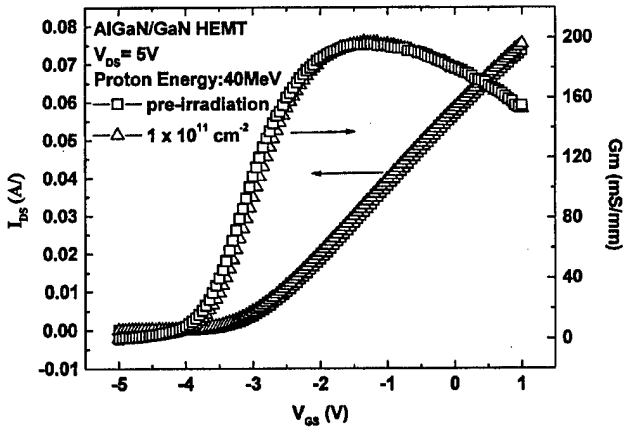

Fig. 6. Transfer characteristics for AlGaN/GaN HEMTs before and after 40-MeV proton irradiation at a fluence of 1×10^{11} cm^{-2}. The measurement was taken one day after irradiation.

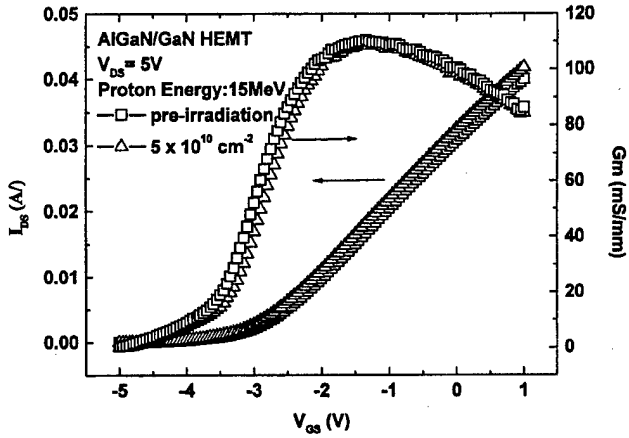

Fig. 7. Transfer characteristics for AlGaN/GaN HEMTs before and after 15-MeV proton irradiation at fluence of 5×10^{10} cm^{-2} at room temperature. The measurement was taken one day after irradiation.

decreases with proton fluence up to 3×10^{12} cm^{-2}; after a fluence of 10^{13} cm^{-2} and 5 h of room-temperature annealing, the reverse characteristics partially recover and approach the pre-irradiation characteristics.

To understand the energy dependence of the radiation response, devices also were irradiated with 40-, 15-, and 1.8-MeV protons. The transfer characteristics for these energies are shown in Figs. 6–8. Fig. 9 shows drain-source current as a function of drain-source voltage ($I_{ds} - V_{ds}$) for an AlGaN/GaN HEMT before and after 1.8-MeV proton irradiation. No significant degradation is observed for the 40- and 15-MeV proton irradiations at the highest fluences used here (5×10^{10} cm^{-2} and 10^{11} cm^{-2}, respectively). For the 1.8-MeV proton irradiation, the drain current and transconductance decreased 4% and 1.4%, respectively, at a fluence of 5×10^{11} cm^{-2}; at 10^{12} cm^{-2}, the drain current and transconductance decreased 10.6% and 6.1%, respectively.

To check the effects of total ionizing dose on the devices, 10-keV X-ray irradiation was also performed. Fig. 10 shows the transfer characteristics for HEMTs before and after X-ray irradiation. No significant degradation was found for a dose of 30 Mrad(SiO_2).

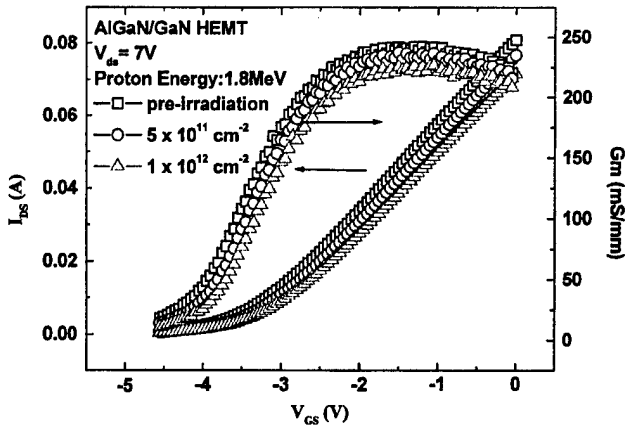

Fig. 8. Transfer characteristics for AlGaN/GaN HEMTs before and after 1.8-MeV proton irradiation at different fluences.

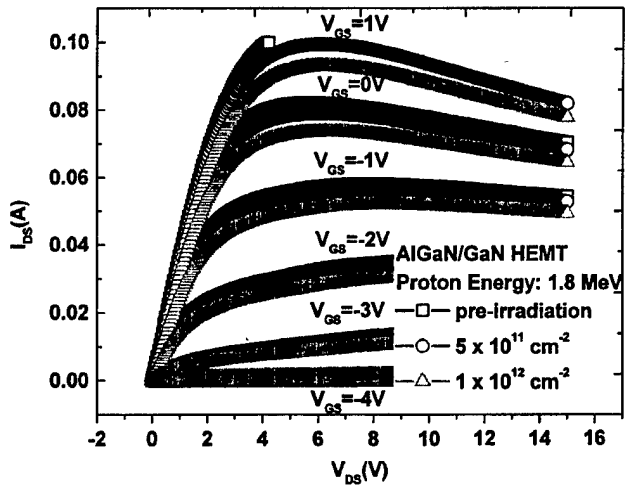

Fig. 9. $I_{DS} - V_{DS}$ characteristics for AlGaN/GaN HEMTs before and after 1.8-MeV proton irradiation at different fluences at room temperature.

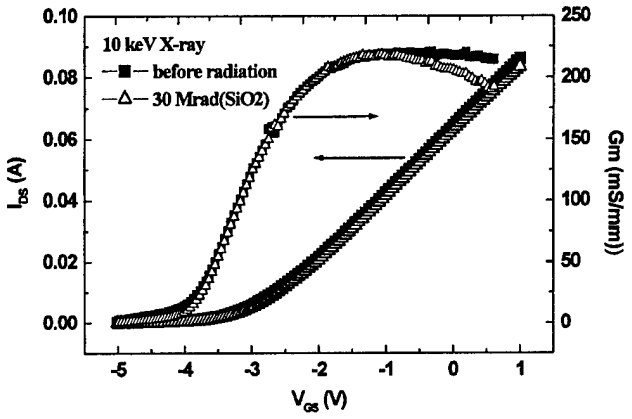

Fig. 10. Transfer characteristics for AlGaN/GaN HEMTs before and after 10-keV X-ray irradiation at fluences up to 30 Mrad (SiO_2).

IV. Discussion

From Fig. 10, ionization effects are relatively unimportant in determining the radiation response of these AlGaN/GaN HEMTs. Hence, we expect the degradation in device performance to be caused by displacement damage.

The displacement damage effects from a variety of different particles can be correlated on the basis of the nonionizing energy loss (NIEL). Monte Carlo simulations using the SRIM program [8] show that the NIEL of 1.8-MeV protons is much greater than that of the higher-energy protons considered here in the first 3.54 μm of the device's sensitive area. The NIEL values for all energies are summarized in Table II. The greater NIEL explains why the degradation due to 1.8-MeV proton irradiation is much larger than that which occurs at the higher energies.

Cai *et al.* [6] reported that the transconductance of AlGaN/GaN HEMTs degraded from about 80 mS/mm to 26 mS/mm at 1.8-MeV proton fluences of 10^{14} cm^{-2} (67.5% degradation), which is consistent with the results reported here. However, Luo reported that the transonductance, g_m, of similar devices decreased 30% at 40-MeV proton fluences of 5×10^{10} cm^{-2}. The pre-irradiation transconductance was approximately 135 mS/mm and the measurements were performed ~50 h after irradiation. This is a surprising result because 5×10^{10} cm^{-2} is a very low fluence compared to the levels at which significant displacement-damage effects are measured in other devices. In order to understand this discrepancy, the experiments described here were performed using the same system for irradiation, but higher fluences. Compared with the results of Luo *et al.*, the results reported here show no significant degradation for 40-MeV proton irradiation. Based on the results presented here, we do not believe that the different radiation response is due to the device structure itself, but rather to an experimental anomaly in the earlier results.

The HEMT devices described here show very good resistance to proton irradiation. This agrees well with the expectation that GaN-based electronic devices should be very radiation hard (more so than GaAs-based electronic devices) [9]. GaN has a higher displacement threshold energy (*Td*) than GaAs and it has been observed empirically that *Td* is inversely proportional to lattice constant ($a = 0.319$ nm, and $c = 0.519$ nm for hexagonal GaN, compared to $a = 0.5653$ nm for the zinc-blende GaAs) [10], [11].

V. Summary

The effects of proton irradiation on AlGaN/GaN HEMTs were studied at four proton energies. Very little degradation was found for proton energies larger than 15 MeV. For a fluence of 10^{12} cm^{-2} 1.8-MeV protons, the drain current decreased approximately 10% and the maximum transconductance decreased 6.1%. The energy dependence of the proton-induced degradation is consistent with NIEL calculations.

AlGaN/GaN HEMTS appear to be excellent candidates for use in space systems. At the proton energies encountered in actual systems, the amount of degradation at typical mission fluences should be negligible for these kinds of devices.

Acknowledgment

The authors would like to thank E. Blackmore for assistance with the 105-MeV proton irradiations.

REFERENCES

[1] M. A. Khan, J. N. Kuznia, D. T. Olson, W. J. Schaff, J. W. Burm, and M. S. Shur, "Microwave performance of a 0.2 μm gate AlGaN/GaN heterostructure field effect transistor," *Appl. Phys. Lett.*, vol. 65, pp. 1121–1123, 1994.

[2] S. Keller, R. Vetury, G. Parish, S. P. DenBaars, and U. K. Mishra, "Effect of growth termination conditions on the performance of AlGaN/GaN high electron mobility transistors," *Appl. Phys. Lett.*, vol. 78, pp. 3088–3090, 2001.

[3] S. Keller, Y.-F. Wu, G. Parish, N. Ziang, J. J. Xu, B. P. Keller, S. P. DenBaars, and U. K. Mishra, "Gallium nitride based high power heterojunction field effect transistors: Process development and present status at UCSB," *IEEE Trans. Electron Devices*, vol. 48, pp. 552–559, 2001.

[4] B. Luo, J. W. Johnson, F. Ren, K. K. Allums, C. R. Abernathy, S. J. Pearton, R. Dwivedi, T. N. Fogarty, R. Wilkins, A. M. Dabiran, A. M. Wowchack, C. J. Polley, P. P. Chow, and A. G. Baca, "DC and RF performance of proton-irradiated AlGaN/GaN high electron mobility transistors," *Appl. Phys. Lett.*, vol. 79, pp. 2196–2199, 2001.

[5] B. Luo, J. W. Johnson, F. Ren, K. K. Allums, C. R. Abernathy, S. J. Pearton, A. M. Dabiran, A. M. Wowchack, C. J. Polley, P. P. Chow, D. Schoenfeld, and A. G. Baca, "Influence of Co-60 γ-rays on DC performance of AlGaN/GaN high electron mobility transistors," *Appl. Phys. Lett.*, vol. 80, pp. 604–606, 2002.

[6] S. J. Cai, Y. S. Tang, R. Li, Y. Wei, L. Wong, Y. L. Chen, K. L. Wang, M. Chen, Y. F. Zhao, R. D. Schrimpf, J. C. Keay, and K. F. Galloway, "Annealing behavior of a proton irradiated Al_x Ga_{1-x} N/GaN high electron mobility transistor grown by MBE," *IEEE Trans. Electron Devices*, vol. 47, pp. 304–307, 2000.

[7] S. M. Sze, *Physics of Semiconductor Devices*. New York: Wiley, 1981.

[8] J. F. Ziegler, J. P. Biersack, and U. Littmark, *The Stopping and Range of Ions in Solids*, 2nd ed, New York: Pergamon Press, 1996.

[9] S. M. Khanna, J. Webb, H. Tang, A. J. Houdayer, and C. Carlone, "2 MeV proton radiation damage studies of Gallium nitride films through low temperature photoluminescence spectroscopy measurements," *IEEE Trans. Nucl. Sci.*, vol. 47, pp. 2322–2328, Dec. 2000.

[10] D. C. Look, D. C. Reynolds, J. W. Hemsky, J. R. Sizelove, R. L. Jones, and R. J. Molnar, "Defect donor and acceptor in GaN," *Phys. Rev. Lett*, vol. 79, no. 12, pp. 2273–2276, 1997.

[11] J. W. Corbett and J. C. Bourgoin, "Defect creation in semiconductors," in *Point Defects in Solids*, J. H. Crawford and F. F. Slifkin, Eds, New York: Plenum Press, 1975, vol. 2, ch. 1.

Appendix F

Characterization of 1.8-MeV Proton-Irradiated AlGaN/GaN Field-Effect Transistor Structures by Nanoscale Depth-Resolved Luminescence Spectroscopy

Characterization of 1.8-MeV Proton-Irradiated AlGaN/GaN Field-Effect Transistor Structures by Nanoscale Depth-Resolved Luminescence Spectroscopy

B. D. White, M. Bataiev, L. J. Brillson, *Fellow, IEEE*, B. K. Choi, *Member, IEEE*, D. M. Fleetwood, *Fellow, IEEE*, R. D. Schrimpf, *Fellow, IEEE*, S. T. Pantelides, *Member, IEEE*, R. W. Dettmer, W. J. Schaff, J. G. Champlain, and U. K. Mishra, *Fellow, IEEE*

***Abstract*—We have used depth-resolved cathodoluminescence spectroscopy to examine AlGaN/GaN modulation-doped field-effect transistors that display degraded source–drain current characteristics after 1.8-MeV proton irradiation, along with bulk heterojunction field-effect transistor material after similar proton irradiation. For both cases, we have observed distinct changes in spectral emission features due to decreased internal electric-field strength and new point defects within different layers of the device structure with nanometer-scale depth resolution. These changes can account for the degraded electrical characteristics.**

***Index Terms*—AlGaN, cathodoluminescence (CL) spectroscopy, defect, displacement, GaN, heterojunction field-effect transistor (HFET), high electron mobility transistor (HEMT), irradiation, modulation-doped FET (MODFET), nitride, proton.**

I. Introduction

NITRIDE-BASED heterostructure devices have received much attention in recent years because of their promise for high-power and high-frequency operational characteristics. Among these devices are the $Al_xGa_{1-x}N/GaN$ heterojunction field-effect transistor (HFET) and modulation-doped field-effect transistor (MODFET), which continue to be intensively studied [1], [2]. Much effort has been concentrated on highly controlled growth of the heterostructure devices, consistent doping methods, and the fabrication of temperature- and time-stable ohmic and Schottky electrical contacts. The effects of irradiation on these devices will become increasingly important as these devices are used in space-radiation environments. Recent investigators [3]–[5] have studied the effects of proton irradiation on electrical-transfer characteristics of the devices, including the decrease in dc saturation current and transconductance as a function of proton energy and fluence. Their results are consistent with the formation of states within the semiconductor bandgaps due to the proton-induced displacement of atoms in the multilayer lattice structure, creating point defects such as vacancies and interstitials. However, although decreases in free-carrier density and increases in trap densities are observed for III-nitrides and other III–V compounds with proton irradiation, relatively little is known about the spatial distribution of such defects, their influence on the internal electric fields within the AlGaN/GaN structure, and their effect on the resultant band structure.

The correlation of radiation-induced transistor performance degradation with spectroscopic characterization of the device material may yield important clues as to the origins of their radiation damage. Spectroscopic techniques such as photoluminescence (PL) [6], Raman spectroscopy [7], and deep-level transient spectroscopy (DLTS) [8]–[11] have been previously used to characterize AlGaN and GaN bulk structures after proton irradiation. Spectroscopy of nitride-based light-emitting diode (LED) structures has also been reported in conjunction with the measurement of electrical characteristics [12], [13]. In this paper, we have used low-energy electron-excited nanoscale- luminescence (LEEN) spectroscopy to characterize nitride-transistor structures before and after proton irradiation. The LEEN technique is a low-energy analog of cathodoluminescence and is sensitive to the deep-level electronic properties of native defects, impurities, chemically induced interface traps, and interfacial compounds. The depth of free-carrier excitation and recombination varies from nanometers to microns as the beam energy varies, thereby discriminating among spectroscopic contributions from different layers of a multilayer interface [14], [15]. We have previously used the LEEN technique to characterize the effects of X-ray irradiation on both thin (~5 nm) SiO_2 layers thermally deposited on Si [16], and thick-oxide SiO_2 capacitor structures analyzed

Manuscript received July 16, 2002; revised September 12, 2002. This work is supported by the Physics and Electronics Directorate, Air Force Office of Scientific Research (AFOSR/NE) under MURI Grant F49620-99-1-0289.

B. D. White and L. J. Brillson are with the Department of Electrical Engineering, The Ohio State University, Columbus, OH 43210 USA (e-mail: whiteb@ee.eng.ohio-state.edu; brillson.1@osu.edu).

M. Bataiev is with the Department of Physics, The Ohio State University, Columbus, OH 43210 USA (e-mail: batayev@mps.ohio-state.edu).

B. K. Choi, D. M. Fleetwood, and R. D. Schrimpf are with the Department of Electrical and Computer Engineering, Vanderbilt University, Nashville, TN 37235 USA (e-mail: bo.choi@vanderbilt.edu; dan.fleetwood@vanderbilt.edu; ron.schrimpf@vanderbilt.edu).

S. T. Pantelides is with the Department of Physics and Astronomy, Vanderbilt University, Nashville, TN 37235 USA.

R. W. Dettmer is with the Air Force Research Lab, Wright-Patterson AFB, OH 45433 USA.

W. J. Schaff is with the Department of Electrical Engineering, Cornell University, Ithaca, NY 14850 USA.

J. G. Champlain and U. K. Mishra are with the Department of Electrical and Computer Engineering, University of California, Santa Barbara, CA 93106 USA.

Digital Object Identifier 10.1109/TNS.2002.805427

in a cross-sectional geometry [17]. The low beam energies employed using LEEN make this technique additionally well suited for analyzing HFET and MODFET structures, since the total thickness of these structures is typically on the order of tens of nanometers. The direct correlation of LEEN spectroscopy with device-electrical characteristics adds physical insight into the changes in material properties that can explain degraded electrical characteristics after proton irradiation.

Additionally, the comparison of different heterostructure-growth techniques may indicate a favorable method for fabricating radiation-hardened devices. In addition to studying the electrical and spectroscopic characteristics of metal-organic chemical-vapor deposition (MOCVD)-grown MODFET structures, we include spectroscopic data for bulk HFET structures grown by molecular-beam epitaxy (MBE), thereby illustrating that irradiation effects can differ based on the device growth and/or fabrication technique.

II. Experimental Procedure

All devices and bulk material characterized in this study were irradiated at room temperature with 1.8-MeV protons at Vanderbilt University, Nashville, TN, using a Van de Graaff accelerator (flux between 1 and 5×10^{10} protons $\text{cm}^{-2} \cdot \text{s}^{-1}$ depending on target fluence). All device terminals were grounded during irradiation. DC electrical characteristics were obtained at room temperature using a HP4156A semiconductor-parameter analyzer.

LEEN analysis was performed at The Ohio State University, Columbus, using a JEOL 7800F ultrahigh vacuum (UHV) scanning-electron microscope (SEM) with an Oxford liquid-helium-cooled sample stage. The SEM electron beam excites electronic transitions into the conduction band, and luminescence from carrier recombination is collected using an Oxford MonoCL apparatus consisting of a parabolic mirror on the UHV side coupled through a sapphire viewport to an airside photomultiplier tube and monochromator with a maximum spectral resolution of 0.15 nm. LEEN spectra were measured in the 200–850-nm range for temperatures in the range of 10–300 K. The depth of excitation for different electron-beam energies can be represented by a CASINO [18] Monte Carlo simulation as shown in Fig. 1. For electron-beam energies E_B between 0.5 and 4 keV, corresponding peak-excitation depth varies between <5 nm and ~50 nm.

Two sets of samples were employed in this study. The first set was grown by MOCVD at the University of California, Santa Barbara, and consisted of 3.5 μm of unintentionally doped GaN grown on a sapphire substrate, followed by a 2.8-nm undoped $Al_{0.36}Ga_{0.64}N$ spacer, a 16-nm $Al_{0.36}Ga_{0.64}N$ donor layer (~10^{18} cm^{-3} Si doped), and capped by an undoped $Al_{0.36}Ga_{0.64}N$ layer of 3–6 nm thickness. Mesa isolation was performed by reactive-ion etching (RIE). Ohmic and Schottky contacts were patterned using photolithography to form the devices on the MODFET structure. The Ohmic metallization consisted of Ti/Al/Ni/Au (20/200/55/45 nm) and the Schottky contact was Ni/Au (20/350 nm). The gate length for the electrically characterized devices is 0.7 μm. After fabrication, the wafers were cut into individual die and packaged. For each package, two transistors were wire-bonded prior to 1.8-MeV proton irradiation. Source–drain dc current–voltage (I–V) characteristics were measured as a function of gate bias immediately prior to irradiation, then at intervals during irradiation. This process was repeated until the devices no longer functioned. The devices were subsequently debonded and depackaged for LEEN analysis. LEEN was performed on a large unmetallized mesa region adjacent to the transistor used for electrical characterization. Multiple spectra were consecutively acquired in the same spot to monitor any possible time effects due to our electron beam. No significant effects were observed.

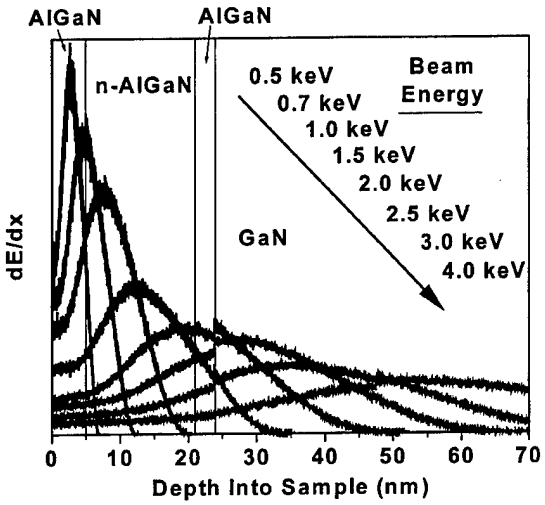

Fig. 1. Monte Carlo simulation of energy loss per unit length dE/dx versus electron-beam penetration depth in the MODFET structure for multiple beam energies.

The second set of samples was from Cornell University, Ithaca, NY, and consisted of MBE-grown HFET bulk material (i.e., without mesa isolation and patterned devices). These structures consisted of a 2–3-μm-thick GaN layer grown on a sapphire substrate, followed by a 23-nm undoped $Al_{0.34}Ga_{0.66}N$ layer, and terminated with a 2-nm GaN-cap layer. LEEN analysis was performed inside a large square of side ~100 μm and was checked in several regions to monitor possible spatial-luminescence variation in the material. No significant variations were observed and time effects were also minimal. Transistors fabricated on this material were unavailable at the time of the study, and we include the spectroscopic results for the purpose of comparison to the MOCVD-grown material.

III. Results

Fig. 2 shows the MODFET source–drain dc I–V characteristics before irradiation and after two successive proton fluences of 10^{11} and 10^{12} cm^{-2}. Fig. 3 shows the transconductance as a function of proton fluence for the same device, with $V_{ds} = 7$ V. The postirradiation curves exhibit a reduction in saturation current with increasing proton fluence, compared with the pre-irradiation data. A ~15% reduction in saturation current and a ~10% decrease in transconductance were measured after a proton fluence of 10^{12} cm^{-2}. LEEN analysis was performed on a reference (unirradiated) die and a die with total fluence of 10^{13} cm^{-2}. Both die were taken from the same wafer and exhibited similar electrical characteristics prior to irradiation.

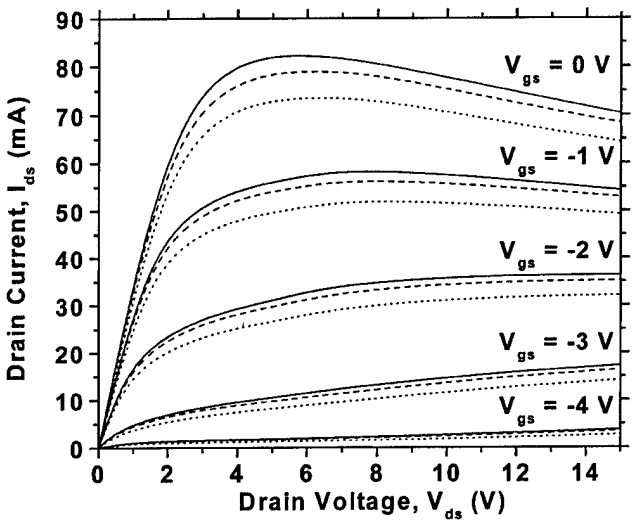

Fig. 2. Common-source dc I–V characteristics for the same transistor pre-irradiation (solid curves), post-10^{11} cm^{-2} fluence (dashed curves), and post-10^{12} cm^{-2} fluence (dotted curves).

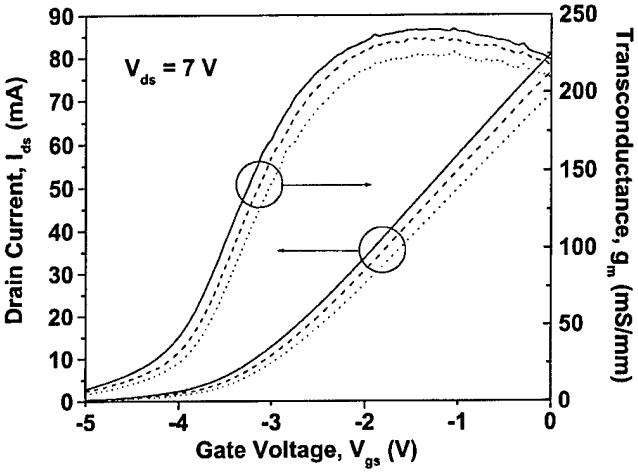

Fig. 3. Common-source drain current as a function of gate voltage and transconductance of the same transistor pre-irradiation (solid curves), post-10^{12} cm^{-2} fluence (dashed curves), and post-5 × 10^{12} cm^{-2} fluence (dotted curves).

LEEN spectra of the MODFET were acquired at room temperature in a ~30 μm square mesa region adjacent to the electrically characterized transistor. Spectra were acquired for beam energies between 0.5–4 keV, with the beam current set at 1 nA for 0.5 keV and adjusted for constant power with increasing energies. Fig. 4 shows a semilog intensity plot of the LEEN spectra for the reference and irradiated die. In this plot, four features are identified: a broad midgap "yellow" luminescence from 2.0–2.5 eV, centered at approximately 2.25 eV, the GaN near-bandedge (NBE) transition at 3.41 eV, a broad emission at ~3.8 eV, and a narrower emission at ~4.1 eV due to the AlGaN NBE. The small apparent features at ~1.7 eV and ~2.0 eV are second-order diffraction effects from our grating monochromator related to the 3.4-eV GaN and 4.1-eV AlGaN emissions, respectively. The reference and irradiated spectra for all energies have been arbitrarily normalized to the GaN NBE for relative comparisons of other spectral features. This normalization

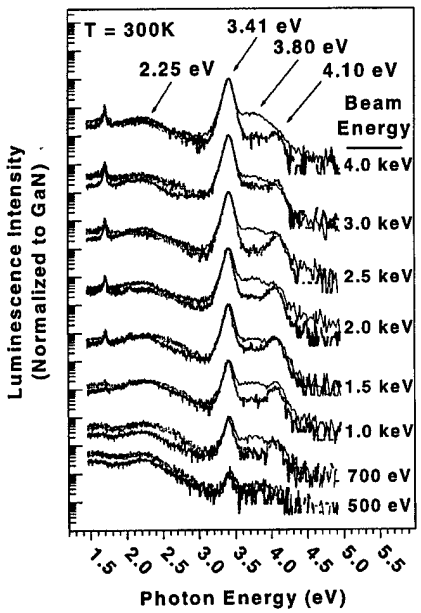

Fig. 4. LEEN spectra for MOCVD-grown MODFET die. A reference die (thin black curves) is compared with a die receiving a fluence of 10^{13} protons/cm^2 (thick gray curves). All intensities are normalized to the GaN NBE emission.

method is validated by the good agreement of the 4.1-eV emission for all energies in both samples, as well as reasonable agreement in the lower (<3.0 eV) emissions.

The presence of multiple emissions above the GaN NBE has been previously reported in cathodoluminescence studies of AlGaN/GaN HFET structures grown by MBE [19]. Here, we attribute the 4.1-eV emission to the Franz–Keldysh-shifted NBE recombination for the thin strained AlGaN film, which for unstrained thick films with 36% Al mole fraction is observed at 4.24 eV [20]. This feature, taken together with the 3.8-eV emission, may represent two different Franz–Keldysh energy shifts originating from the two different types of AlGaN layers (i.e., with and without Si doping). This phenomenon is treated in detail in Section IV.

After normalization, the prominent difference between the reference and irradiated sample is the significant decrease in the 3.8-eV emission for all electron-beam energies. By contrast, the 4.1-eV AlGaN emission is unchanged relative to the GaN NBE in all cases. As the sample temperature is decreased to ~10 K, the GaN and AlGaN NBE transitions exhibit increased intensity and narrower lineshapes, as commonly observed for excitonic luminescence features at low temperature. The 3.8-eV feature does not change in intensity on an absolute scale as temperature is decreased. The lineshape of the 3.8-eV emission is also unaffected by low temperatures, as shown in Fig. 5. In this figure, all data were obtained with a beam voltage of 2 keV and the spectra have again been normalized to the GaN NBE emission. Sub-GaN NBE emissions are increasingly resolved as temperature is decreased, and have been previously attributed to phonon replica emissions associated with the various GaN excitons [21]. No significant temperature evolution was observed for the small yellow luminescence.

The depth dependence of the ~2.25-, 3.8-, and 4.1-eV emissions can be extracted from the variations in spectral features

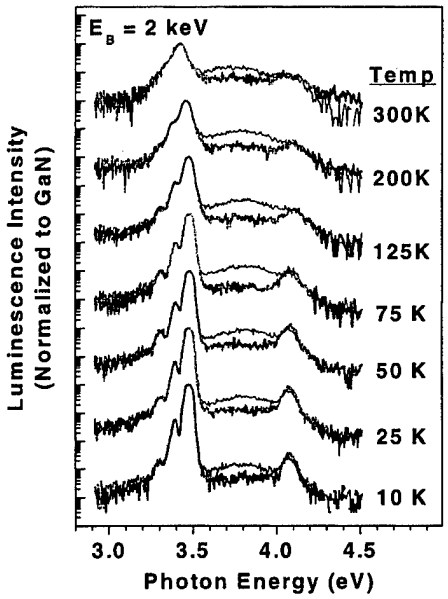

Fig. 5. Temperature dependence of the LEEN MODFET spectra for the reference (thin black curves) and 10^{13} protons/cm^2 fluence (thick gray curves) die. All intensities are normalized to the GaN NBE emission.

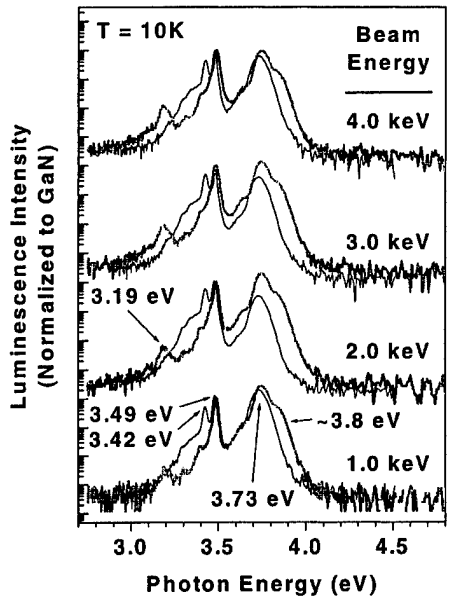

Fig. 7. 10-K LEEN spectra as a function of electron-beam energy E_B for MBE grown HFET samples before irradiation (thin black curves) and after 10^{13} protons/cm^2 fluence (thick gray curves). All intensities are normalized to the GaN-NBE emission.

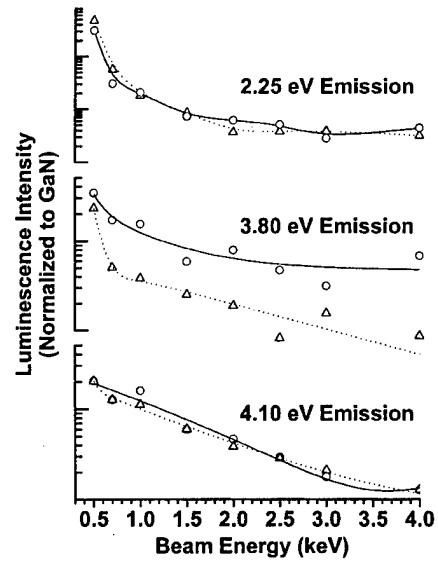

Fig. 6. Intensities and least-squares fits of the 2.25-, 3.8-, and 4.1-eV emissions as a function of electron-beam energy for the MODFET reference die (circle symbols, solid curves) and the 10^{13} protons/cm^2 irradiated die (triangle symbols, dotted curves). These intensities are extracted after normalizing to the GaN NBE.

with incident beam energy E_B. Fig. 6 shows the intensities of these emissions as a function of E_B, with the intensities normalized to the GaN NBE, as in Fig. 4. The 4.1-eV AlGaN emission exhibits an exponential decay with increasing beam energy, consistent with its near-surface location and the increasing depth of excitation with increasing E_B. For $0.5 < E_B < 1.5$ keV corresponding to excitation almost entirely within the AlGaN layers (see Fig. 1), the relative-intensity decay of the 3.8-eV emission is ~50% faster than that of the 4.1-eV feature. This difference indicates that the 3.8-eV feature is associated with a layer located closer to the free surface than that of the 4.1-eV feature. For $0.5 < E_B < 3$ keV, corresponding to overall decay well past the AlGaN/GaN interface, the 3.8-eV and 4.1-eV features exhibit nearly the same decrease. The 2.2–2.4 eV emission normalized to the GaN NBE intensity also exhibits a decrease with increasing E_B, indicating that this luminescence is primarily in the AlGaN layers, rather than the GaN.

Irradiation also produces significant spectral changes in AlGaN/GaN unpatterned HFET layers grown by MBE. Fig. 7 shows 10-K LEEN spectra for reference and irradiated bulk samples for the HFET structure. As before, all spectra have been normalized to the GaN NBE emission. The electron-beam currents were chosen by the method described for the MODFET die, and the total proton fluence of the irradiated specimen was 10^{13} cm^{-2}. The reference HFET sample exhibits emission at 3.49 and 3.73 eV, corresponding to the GaN and AlGaN NBE emissions, respectively. The peak at 3.42 eV can be attributed to a characteristic neutral donor-acceptor (D–A) pair recombination [21]. Additionally, the GaN NBE exhibits a broad sub-GaN shoulder from 3.2–3.4 eV combined with a narrow emission at 3.42 eV. The broad emission may represent Franz–Keldysh red-shifted NBE emission from strained GaN at the two-dimensional electron gas (2DEG) AlGaN/GaN interface or in the thin GaN-cap layer at the free surface.

The irradiated specimen exhibits significant differences compared with the reference spectra. A 3.19-eV emission appears, and its intensity relative to the GaN NBE increases with increasing E_B and proximity to the GaN. This implies the emission originates past the AlGaN layer. Emission at ~3.2 eV has previously been reported for bulk GaN films [22] and has been attributed to a D–A pair transition. A significant decrease in the 3.2–3.4 eV shoulder emission is also observed for all beam energies. A final postirradiation change is the appearance of a

higher energy component of the AlGaN NBE emission, with an apparent peak in the vicinity of ~3.8 eV, when corrected for convolution with the 3.73-eV emission.

IV. Discussion

From the 300-K LEEN spectra of the MOCVD-grown AlGaN/GaN MODFET structures, no significant changes are observed after irradiation in the relative-emission intensities for the AlGaN NBE (4.1 eV) and "yellow" luminescence (2.2–2.4 eV), when normalized to the GaN NBE (3.41 eV). Absolute intensities of the GaN NBE (and consequently the AlGaN NBE and "yellow") were also unchanged, within the uncertainty of optical-collection efficiency for slightly different sample positioning within our SEM (~10)%. Similar GaN-NBE intensity comparisons can be made for the MBE-grown HFET structures. These observations indicate the AlGaN and GaN films are not strongly degraded upon 10^{13} cm^{-2} proton irradiation. Similar results have been observed for photoluminescence studies of thick GaN films, for which the luminescence intensity decreased significantly (nearly three orders of magnitude) only after proton fluences in excess of 10^{13} cm^{-2} [6].

Stopping and range of ions in matter (SRIM) [23] simulations of 1.8-MeV proton irradiation indicate that ionization events dominate the proton energy loss within the AlGaN/GaN structure, with the nonionizing energy loss (NIEL) events comprising only a small fraction (2.4 eV/ion versus 1.24×10^5 eV/ion) [24] of the total. Ionizing irradiation does not produce significant degradation of the films, because the resulting electron-hole pairs recombine quickly. NIEL events are comprised of the generation of lattice phonons and vacancy-interstitial (V–I) pair formation. Even for the low NIEL component of the energy loss, our SRIM simulations indicate the formation of ~10^{16} vacancies/cm^3 in the thin AlGaN layers, based on a displacement-damage threshold of 20 eV. Since V–I pairs can easily recombine after formation, this density can be regarded as an upper limit. However, multiple defect complexes can form that do not readily recombine [25]. Also, GaN damage-threshold energies are not well established and lower values produce significantly higher densities [4]. Our SRIM calculations also show the implanted proton concentration resides far from the AlGaN/GaN layers, with a highly concentrated proton-penetration depth of ~40 μm.

The predominant irradiation-induced change in the MODFET spectral emission is the significant decrease in 3.8-eV emission. A plausible explanation for this feature is a red shift, i.e., a shift to lower luminescence energy, of the AlGaN NBE emission induced by Franz–Keldysh band gap "narrowing," in turn due to the high piezoelectric field of the strained film [26]. Such piezoelectric fields are induced by lattice mismatch between AlGaN and GaN layers, but smaller fields are also present in ultrathin III-nitride films without strain as well [27]. These fields induce a positive-sheet charge at the AlGaN/GaN interface, which in turn induces the 2DEG charge in the MODFET channel. The undoped AlGaN layer is expected to have a high piezoelectric field. A band diagram for this structure, as generated by a one-dimensional Poisson-solver program [28], is shown in Fig. 8, with piezoelectric parameters taken from [29]. The 2DEG region is shown on the GaN side of the AlGaN/GaN interface, and in this region the conduction band is below the GaN Fermi level. With the additional, 10^{18} cm^{-3} Si doped AlGaN layer, the band diagram for this structure exhibits higher electric fields with the outer AlGaN layers (~8×10^5 V/cm) versus the undoped layer (~4×10^5 V/cm) near the AlGaN/GaN interface. Thus, we argue that the higher energy AlGaN emission at 4.1-eV originates in the undoped portion of the AlGaN film near the AlGaN/GaN interface, whereas the red-shifted 3.8-eV emission originates from the higher electric field strength regions of the outer AlGaN layers.

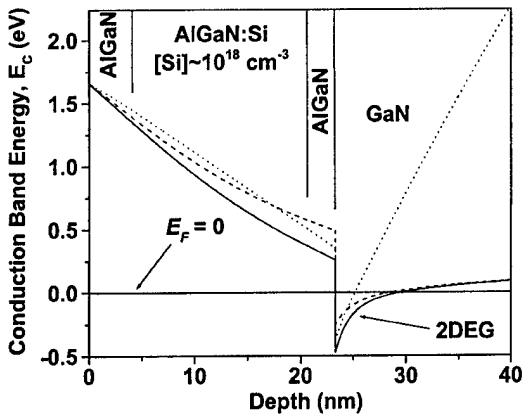

Fig. 8. Band diagram for the MODFET conduction band E_C. The Fermi level E_F is at 0 eV. The solid curve represents the as-received reference sample. The dashed curve represents the effect of changing the polarization parameters and decreasing the maximum internal electric field from ~0.8 MV/cm to ~0.6 MV/cm. The dotted curve represents the effect of adding 10^{18} cm^{-3} acceptors uniformly throughout all layers. In each case, the effect is to decrease the depth and/or effective width of the 2DEG well, thereby reducing the sheet charge in the FET channel.

The LEEN intensities versus depth shown in Fig. 6 support this hypothesis. This figure indicates that the 3.8-eV emission originates from shallower in the multilayer structure than the 4.1-eV emission, indicating preferential 3.8-eV emission from the layers nearest to the free surface. The post-irradiation decrease in the 3.8-eV emission can be interpreted as a decrease in electric field within the AlGaN layers. This decrease could be due to internal electric field screening resulting from charged complexes formed in the AlGaN lattice. Such complexes would need to have areal densities within the AlGaN film comparable to that of the 2DEG channel, e.g., 10^{13} cm^{-2} [27]. New defect complexes can also passivate existing donors [30], thereby reducing carrier concentrations and channel densities. Alternatively, lattice disruption due to such defects may induce sufficient reordering to reduce the as-grown strain and thereby reduce the piezoelectric fields.

The observation that irradiation decreases the electric field is useful in developing physical models for the degradation processes that affect the device-electrical characteristics. Fig. 8 illustrates each effect as calculated by the Poisson solver by independently reducing the polarization-induced sheet charge (and hence the strain in the AlGaN film) or by adding a uniform-acceptor concentration of ~10^{18} cm^{-3} throughout the heterostructure. In each case, the effects are to decrease

the effective AlGaN electric field and increase the energy of the 2DEG well with respect to the GaN Fermi level. These effects will produce the degradation in MODFET saturation current shown in Fig. 2 since the sheet charge density in the 2DEG channel would decrease. The decreases in drain current and transconductance shown in Fig. 3 are also consistent with decreases in 2DEG channel density. Similar effects have been modeled for AlGaN/GaN transistor structures [31]. Using this model, postirradiation changes in threshold voltage extracted from Fig. 3 can be accounted for by a 2.5% reduction in polarization sheet charge, if the n-type carrier concentration is held constant. Such polarization-charge reduction could be due to strain relaxation or preferential acceptor trapping at the AlGaN interfaces. Alternatively, the threshold voltage shift can be accounted for by decreasing net n-type carrier concentration by $\sim 5 \times 10^{17}$ cm^{-3}, while holding the polarization charge constant. This acceptor concentration is ~10–20 times larger than the maximum postirradiation vacancy concentration projected from SRIM. However, it is possible that each simple-point defect projected by SRIM results in multiple-trap complexes that could decrease the donor concentration further [32]. Carrier removal by the formation of defect complexes and/or a reduction in channel mobility will further degrade the device electrical characteristics. However, carrier removal or mobility decreases alone cannot account for the spectral differences observed. Experiments in progress will track changes in free-carrier density, mobility, electrical characteristics, and band bending to distinguish these different mechanisms.

Evidence of AlGaN/GaN electric-field reduction is also present in the HFET bulk samples. The AlGaN emission observed at 3.73 eV prior to irradiation evolves a higher energy component at $\sim$ 3.8 eV after irradiation, suggesting a lower electric field and a resultant shift of the AlGaN emission to higher energy. Since only one undoped AlGaN layer is present in this structure, the AlGaN emission is expected to have only one red-shifted component before irradiation. This is indeed observed as a single 3.73-eV peak. The additional component induced with irradiation can be attributed to reduced fields due to partial screening and/or strain relaxation. The depth dependence of the 3.8-eV emission in Fig. 7 indicates increased intensity at intermediate depths (~20–35 nm for 2–3 keV, respectively), corresponding to the AlGaN layer. Since high fields in this layer could separate electron-beam-excited free electron-hole pairs and reduce NBE emission intensity, a reduction in field strength would increase this intensity in the AlGaN as observed.

The narrow peak at 3.19 eV after proton irradiation has been previously observed in GaN films [21] and is commonly attributed to D–A pair transitions. Fig. 7 shows the intensity of this feature increasing with higher values of E_B, indicating the origin of this feature is in the GaN film, below the channel region. Preliminary analysis of the temperature dependence of the peak intensity (not shown) indicates that it involves a relatively shallow state with low (<25 meV) activation energy. For a nitrogen vacancy V_N, the predominant shallow donor in GaN [33], the corresponding acceptor would then have to be deep (>200 meV), and possibilities include gallium-related defects, including V_{Ga}, V_{Ga} + associated H_n, or V_{Ga} complexed with interstitial N [34]. Gallium-vacancy production by high-energy protons in, e.g., GaAs, is well known [35]. Overall, the LEEN results for irradiated MODFET and MBE-grown AlGaN/GaN structures suggest substantial field reductions due to the creation of charged defects within their AlGaN layers.

Although the predominant spectral changes after irradiation for both sample sets can be attributed to field reduction, it is important to emphasize that these changes are different for each set. For example, unlike the HFET structure, the MODFET structure does not exhibit the evolution of a higher energy counterpart of the primary AlGaN-NBE emission. Similarly, the appearance of a D–A pair emission in the HFET specimen is not observed in the MODFET structure. These differences suggest that the effects of proton irradiation are dependent upon the growth method employed. Such growth dependence is not unexpected, given the substantial differences in H and C exposure between the MOCVD and MBE processes. Further study is in progress to determine the corresponding electrical degradation of devices fabricated on the MBE material, and thereby allowing for direct comparison with the MOCVD material. Fluence-dependence experiments for similar MOCVD and MBE samples are also in progress, to more precisely correlate the evolution of LEEN emission with device-electrical characteristics. These results may well indicate a preferred growth method for improving radiation hardness.

V. Conclusion

Spatially resolved cathodoluminescence spectroscopy studies of AlGaN/GaN MODFET and MBE-grown layered HFET transistor structures reveal spectral differences corresponding to spatially localized changes in electronic properties after 1.8-MeV proton irradiation. These changes indicate a reduction in internal electric-field strength within the AlGaN layers and the formation of charged defects. These localized electronic changes and the associated reduction in charge density induced at the AlGaN/GaN 2DEG interface channel can account for the decreases in MODFET saturation current, drain current, and transconductance observed electrically.

Acknowledgment

The authors would like to thank Dr. D. Look, Wright State University, Dayton, OH, and Dr. R. Weller, Vanderbilt University, Nashville, TN, for valuable conversations. They would also like to thank D. Buttari, L. Shen, S. Heikman, and S. Keller, University of California, Santa Barbara, for the growth and processing of the MODFET material.

References

[1] Y.-F. Wu, D. Kapolnek, J. P. Ibbetson, P. Parikh, B. P. Keller, and U. K. Mishra, "Very-high power density AlGaN/GaN HEMT's," *IEEE Trans. Electron Devices*, vol. 48, pp. 586–590, Mar. 2001.

[2] L. F. Eastman, V. Tilak, J. Smart, B. M. Green, E. M. Chumbes, R. Dimitrov, H. Kim, O. S. Ambacher, N. Weimann, T. Prunty, M. Murphy, W. J. Schaff, and J. R. Shealy, "Undoped AlGan/GaN HEMT's for microwave power amplification," *IEEE Trans. Electron Devices*, vol. 48, pp. 479–485, Mar. 2001.

[3] S. J. Cai, Y. S. Tang, R. Li, Y. Wei, L. Wong, Y. L. Chen, K. L. Wang, M. Chen, Y. F. Zhao, R. D. Schrimpf, J. C. Keay, and K. F. Galloway, "Annealing behavior of a proton irradiated AlxGa1-xN/GaN high electron mobility transistor grown by MBE," *IEEE Trans. Electron Deices*, vol. 47, pp. 304–307, Feb. 2000.

[4] B. Luo, J. W. Johnson, F. Ren, K. K. Allums, C. R. Abernathy, S. J. Pearton, R. Dwivedi, T. N. Fogarty, R. Wilkins, A. M. Dabiran, A. M. Wowchack, C. J. Polley, P. P. Chow, and A. G. Baca, "DC and RF performance of proton-irradiated AlGaN/GaN high electron mobility transistors," *Appl. Phys. Lett.*, vol. 79, no. 14, pp. 2196–2199, Feb. 2001.

[5] ——, "High-energy proton irradiation effects on AlGan/GaN high-electron mobility transistors," *J. Electron. Mater.*, vol. 31, pp. 437–441, May 2002.

[6] S. M. Khanna, J. Webb, H. Tang, A. J. Houdayer, and C. Carlone, "2 MeV proton radiation damage studies of gallium nitride films through low temperature photoluminescence spectroscopy measurements," *IEEE Trans. Nucl. Sci.*, vol. 47, pp. 2322–2328, Dec. 2000.

[7] V. V. Emtsev, V. Y. Davydov, E. E. Haller, A. A. Klochikhin, V. V. Kozlovskii, G. A. Oganesyan, D. S. Poloskin, N. M. Shmidt, V. A. Vekshin, and A. S. Usikov, "Radiation-induced defects in n-type GaN and InN," *Phys. B*, vol. 308–310, pp. 58–61, 2001.

[8] S. A. Goodman, F. D. Auret, F. K. Koschnick, J.-M. Spaeth, B. Beaumont, and P. Gibart, "Radiation induced defects in MOVPE grown n-GaN," *Mater. Sci. Eng. B*, vol. 71, pp. 100–103, 2000.

[9] F. D. Auret, S. A. Goodman, M. Hayes, M. J. Legodi, S. S. Hullavarad, E. Friedland, B. Beaumont, and P. Gibart, "Electrical characterization of epitaxially grown n-GaN bombarded with high- and low-energy protons," *Nucl. Instrum. Methods Phys. Res. B, Beam Interact. Mater. Al.*, vol. 175–177, pp. 292–295, 2001.

[10] M. J. Legodi, S. S. Hullavarad, S. A. Goodman, M. Hayes, and F. D. Auret, "Defect characterization by DLTS and AlGaN UV Schottky photodetectors," *Phys. B*, vol. 308–310, pp. 1189–1192, 2001.

[11] G. A. Umana-Membreno, J. M. Dell, T. P. Hessler, B. D. Nener, G. Parish, L. Faraone, and U. K. Mishra, "^{60}co gamma-irradiation-induced defects in n-GaN," *Appl. Phys. Lett.*, vol. 80, pp. 4354–4356, Jun. 2002.

[12] F. Gaudreau, C. Carlone, A. Houdayer, and S. M. Khanna, "Spectral properties of proton irradiated gallium nitride blue diodes," *IEEE Trans. Nucl. Sci.*, vol. 48, pp. 1778–1784, Dec. 2001.

[13] M. Osinski, P. Perlin, H. Schone, A. H. Paxton, and E. W. Taylor, "Effects of proton irradiation on AlGaN/InGaN/GaN green light emitting diodes," *Electron. Lett.*, vol. 33, pp. 1252–1254, July 1997.

[14] L. J. Brillson, A. P. Young, G. H. Jessen, T. M. Levin, S. T. Bradley, S. H. Goss, J. Bae, F. A. Ponce, M. J. Murphy, W. J. Schaff, and L. F. Eastman, "Low energy electron-excited nano-luminescence spectroscopy of GaN surfaces and interfaces," *Appl. Surf. Sci.*, vol. 175–176, pp. 442–449, May 2001.

[15] L. J. Brillson, "Nanoscale luminescence spectroscopy of defects at buried interfaces and ultrathin films," *J. Vac. Sci. Technol. B*, vol. 19, pp. 1762–1768, Sept./Oct. 2001.

[16] B. D. White, L. J. Brillson, S. C. Lee, D. M. Fleetwood, R. D. Schrimpf, S. T. Pantelides, Y.-M. Lee, and G. Lucovsky, "Low energy electron-excited nanoscale luminescence: A tool to detect trap activation by ionizing radiation," *IEEE Trans. Nucl. Sci.*, vol. 47, pp. 2276–2280, Dec. 2000.

[17] B. D. White, M. Bataiev, L. J. Brillson, D. M. Fleetwood, R. D. Schrimpf, B. K. Choi, and S. T. Pantelides, "Detection of trap activation by ionizing radiation in SiO_2 by spatially localized cathodoluminescence spectroscopy," *J. Appl. Phys.*, vol. 92, pp. 5729–5734, Nov. 2002.

[18] D. Drouin, A. R. Couture, and R. Gauvin, "Casino V2.0: An advance simulation tool for scanning electron microscope users," *Micro. Microanal.*, vol. 7, no. 2, pp. 684–685, 2001.

[19] A. P. Young, J. Bae, L. J. Brillson, M. J. Murphy, and W. J. Schaff, "Depth-resolved spectroscopy of interface defects in GlNaN/GaN heterostructure field effect transistors device structures," *J. Vac. Sci. Technol. B*, vol. 18, pp. 2309–2312, Jul./Aug. 2000.

[20] B. K. Meyer, G. Steude, A. Goldner, A. Hoffmann, H. Amano, and I. Akasaki, "PL investigations of AlGaN on GaN," *Phys. Stat. Sol. B*, vol. 216, pp. 187–191, 1999.

[21] M. Leroux, N. Grandjean, B. Beaumont, G. Nataf, F. Semond, J. Massies, and P. Gibart, "Temperature quenching of photoluminescence intensities in undoped and doped GaN," *J. Appl. Phys.*, vol. 86, pp. 3721–3728, Oct. 1999.

[22] A. Y. Polyakov, A. S. Usikov, B. Theys, N. B. Smirnov, A. V. Govorkov, F. Jomard, N. M. Shmidt, and W. V. Lundin, "Effects of proton implantation on electrical and recombination properties of n-GaN," *Solid-State Electron.*, vol. 44, pp. 1971–1983, 2000.

[23] J. F. Ziegler, J. P. Biersack, and U. Littmark, *The Stopping and Range of Ions in Solids*, 2nd ed. New York: Pergamon, 1996.

[24] X. Hu, B. K. Choi, H. J. Barnaby, D. M. Fleetwood, R. D. Schrimpf, S. C. Lee, S. Shojah-Ardalan, R. Wilkins, U. K. Mishra, and R. Dettmer, "The Energy Dependence of Proton-Induced Degradation in AlGaN/GaN High Electron Mobility Transistors," in *RADECS2002 Workshop Proc.*, 2002, pp. 17–20.

[25] G. P. Summers, E. A. Burke, M. A. Xapsos, C. J. Dale, P. W. Marshall, and E. L. Petersen, "Displacement damage in GaAs structures," *IEEE Trans. Nucl. Sci.*, vol. 35, pp. 1221–1226, Dec. 1988.

[26] C. Wetzel, T. Takeuchi, H. Amano, and I. Akasaki, "Piezoelectric Franz-Keldysh effect in strained GaInN/GaN heterostructures," *J. Appl. Phys.*, vol. 85, pp. 3786–3791, Apr. 1999.

[27] O. Ambacher, J. Majewski, C. Miskys, A. Link, M. Hermann, M. Eickhoff, M. Stutzmann, F. Bernardini, V. Fiorentini, V. Tilak, B. Schaff, and L. F. Eastman, "Pyroelectric properties of Al(In)GaN/GaN hetero- and quantum well structures," *J. Phys. Cond. Matt.*, vol. 13, pp. 1–36, 2001.

[28] G. Snider. 1D Poisson Band Diagram Calculator. Univ. Notre Dame, South Bend, IN. [Online]. Available: http://www.nd.edu/~gsnider/

[29] O. Ambacher, B. Foutz, J. Smart, R. Shealy, N. G. Weimann, K. Chu, M. Murphy, A. J. Sierakowski, W. J. Schaff, L. F. Eastman, R. Dimitrov, A. Mitchell, and M. Stutzmann, "Two dimensional electron gases induced by spontaneous and piezoelectric polarization in undoped and doped AlGaN/GaN heterostructures," *J. Appl. Phys.*, vol. 87, pp. 334–344, Jan. 2001.

[30] D. C. Look, J. W. Hemsky, and J. R. Sizelove, "Residual native shallow donor in ZnO," *Phys. Rev. Lett.*, vol. 82, Mar. 1999.

[31] Rashmi, A. Kranti, S. Haldar, and R. S. Gupta, "Impact of strain relaxation of AlGaN layer on 2-DEG sheet charge density and current voltage characteristics of lattice mismatched AlGaN/GaN HEMT's," *Microelectron. J.*, vol. 33, pp. 205–212, Mar. 2002.

[32] L. Polenta, Z.-Q. Fang, and D. C. Look, "On the main irradiation-induced defect in GaN," *Appl. Phys. Lett.*, vol. 76, pp. 2086–2088, Apr. 2000.

[33] D. C. Look, D. C. Reynolds, J. W. Hemsky, J. R. Sizelove, R. L. Jones, and R. J. Molnar, "Defect donor and acceptor in GaN," *Phys. Rev. Lett.*, vol. 79, pp. 2273–2276, Sep. 1997.

[34] D. C. Look, "Defect-related donors, acceptors, and traps in GaN," *Phys. Stat. Sol. B*, vol. 228, pp. 293–302, Nov. 2001.

[35] S. M. Khanna, A. Jorio, C. Carlone, M. Parenteau, A. Houdayer, and J. W. Gerdes Jr., "Particle dependence of the gallium vacancy production rate in irradiated n-type GaAs," *IEEE Trans. Nucl. Sci.*, vol. 42, pp. 2095–2103, Dec. 1995.

Appendix G

Proton-irradiation effects on AlGaN/AlN/GaN high electron mobility transistors

Proton-Irradiation Effects on AlGaN/AlN/GaN High Electron Mobility Transistors

Xinwen Hu, *Member, IEEE*, Aditya P. Karmarkar, *Student Member, IEEE*, Bongim Jun, *Member, IEEE*, Daniel M. Fleetwood, *Fellow, IEEE*, Ronald D. Schrimpf, *Fellow, IEEE*, Robert D. Geil, Robert A. Weller, *Member, IEEE*, Brad D. White, Mykola Bataiev, Leonard J. Brillson, *Fellow, IEEE*, and Umesh K. Mishra, *Fellow, IEEE*

***Abstract*—The degradation of AlGaN/AlN/GaN high electron mobility transistors due to 1.8-MeV proton irradiation was measured at fluences up to 3×10^{15} cm^{-2}. The devices have much higher mobility than AlGaN/GaN devices, but they possess similarly high radiation tolerance, exhibiting little degradation at fluences up to 1×10^{14} cm^{-2}. Decreased sheet carrier mobility due to increased carrier scattering and decreased sheet carrier density due to carrier removal are the primary damage mechanisms. The device degradation is observed as a decrease in the maximum transconductance, an increase in the threshold voltage, and a decrease in the drain saturation current.**

***Index Terms*—Gallium alloys, MODFETs, proton radiation effects.**

I. Introduction

GALLIUM nitride-based high electron mobility transistors (HEMT) have attracted much research interest and have emerged as promising candidates for high-power applications at microwave frequencies. The most important advantages of these devices are the large energy bandgap difference (GaN: 3.4 eV; AlN: 6.2 eV) and high electron velocity (10^7 cm/s), which lead to a high density of sheet charge and high current density. Moreover, gallium nitride-based thin film structures are suitable for bandgap engineering, resulting in a wide variety of electrical characteristics. These properties, combined with the high thermal stability, make gallium nitride-based devices suitable for high-power, high-frequency applications. Gallium nitride-based devices also have the potential to exhibit extremely high radiation hardness [1], [2]. These devices can be more radiation tolerant than gallium-arsenide-based devices because of a higher displacement threshold energy (T_d), which is inversely proportional to the lattice constant [1]–[3]. For hexagonal gallium nitride, the lattice constants are $a = 0.319$ nm and $c = 0.519$ nm, as compared with $a = 0.5653$ for zinc-blende gallium arsenide [2], [4]. The electrical properties of gallium-nitride-based devices, i.e., the ability to handle high power and high frequencies, make these devices suitable for broadband communication systems. Systems employing GaN devices will be deployed in space, where they are exposed to both particle and electromagnetic radiation. Hence, it is important to understand the radiation tolerance of gallium-nitride-based electronic devices.

Previous studies observed significant total-dose-induced degradation in AlGaN/GaN HEMTs only after a γ-ray (^{60}Co) dose of 600 Mrad(Si) [5]. Deterioration in electrical properties was reported at the relatively low fluence of 5×10^9 cm^{-2} 40-MeV protons, but this was a surprising result that was not confirmed in the other studies mentioned below [5], [6]. Other investigators [7] observed significant degradation in the maximum transconductance of AlGaN/GaN HEMTs only after a fluence of 10^{14} cm^{-2} 1.8-MeV protons. The energy dependence of proton-induced degradation in AlGaN/GaN HEMTs was previously investigated using 1.8-, 15-, 40-, and 105-MeV proton irradiations [8]. No significant degradation was observed at fluences of 10^{13} cm^{-2} or less for 15-, 40-, and 105-MeV proton irradiations. However, significant degradation occurred due to 1.8-MeV proton irradiations. These results lead us to conclude that the gallium-nitride-based devices studied to date are extremely radiation tolerant and displacement damage is the primary phenomenon responsible for the degradation.

In this work, we describe the radiation response of a novel AlGaN/AlN/GaN heterostructure [9], irradiated with 1.8-MeV protons at fluences from 3×10^{11} cm^{-2} to 3×10^{15} cm^{-2}. We compare these results with results previously obtained for conventional AlGaN/GaN devices. Introduction of a thin AlN layer in the heterostructures enhances the physical properties and results in better performance. We find that the AlGaN/AlN/GaN devices examined here exhibit improved sheet carrier mobility compared with AlGaN/GaN devices without a significant change in the radiation response of the

Manuscript received July 22, 2003; revised September 8, 2003. This work was supported in part by the AFOSR Multidisciplinary University Research Initiative (MURI).

X. Hu was with the Department of Electrical Engineering, Vanderbilt University, Nashville, TN 37235 USA. He is now with Spang and Company, Pittsburgh, PA 15238 USA (e-mail: xinwen.hu@vanderbilt.edu).

A. P. Karmarkar is with the Interdisciplinary Program in Materials Science, Vanderbilt University, Nashville, TN 37235 USA (e-mail: a.karmarkar@vanderbilt.edu).

B. Jun, D. M. Fleetwood, R. D. Schrimpf, and R. A. Weller are with the Department of Electrical Engineering, Vanderbilt University, Nashville, TN 37235 USA (e-mail: bongim.jun@vanderbilt.edu; dan.fleetwood@vanderbilt.edu; ron.schrimpf@vanderbilt.edu; Robert.a.weller@vanderbilt.edu).

R. D. Geil is with the Department of Chemical Engineering, Vanderbilt University, Nashville, TN 37235 USA (telephone: 615-322-1564, e-mail: bob.geil@vanderbilt.edu).

B. D. White and L. J. Brillson are with the Department of Electrical Engineering, Ohio State University, Columbus, OH 43210 USA (e-mail: whiteb@ece.eng.ohi-state.edu; brillson.1@osu.edu).

M. Bataiev is with Department of Physics, Ohio State University, Columbus, OH 43210 USA (e-mail: batayev@mps.ohio-state.edu).

U. K. Mishra is with the Department of Electrical Engineering, University of California at Santa Barbara, Santa Barbara, CA 93106 USA (e-mail: misra@ece.ucsb.edu).

Digital Object Identifier 10.1109/TNS.2003.820792

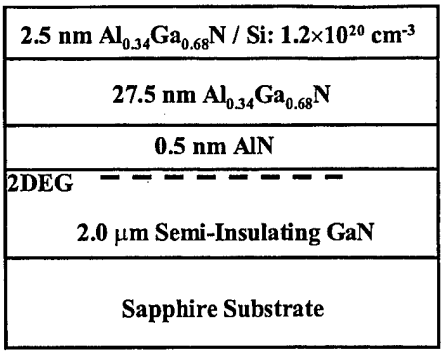

Fig. 1. Schematic cross-section of an AlGaN/AlN/GaN HEMT. Conduction is through the 2DEG. The gate length (L_g) is 1.0 μm and the gate width (W) is 150 μm.

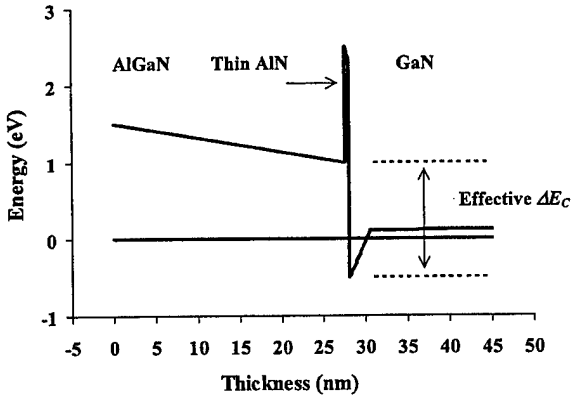

Fig. 2. Schematic conduction band diagram of an AlGaN/AlN/GaN HEMT [9].

devices. To the best of our knowledge, this is the first time that radiation effects in AlGaN/AlN/GaN devices have been studied, including proton radiation effects.

II. Experiment

The AlGaN/AlN/GaN HEMTs were fabricated at the University of California at Santa Barbara (UCSB) and packaged at the Air Force Research Laboratory (AFRL). The AlGaN/AlN/GaN heterostructures were fabricated by metallorganic chemical vapor deposition (MOCVD) on a c-plane sapphire substrate. The gate length is 1 μm, and the gate width is 150 μm. The distance between the gate and the drain is 1.4 μm. The distance between the gate and the source is 1 μm. A schematic cross section of the device is shown in Fig. 1.

The structure consists of 2 μm of semi-insulating GaN on top of the c-plane sapphire substrate, a 0.5-nm interfacial layer, a 27.5-nm unintentionally doped (UID) $Al_{0.34}Ga_{0.68}N$ spacer layer, and on top of a 2.5-nm $Al_{0.34}Ga_{0.68}N$ silicon-doped cap layer with doping concentration of 1.2×10^{20} cm^{-3}. The schematic band diagram for the AlGaN/AlN/GaN structure is shown in Fig. 2 [9]. In this structure, the difference in values of spontaneous polarization and band gap for GaN ($P_{sp} = -2.9 \times 10^{-6}$ C/cm^2) and AlN ($P_{sp} = -8.1 \times 10^{-6}$ C/cm^2) result in a large discontinuity in the conduction band [10]. AlGaN, on the other hand, has a lower band gap and lower spontaneous polarization than AlN and, consequently, the conduction band discontinuity is smaller for the AlGaN/GaN structure. Since the sheet carrier mobility depends on the conduction band discontinuity, insertion of the thin AlN ($\sim$ 0.5 nm) layer increases the sheet carrier mobility compared with conventional AlGaN/GaN heterostructures devices having equivalent AlGaN parameters [9]. Hall measurements at 300 K show that, prior to irradiation, the sheet carrier mobility for the AlGaN/AlN/GaN structure is 1600 cm^2/V $\cdot$ s and that for the AlGaN/GaN structure is 1000 cm^2/V $\cdot$ s.

Samples were diced and mounted in 40-pin dual inline packages (DIPs). Proton irradiations were performed at Vanderbilt University using a 2-MeV Van de Graaff accelerator with raster scanning. The devices were irradiated at room temperature with a proton energy of 1.8 MeV; the ion currents were between 6 nA and 40 nA; the proton fluences ranged from 3×10^{11} cm^{-2} to 3×10^{15} cm^{-2}. All the terminals were grounded during irradiation. After irradiation, the samples were measured immediately using a HP4156A semiconductor parameter analyzer. All of the measurements were performed at room temperature. In addition to packaged devices, thin films were also irradiated and characterized for sheet charge density and mobility using the Van der Pauw method.

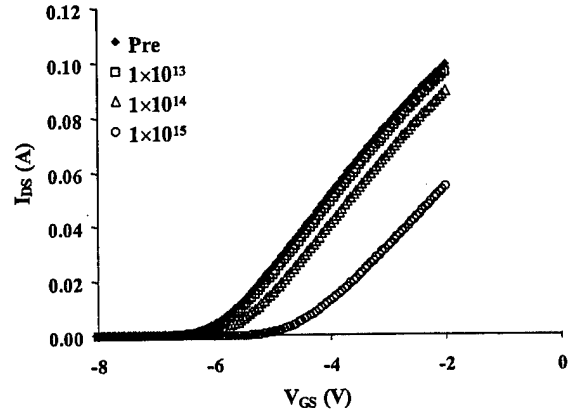

Fig. 3. I_{DS} versus V_{GS} for AlGaN/AlN/GaN HEMTs before and after 1.8-MeV proton irradiation at RT with fluences between 1×10^{13} cm^{-2} and 1×10^{15} cm^{-2}.

III. Results

The transfer characteristics (I_{DS} versus V_{GS} and g_m versus V_{GS}) of a HEMT before and after 1.8-MeV proton irradiation are shown in Figs. 3 and 4. No significant degradation is observed for proton fluences below 1×10^{14} cm^{-2}. As the fluence increases further, the drain current decreases and the threshold voltage V_{TH} shifts toward more positive values.

The dependence of the drain saturation current on proton fluence is presented in Fig. 5. The results for $V_{GS} = -2$ V and -3 V are shown. The saturation current does not degrade significantly for fluences less than 1×10^{14} cm^{-2}. Beyond this level, the device degradation becomes significant and the drain saturation current drops to about 50% and 80% of its pre-irradiation level at fluences of 1×10^{15} cm^{-2} and 3×10^{15} cm^{-2}, respectively.

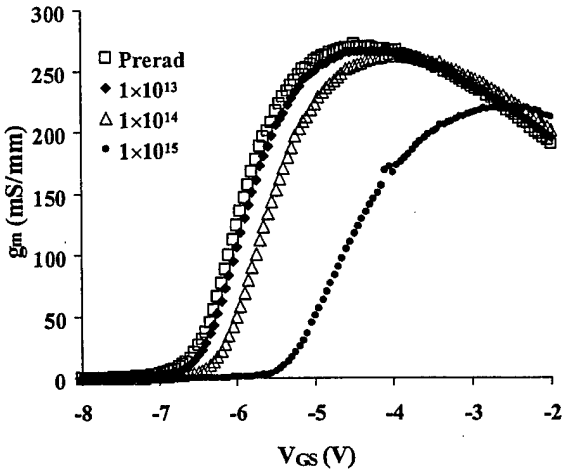

Fig. 4. g_m versus V_{GS} for AlGaN/AlN/GaN HEMTs before and after 1.8-MeV proton irradiation at RT with fluences between 1×10^{13} cm^{-2} and 1×10^{15} cm^{-2}.

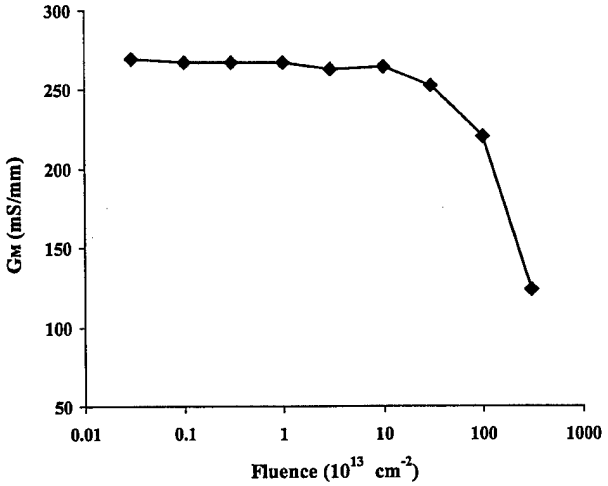

Fig. 6. Maximum transconductance G_M before and after 1.8-MeV proton irradiation at RT with fluences between 3×10^{11} cm^{-2} and 3×10^{15} cm^{-2}.

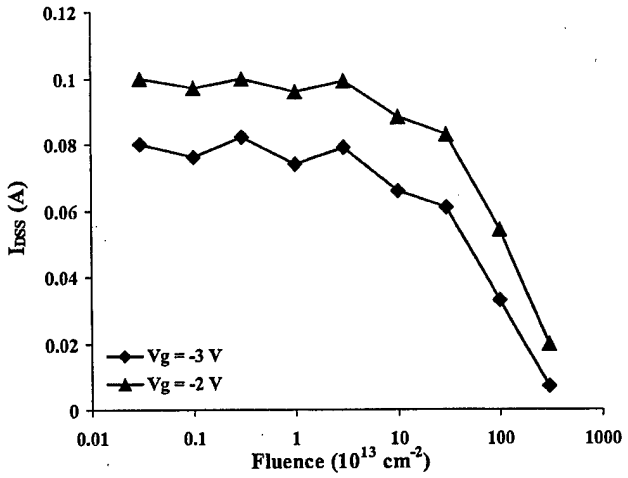

Fig. 5. Drain saturation current I_{DSS} before and after 1.8-MeV proton irradiation at RT with fluences between 3×10^{11} cm^{-2} and 3×10^{15} cm^{-2}.

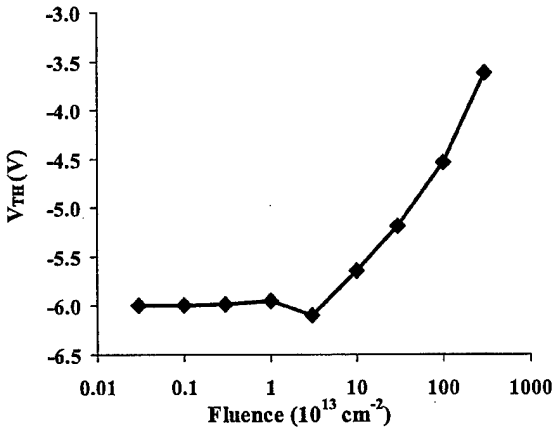

Fig. 7. Threshold voltage versus 1.8-MeV proton fluence.

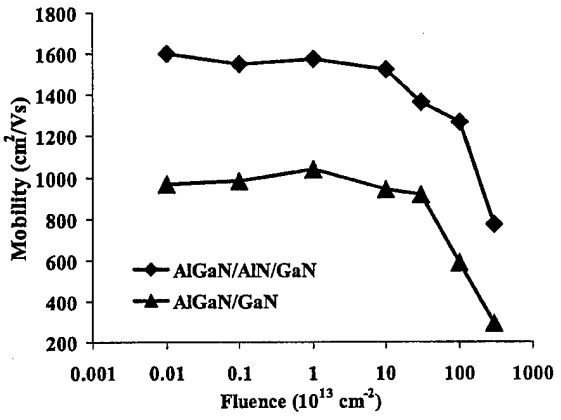

Fig. 8. Mobility versus 1.8-MeV proton fluence (determined from Hall effect measurement).

Fig. 6 shows the maximum transconductance (G_M) for different proton fluences. Prior to irradiation, G_M is 272 mS/mm, and for fluences up to 1×10^{14} cm^{-2}, it is nearly constant. It degrades at higher fluences, decreasing by $\sim 55\%$ at a fluence of 3×10^{15} cm^{-2}.

The threshold-voltage shift is plotted as a function of the proton fluence in Fig. 7. The devices are depletion-mode, so the threshold voltage is negative. Since these devices are expected to handle high power at microwave frequencies, a high threshold voltage may prove to be advantageous. Threshold voltages of the order of ~ -4.0 V have previously been reported for AlGaN/GaN devices and the value can be controlled by altering the doping levels in the thin-film structure [8]. For the present devices, the threshold voltage, V_{TH}, changes very little from its pre-irradiation value of -6.0 V for fluences below 1×10^{14} cm^{-2}. However, V_{TH} shifts to -3.5 V at a fluence of 3×10^{15} cm^{-2}.

Figs. 8 and 9 show the sheet carrier mobility and sheet carrier density as functions of proton fluence for AlGaN/AlN/GaN and AlGaN/GaN thin films, measured using the Van Der Pauw method. The AlGaN/AlN/GaN thin films exhibit consistently higher mobility than the AlGaN/GaN thin films. The AlGaN/AlN/GaN films have a preirradiation mobility

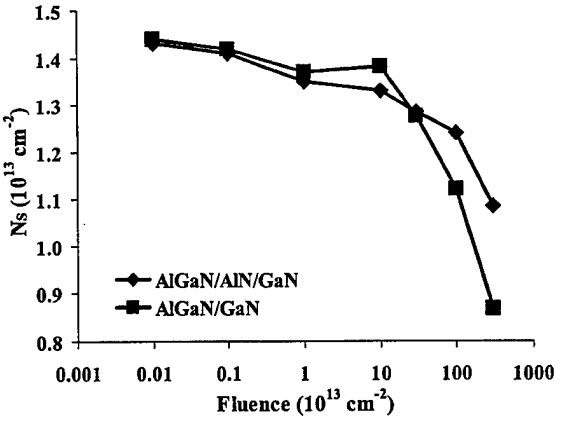

Fig. 9. Sheet carrier density versus 1.8-MeV proton fluence (determined from Hall effect measurement).

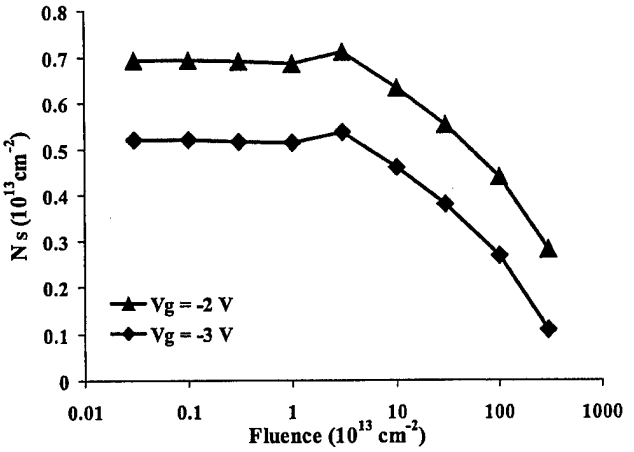

Fig. 10. Sheet carrier density calculated from the electrical characterization data versus 1.8-MeV proton fluence.

of $\sim$ 1600 cm^2/V $\cdot$ s, whereas the AlGaN/GaN thin films have a preirradiation mobility of $\sim$ 1000 cm^2/V $\cdot$ s. Both types of thin film structures have similar sheet carrier densities ($\sim 1.5 \times 10^{13}$ cm^{-2}) prior to irradiation. For all the data plotted as a function of fluence, the pre-irradiation values are virtually the same as the values measured at a fluence of 3×10^{11} cm^{-2}.

IV. Discussion

A. Ionization Effects

Previous researchers observed very little degradation in gallium nitride-based devices after exposure to γ radiation [5]. Earlier 10-keV X-ray experiments with the AlGaN/GaN high electron mobility transistors found no significant changes after a total ionizing dose of 30 Mrad(SiO_2) [8]. These results lead to the conclusion that ionization effects are relatively unimportant in determining the radiation response of GaN-based high electron mobility transistors. Moreover, the AlGaN/AlN/GaN devices considered here are structurally very similar to the AlGaN/GaN devices, which showed little degradation after exposure to X-ray irradiation. Therefore, the experiments reported here focused on displacement damage caused by proton irradiation.

B. Displacement Damage Effects

Proton irradiation displaces atoms in the crystal lattice and introduces defect centers in the device. These defect centers influence the sheet carrier density and mobility [3], [10]–[12]. To check the influence of radiation on the sheet carrier density and mobility of the two-dimensional electron gas (2DEG), a simple charge control model for the AlGaN/GaN system is used, similar to the charge control model used to describe GaAs-based HEMTs [13].

Placing a Schottky gate on the AlGaN layer results in depletion beneath the gate. If the AlGaN layer is thin enough, or a sufficiently large negative gate voltage is applied, the gate depletion and junction depletion regions will overlap. In this case the sheet carrier density of the 2DEG is given by

$$n_s = \frac{\varepsilon}{qd}\left[V_{GS} - (\phi_b - V_P - \Delta E_C)\right] \tag{1}$$

where ϕ_b is the Schottky barrier height and

$$V_P = \frac{qN_d d_d^2}{2\varepsilon} \tag{2}$$

is the pinch-off voltage of the AlGaN layer. Here d_d is the thickness of the AlGaN beneath the gate.

The charge control model assumes that, in the linear regions of the I_D-V_D plot, the drain current is proportional to the sheet carrier density, channel length, and the electric field. The electric field is proportional to the drain voltage and the sheet carrier density depends on the applied gate voltage. Using these approximations, the following relation can be obtained from the charge control model:

$$\frac{V_{DS}}{I_{DS}} = R_S + R_D + \frac{Ld}{\mu W \varepsilon (V_{GS} - V_{\mathrm{OFF}})} \tag{3}$$

where R_S and R_D are the source and drain access resistances, and L and W are the gate length and width. V_{OFF} is the "off voltage" that annihilates the 2DEG:

$$V_{\mathrm{OFF}} = \phi_b - \Delta E_C - V_P. \tag{4}$$

For the present devices, $V_P = 0$, because the AlGaN layer is not intentionally doped. The off voltage, V_{OFF}, is then equal to the threshold voltage V_{TH}:

$$V_{\mathrm{OFF}} = \phi_b - \Delta E_C = V_{TH}. \tag{5}$$

Combining (1) and (5) and using the fact that $V_P = 0$, the sheet carrier density can be calculated from

$$n_s = \frac{\varepsilon}{qd}\left[V_{GS} - V_{TH}\right]. \tag{6}$$

The threshold voltage is determined from the I_{DS}-V_{GS} characteristics. The calculated sheet carrier density is plotted as a function of proton fluence in Fig. 10. To calculate the mobility, V_{DS}/I_{DS} is calculated in the linear region of the I-V curve, i.e., at low drain voltages. The V_{DS}/I_{DS} values are plotted versus $1/(V_{GS} - V_{OFF})$. Fig. 11 shows a representation of the V_{DS}/I_{DS} versus $1/(V_{GS} - V_{OFF})$ plot. The slope of this plot is related to the sheet carrier mobility and the intercept is related to

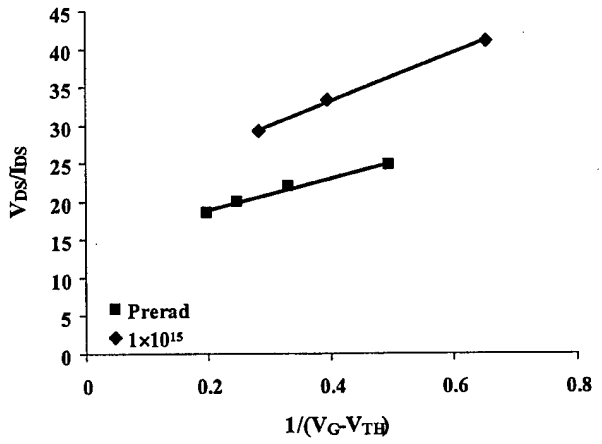

Fig. 11. Example of the V_{DS}/I_{DS} versus $1/(V_G - V_{TH})$ plots used to determine the mobility.

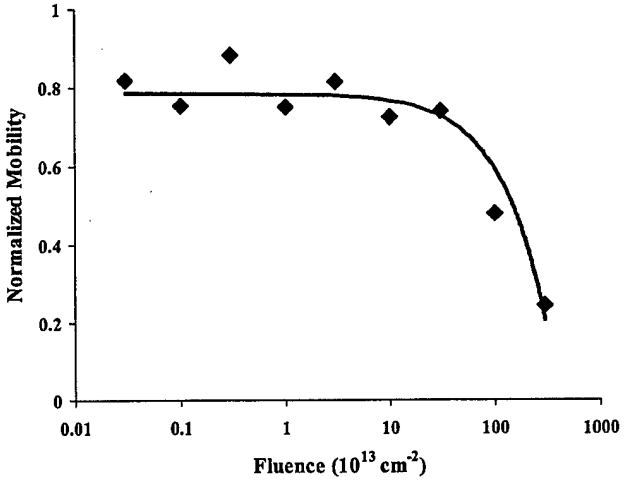

Fig. 12. Normalized mobility calculated from the I_{DS}-V_{DS} plots versus 1.8-MeV proton fluence.

the source and drain access resistance. Variation of sheet carrier mobility with proton fluence is calculated using a linear fit of the I_{DS}-V_{DS} data. The calculated mobility is shown in Fig. 12 for different proton fluences. No significant degradation is found for proton fluences below 10^{14} cm^{-2}. At higher fluences, a significant decrease in mobility is observed.

For 1.8-MeV proton irradiation, these AlGaN/AlN/GaN HEMTs exhibited no significant degradation at proton fluences up to 10^{14} cm^{-2}. Including the AlN layer in the AlGaN/AlN/GaN structure results in a large decrease in alloy disorder scattering at the AlN/GaN interface, leading to an increase in mobility. The difference in the band gaps of AlN and GaN leads to a higher conduction-band discontinuity that results in lower electron penetration into the AlGaN. All of these effects combine to yield a higher mobility of carriers in the sheet charge [14] and, hence, improved device performance.

Similar behavior is observed in the thin film structures. Figs. 8 and 9 show the sheet carrier mobility and sheet carrier density for AlGaN/AlN/GaN and AlGaN/GaN heterostructures at different fluences. Fig. 8 shows that the AlGaN/AlN/GaN devices exhibit consistently higher mobility than the AlGaN/GaN devices over the entire fluence range. Fig. 9 shows that both the AlGaN/AlN/GaN and AlGaN/GaN devices exhibit similar degradation patterns for the sheet carrier density. These results support the conclusion that introduction of the thin AlN layer results in improved mobility, and hence better performance, without decreasing the radiation tolerance of the devices.

C. Damage Mechanisms

At very high proton fluences, displacement damage degrades the characteristics of the devices studied here. Incident protons displace atoms from their lattice sites and create charged defect centers. Interaction of carriers with charged defect centers in the lattice is responsible for carrier scattering and overall degradation in electrical properties in these devices [15].

A number of mechanisms have been postulated to explain device degradation in HEMTs due to interaction between carriers and defect centers [11], [12]. Defect centers can be introduced inside or outside the 2-D electron gas. As the 2-D electron gas has an infinitesimal thickness, the probability of an incident proton creating a defect center inside the 2-D electron gas is small. Thus, the majority of the defect centers are formed outside the 2-D electron gas. However, the charged defect centers outside the 2-D electron gas scatter the carriers through Coulomb interactions and significantly affect the mobility in the 2-D electron gas. At higher fluence levels, mobility degradation is the dominant mechanism responsible for the device-level effects described above.

Proton irradiation may also increase the interface roughness at the AlN/GaN interface [10]. Since the 2-D electron gas is situated in the GaN near the AlN/GaN interface, increased roughness at that interface may increase carrier scattering and consequently lead to lower mobility. However, for the experiments described here, mobility degradation due to increased interface roughness is not important since it is a significant mechanism only at low temperatures [10].

Defect centers that are created inside the 2-D electron gas may trap the carriers and lead to a decrease in sheet carrier density [11], [12]. For these devices, $\sim$ 30% degradation in the sheet carrier density is observed at a proton fluence of 1×10^{14} particles/cm^2. The sheet carrier mobility also shows a similar decrease at a fluence of $\sim 3\times10^{14}$ particles/cm^2. From these results, it is evident that the device degradation after proton irradiation is due to both the decrease in the sheet carrier mobility and the decrease in the sheet carrier density.

V. Summary

We report the proton-radiation response of a new type of AlGaN/AlN/GaN HEMT. The introduction of a thin AlN barrier layer improves the sheet carrier mobility due to the higher conduction band discontinuity. The AlGaN/AlN/GaN devices show improved properties over the AlGaN/GaN devices without compromising the radiation tolerance. The devices show no significant degradation for 1.8-MeV proton irradiation at fluences up to 10^{14} cm^{-2}. This strongly suggests these devices are well suited for most space applications. Moreover, the device degradation due to higher energy protons would be significantly lower than that due to lower energy protons, as suggested

by previous studies with similar devices [8]. As the fluence goes up, the drain saturation current and maximum transconductance decrease and the threshold voltage becomes more positive, which is mainly due to displacement damage-induced decreases of carrier density and mobility in the sheet charge. Carrier scattering and carrier removal due to radiation-induced defect centers are the primary degradation mechanisms.

ACKNOWLEDGMENT

The authors would like to thank R. Dettmer of the Air Force Research Laboratory for packaging the devices.

REFERENCES

[1] S. M. Khanna, J. Webb, H. Tang, A. J. Houdayer, and C. Carlone, "2 MeV proton radiation damage studies of gallium nitride films through low temperature photoluminescence spectroscopy measurements," *IEEE Trans. Nucl. Sci.*, vol. 47, pp. 2322–2328, Dec. 2000.

[2] J. W. Corbett and J. C. Bourgoin, *Defect Creation in Semiconductors, Point Defects in Solids*, J. H. Crawford and F. F. Slifkin, Eds. New York: Plenum, 1975, vol. 2, ch. 1.

[3] A. Ionascut-Nedelcescu, C. Carlone, A. Houdayer, H. J. von Bardeleben, J.-L. Cantin, and S. Raymond, "Radiation hardness of gallium nitride," *IEEE Trans. Nucl. Sci.*, vol. 49, pp. 2733–2738, Dec. 2002.

[4] D. C. Look, D. C. Reynolds, J. W. Hemsky, J. R. Sizelove, R. L. Jones, and R. J. Molnar, "Defect donor and acceptor in GaN," *Phys. Rev. Lett.*, vol. 79, no. 12, pp. 2273–2276, 1997.

[5] B. Luo, J. W. Johnson, F. Ren, K. K. Allums, C. R. Abernathy, S. J. Pearton, A. M. Dabiran, A. M. Wowchack, C. J. Polley, P. P. Chow, D. Schoenfeld, and A. G. Baca, "Influence of Co-60 γ-rays on DC performance of AlGaN/GaN high electron mobility transistors," *Appl. Phys. Lett.*, vol. 80, pp. 604–606, 2002.

[6] B. Luo, J. W. Johnson, F. Ren, K. K. Allums, C. R. Abernathy, S. J. Pearton, R. Dwivedi, T. N. Fogarty, R. Wilkins, A. M. Dabiran, A. M. Wowchack, C. J. Polley, P. P. Chow, and A. G. Baca, "DC and RF performance of proton-irradiated AlGaN/GaN high electron mobility transistors," *Appl. Phys. Lett.*, vol. 79, pp. 2196–2199, 2001.

[7] S. J. Cai, Y. S. Tang, R. Li, Y. Wei, L. Wong, Y. L. Chen, K. L. Wang, M. Chen, Y. F. Zhao, R. D. Schrimpf, J. C. Keay, and K. F. Galloway, "Annealing behavior of a proton irradiated $Al_xGa_{1-x}N$/GaN high electron mobility transistor grown by MBE," *IEEE Trans. Electron Devices*, vol. 47, pp. 304–307, Feb. 2000.

[8] X. Hu, B. K. Choi, H. J. Barnaby, D. M. Fleetwood, R. D. Schrimpf, S. C. Lee, S. Shojah-Ardalan, R. Wilkins, U. K. Mishra, and R. Dettmer, "The energy dependence of proton-induced degradation in AlGaN/GaN high electron mobility transistors," in *Proc. 2002 Radiation and its Effect on Components and Systems (RADEC) Workshop*, Padova, Italy, Sept. 2002.

[9] L. Shen, S. Heikman, B. Moran, R. Coffie, N.-Q. Zhang, D. Buttari, I. P. Smorchkova, S. Keller, S. P. DenBaars, and U. K. Mishra, "AlGaN/AlN/GaN high-power microwave HEMT," *IEEE Electron Device Lett.*, vol. 22, pp. 457–459, Oct. 2001.

[10] Y. Zhang, I. P. Smorchkova, C. R. Elsass, S. Keller, J. P. Ibbetson, S. DenBaars, U. K. Mishra, and J. Singh, "Charge control and mobility in AlGaN/GaN transistors: Experimental and theoretical studies," *J. Appl. Phys.*, vol. 87, no. 11, pp. 7981–7987, 2000.

[11] F. Gaudreau, P. Fournier, C. Carlone, S. M. Khanna, H. Tang, J. Webb, and A. Houdayer, "Transport properties of proton-irradiated gallium nitride-based two-dimensional electron-gas system," *IEEE Trans. Nucl. Sci.*, vol. 49, pp. 2702–2707, Dec. 2002.

[12] B. Jun and S. Subramanian, "Carrier removal rate and mobility degradation in heterojunction field effect transistor structures," *IEEE Trans. Nucl. Sci.*, vol. 49, pp. 3222–3229, Dec. 2002.

[13] M. Shur, *GaAs Devices and Circuits*. New York: Plenum, 1986.

[14] L. Hsu and W. Walukiewicz, "Effect of polarization fields on transport properties in AlGaN/GaN heterostructures," *J. Appl. Phys.*, vol. 89, pp. 1783–1789, 2001.

[15] ——, "Electron mobility in $Al_xGa_{1-x}N$/GaN heterostructures," *Phys. Rev. B.*, vol. 56, no. 3, pp. 1520–1528, 1997.

Appendix H

Proton-Induced Degradation in AlGaAs/GaAs Heterojunction Bipolar Transistors

Proton-Induced Degradation in AlGaAs/GaAs Heterojunction Bipolar Transistors

Xinwen Hu, *Member, IEEE*, Bo K. Choi, *Member, IEEE*, Hugh J. Barnaby, Daniel M. Fleetwood, *Fellow, IEEE*, Ronald D. Schrimpf, *Fellow, IEEE*, Kenneth F. Galloway, *Fellow, IEEE*, Robert A. Weller, *Member, IEEE*, Kyle McDonald, Umesh K. Mishra, *Fellow, IEEE*, and Ross W. Dettmer

***Abstract*—The effects of 1.8-MeV and 105-MeV proton irradiation on AlGaAs/GaAs heterojunction bipolar transistors (HBTs) are reported. For 1.8-MeV protons, the degradation of the transistors is caused by an increase in the base current and a large decrease in the collector current. The device degradation is much less after irradiation with 105-MeV protons, because of lower nonionizing energy loss (NIEL) in the sensitive region of the device. There is no improvement in device performance after three months of room temperature annealing.**

***Index Terms*—Displacement damage, GaAs, heterojunction bipolar transistors (UBTs), nonionizing energy loss (NIEL), proton radiation effects.**

TABLE I
TYPICAL VERTICAL STRUCTURE OF THE GaAs HBT

Doping	Layers	Thickness (Å)	X	Concentration (cm^{-3})
n^+	InGaAs	500	0.6	1×10^{19}
n^+	InGaAs	500	0->0.6	1×10^{19}
n	GaAs	1000		5×10^{18}
n	AlGaAs	300	0.28->0	4×10^{18}
n	AlGaAs	700	0.28	1.5×10^{17}
n	AlGaAs	300	0->0.28	1.5×10^{17}
p^+	GaAs	800		4×10^{19}
n	GaAs	10000		1×10^{16}
n	GaAs	6000		5×10^{18}
n	AlGaAs	100	0.28	-
n	GaAs	100		-

I. INTRODUCTION

AlGaAs/GaAs heterojunction bipolar transistors (HBTs) are promising devices for high-speed and high-frequency operation. Their superior high-speed potential and high-current handling capabilities have made AlGaAs/GaAs HBTs an important option for RF and microwave circuit technologies in space communication systems. Understanding the radiation response of these devices is of high interest for space applications. Many papers have reported the radiation response of SiGe HBTs (see, for example, [1]–[4]), but less work has been done on GaAs-based HBTs [2], [5], and [6]. In this paper, we report the effects of proton irradiation on AlGaAs/GaAs HBTs. The devices are very radiation tolerant in the high-energy proton environment (105 MeV) examined here, suggesting that they are excellent candidates for space applications. Lower energy (1.8-MeV) proton irradiations were conducted to understand the degradation mechanisms in the devices. Low-energy protons are much more damaging because they deposit more energy in the active device region. At the lower energy, a large decrease in the collector current occurred due to decreased electron injection efficiency. Monte Carlo simulation is used to calculate the nonionizing energy loss (NIEL) in the device and good correlation with device degradation is found.

II. EXPERIMENTS

The AlGaAs/GaAs HBT devices were fabricated at the University of California at Santa Barbara (UCSB) using MOCVD and packaged at the Air Force Research Laboratory (AFRL). A representative cross section of the vertical epitaxial AlGaAs/GaAs HBTs studied in this work is shown in Table I. The layers are grown in order from the bottom of the chart to the top. The x column refers to the ratio of the corresponding ternary $Al_xGa_{1-x}As$ or $In_xGa_{1-x}As$ material. A graded layer is indicated by an arrow between two ratios—for example, 0.28 → 0 indicates a gradation from 28% Al to no Al from the bottom (or first-grown part) of the layer to the top (or last-grown portion) of the layer. The concentration column is doping in cm^{-3}. Silicon doping is used except for the p^+-type base (the 800-Å GaAs layer doped to 4×10^{19} cm^{-3}), which is carbon-doped. As shown in Table I, from the top to the bottom, the first two 500-Å InGaAs layers are n^+ cap layers; the next 1000-Å GaAs layer also is a cap layer. The AlGaAs layer is the emitter. The 800-Å is also GaAs layer with concentration of 4×10^{19} cm^{-3} is the p^+-type base. The 10 000-Å GaAs layer is the collector, and there is a 6000-Å GaAs n-type subcollector layer.

Fig. 1 shows a cross-sectional view of the HBT device structure. All contacts are identified in the figure. The emitter area is 150 μm^2. The emitter metallization is approximately 8 μm of plated gold. The AlGaAs is the wide-bandgap emitter of the heterostructure—the extra band discontinuity caused by using a heterostructure allows the base to be heavily doped while still maintaining good injection efficiency. The GaAs portion of the emitter

Manuscript received July 16, 2002; revised September 6, 2002.

X. Hu, B. K. Choi, D. M. Fleetwood, R. D. Schrimpf, K. F. Galloway, and R. A. Weller are with the Department of Electrical Engineering and Computer Science, Vanderbilt University, Nashville, TN 37235 USA (e-mail: xinwen.hu@vanderbilt.edu; bo.choi@vanderbilt.edu; dan.fleetwood@vanderbilt.edu; ron.schrimpf@vanderbilt.edu; rkfg@vuse.vanderbilt.edu; robert.a.weller@vanderbilt.edu).

H. J. Barnaby is with the Department of Electrical and Computer Engineering, University of Arizona, Tucson, AZ 85721 USA (e-mail: barnaby@ece.arizona.edu).

K. McDonald was with the Department of Physics, Vanderbilt University, Nashville, TN 37235 USA. He is now with Sandia National Laboratories, Albuquerque, NM 87185 USA (e-mail: kyle.mcdonald@vanderbilt.edu).

U. K. Mishra is with the Department of Electrical and Computer Engineering, University of California at Santa Barbara, Santa Barbara, CA 93106 USA (e-mail: mishra@ece.ucsb.edu).

R. W. Dettmer is with the Air Force Research Laboratory (AFRL), Wright-Patterson AFB, OH 45433 USA (e-mail: ross.dettmer@wpafb.af.mil).

Digital Object Identifier 10.1109/TNS.2002.805399

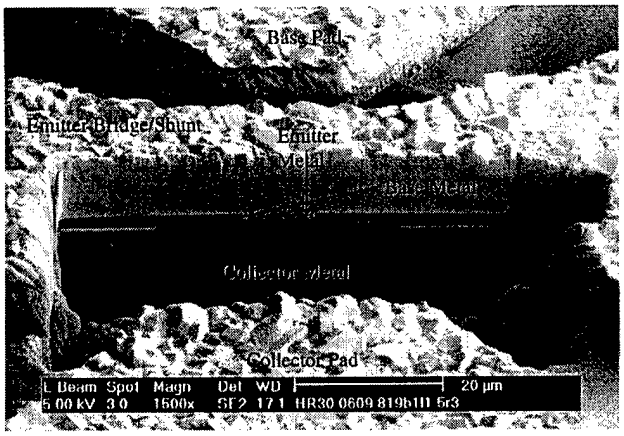

Fig. 1. Focused ion beam (FIB) cross section of a device with the contacts identified.

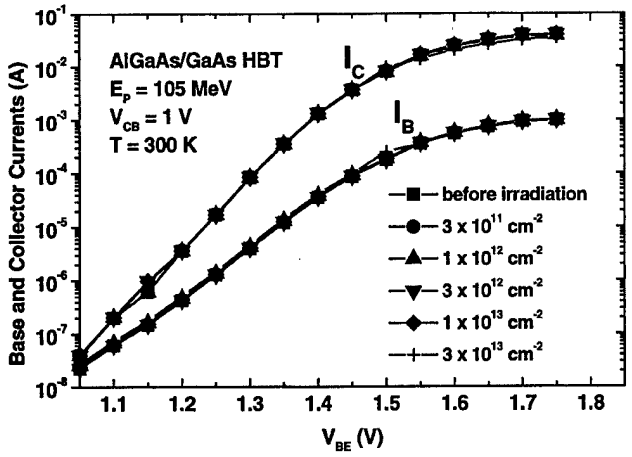

Fig. 2. Gummel characteristics for AlGaAs/GaAs HBT device before and after 105-MeV proton irradiation.

provides a growth transition layer from AlGaAs to InGaAs. The InGaAs layer is used for good contact. The graded layer was inserted to smooth out the conduction-band discontinuity.

Samples were diced and mounted in 40-pin dual in-lin package (DIP) packages. Devices were irradiated at two proton energies. Overall, 1.8-MeV protons were used to study the degradation mechanisms and 105-MeV protons were used to be more representative of the space environment. Two devices from the same wafer were used for each experiment to check the variations. All of them showed the same behavior before and after irradiation.

For the 1.8-MeV proton irradiation, the devices were irradiated at room temperature under vacuum using the Vanderbilt University 2-MeV Van de Graaff accelerator with ion currents from 4.8 to 7.5 nA, and fluences of 3×10^{11}cm^{-2}, 1×10^{12} cm^{-2}, 3×10^{12} cm^{-2}, 1×10^{13} cm^{-2}, and 3×10^{13} cm^{-2}. The dose in rad(GaAs), D, is related to the fluence, ϕ, through the relation [7]

$$D = 1.6 \times 10^{-5} \cdot \Phi \cdot LET \qquad (1)$$

where LET is the linear energy transfer of the material and is given in units of MeV-cm^2/mg. According to calculations [7] and through Monte Carlo simulation with the SRIM program [8], the LET of 1.8-MeV protons in GaAs is 7.86×10^{-2} MeV-cm^2/mg. Thus, the fluences correspond to total (ionizing) doses of 378, 1.3, 3.8, 12.6, and 37.8 Mrad(GaAs), respectively; however, as discussed below, the NIEL is a more relevant quantity for these devices than is the total ionizing dose. Although these ionizing doses are relatively large, X-ray irradiations confirmed that there was no significant degradation due to total ionizing dose.

For the 105-MeV proton irradiation, the experiments were performed at the TRIUMF accelerator at the University of British Columbia, Vancouver, Canada. The fluences were the same as those used in the 1.8-MeV experiment, with proton fluxes of about 9×10^8 cm^{-2}s^{-1}, which correspond to total doses of 22.56 krad(GaAs) to 2.26 Mrad(GaAs), respectively. All terminals were grounded during the irradiation.

After proton radiation, the dc performance of the HBT devices was measured immediately using an HP4156A semiconductor parameter analyzer. All of the measurements were performed at room temperature. The samples were measured again after two days and after three months to check for annealing effects.

III. Results

Fig. 2 shows typical Gummel characteristics [$\log(I_C)$ and $\log(I_B)$ versus V_{BE}] in an HBT device before and after 105-MeV proton irradiation. No significant changes are visible, even at the highest proton fluence (3×10^{13} cm^{-2}). The collector current decreases less than 2% at a fluence of 10^{13} cm^{-2}, and at 3×10^{13} cm^{-2}, it decreases just 15%, which makes the current gain degrade 15%. Although the energy spectrum of protons in space is highly dependent on the orbit, most of the protons reaching the device will have relatively high energies. Thus, the degradation due to 105-MeV protons is a reasonable indicator of the radiation tolerance of these devices in space. The good radiation tolerance of these devices is partly the result of the thin, heavily doped base region [9].

The base current is plotted versus emitter–base voltage before and after 1.8-MeV proton irradiation in Fig. 3. Post-irradiation annealing results are also plotted in the figure. For proton fluences up to 10^{12} cm^{-2}, the base current is nearly constant. When the proton fluence reaches 3×10^{12} cm^{-2}, the base current increases $\sim$25% at $V_{BE} = 1.55$ V; at 10^{13} cm^{-2}, the base current increases 100%; and at 3×10^{13} cm^{-2}, the base current increases 250%. There is almost no change in base current during three months of post-irradiation room temperature annealing in air.

It is interesting to note that the collector current decreases significantly. Fig. 4 shows the collector current versus emitter–base voltage for different proton fluences with $V_{CB} = 1$ V. The collector current changes very little for fluences below 10^{12} cm^{-2}. However, at 3×10^{12} cm^{-2}, the collector current decreases $\sim$20% at $V_{BE} = 1.55$ V; at 10^{13} cm^{-2}, the collector current decreases $\sim$55%; and at 3×10^{13} cm^{-2}, the collector current decreases 97%. The collector current recovers 4% after three months of room temperature annealing, but it remains far less than the pre-irradiation value. All of the irradiated devices show the same behavior.

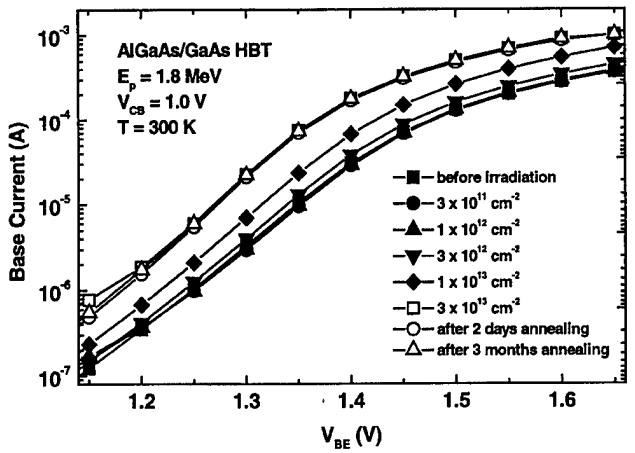

Fig. 3. Logarithm of I_B versus V_{BE} for a typical GaAs HBT device at V_{CB} = 1.0 V before and after 1.8-MeV proton irradiation at 300 K.

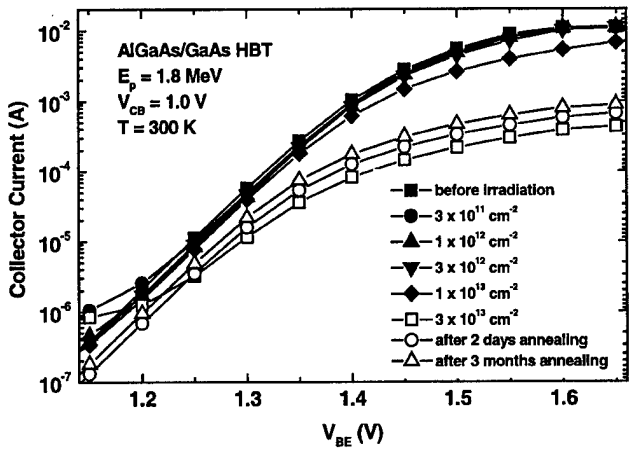

Fig. 4. Logarithm of I_C versus V_{BE} for the device and irradiation conditions of Fig. 3.

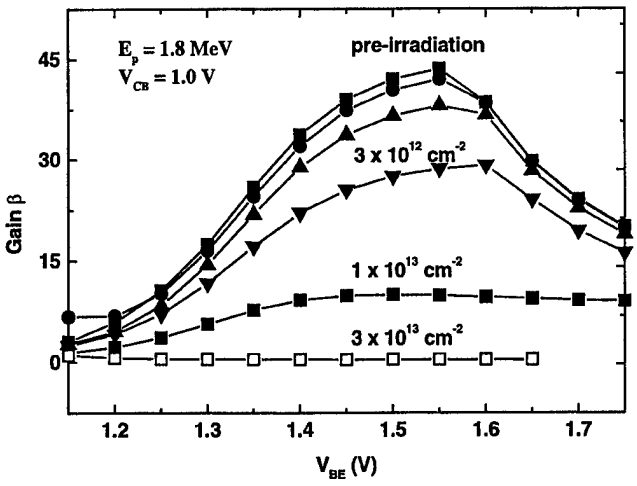

Fig. 5. Pre- and post-radiation current gain (β) for a GaAs HBT device versus the emitter-to-base voltage at 300 K.

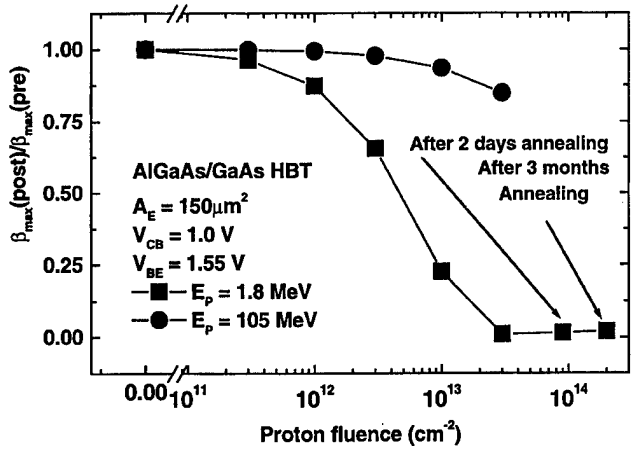

Fig. 6. Normalized current gain as a function of proton fluences for AlGaAs/GaAs HBTs with proton energy of 1.8 MeV and 105 MeV at 300 K.

Because of the increase of the base current and the large decrease of the collector current, the current gain β decreases very significantly after 1.8-MeV proton irradiation. The degradation of the current gain for different values of V_{BE} before and after 1.8-MeV proton irradiation is shown in Fig. 5. A comparison of current-gain degradation due to 1.8- and 105-MeV proton irradiation is shown in Fig. 6.

For 1.8-MeV irradiation, the peak current gain is 44 at a base emitter voltage of 1.55 V before irradiation. After 10^{12}-cm^{-2} proton irradiation, the peak gain shows little degradation; at 3×10^{12} cm^{-2}, it decreases 35%; at 10^{13} cm^{-2}, it decreases 75%. For a fluence of 3×10^{13} cm^{-2}, the current gain has essentially gone to zero. After three months of annealing, the peak current gain recovers very little.

IV. Discussion

Previous work has shown that GaAs devices can be irradiated with gamma rays to levels in excess of 400 Mrad(GaAs) without significant degradation [2], [10]. Our own 10-keV X-ray experiments with the HBT devices also found no significant changes after a total ionizing dose of 30 Mrad(GaAs). Thus, ionization effects are relatively unimportant in determining the radiation response of these devices. Hence, we expect the degradation in device performance to be caused by displacement damage.

The displacement damage effects from a variety of different particles can be correlated on the basis of the NIEL. Estimates using the SRIM program [8] (ignoring nuclear reactions) indicate that the NIEL for 1.8-MeV protons is approximately 70 times higher than the NIEL for 105-MeV protons in the first 2 μm of the device, which explains why the degradation of the current gain due to 1.8-MeV protons is almost 80 times larger than that caused by 105-MeV protons at a fluence of 3×10^{13} cm^{-2} (Fig. 6).

Base current ideality factors [n in the expression $I = I_0 + I_1 \exp(qV/nkT)$] at low V_{BE} are useful in determining the degradation mechanisms. For 1.8-MeV proton irradiation, the base current ideality factor (measured with 1.0 V $< V_{BE} <$ 1.35 V) changes in the range from 1.76 to 1.46 before and after proton irradiation, respectively. This implies that recombination happens both in the base–emitter depletion region and in the neutral base region, because the recombination current in the emitter–base depletion region has an ideality factor of ~2.0,

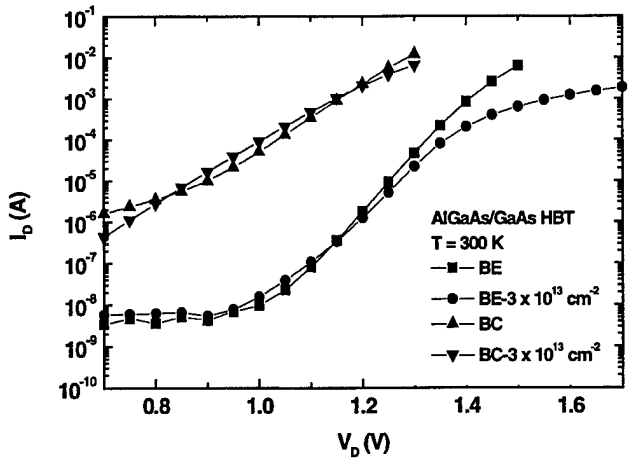

Fig. 7. Current–voltage characteristics of B–E diode and B–C diode after 1.8-MeV proton irradiation. The proton fluence is 3×10^{13} cm^{-2}.

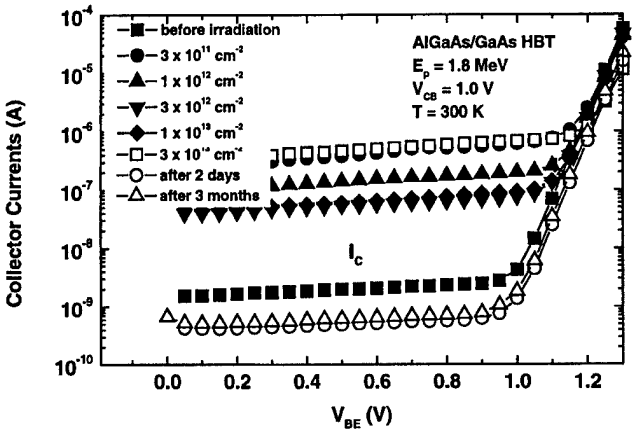

Fig. 8. Collector current at the low emitter–base voltage range before and after 1.8-MeV proton irradiation.

whereas the recombination current in the neutral base region has an ideality factor of ~1.0 [11]. The base–current increase is due to displacement damage-induced traps, which decrease the minority-carrier lifetime.

The great decrease of collector current in the devices irradiated with 1.8-MeV protons is due to the deterioration of the emitter–base diode. The base–emitter and base-collector diode current–voltage characteristics are shown in Fig. 7. The base–emitter heterojunction was degraded more than the base–collector homojunction after 1.8-MeV proton irradiation (e.g., in the active region at $V_{BE} = 1.5$ V, the current level decreased by more than a factor of ten after irradiation), which decreases the emitter injection efficiency. The same phenomenon was previously observed in neutron irradiation experiments [12].

The collector current at low emitter–base voltage (<1.0 V) increases several hundred times after irradiation, and it recovers after annealing, as shown in Fig. 8. The greatly increased leakage current comes from generation current in the reverse-biased base–collector depletion region, which is due to the creation of trapping centers by displacement damage.

V. Summary

GaAs HBTs were irradiated with protons at energies of 1.8 MeV and 105 MeV and at fluences ranging from 3×10^{11} cm^{-2} to 3×10^{13} cm^{-2}. For 1.8-MeV proton irradiation, the increase of the base current and the large decrease of collector current both contribute to the degradation of the device. The increase of the base current is due to displacement damage-induced traps, which decrease the minority carrier lifetime. However, the collector current decrease appears to be mainly due to degradation of the emitter–base diode, which decreases the electron injection efficiency. Although these HBT devices show significant degradation for 1.8-MeV proton irradiation, they are good candidates for applications in space systems because they exhibit relatively little degradation due to high-energy (105 MeV) protons, which are much more representative of space than are 1.8-MeV protons.

Acknowledgment

The authors thank E. Blackmore for proton irradiation and the Air Force Office of Scientific Research MURI program for funding support.

References

[1] J. D. Cressler, M. C. Hamilton, G. S. Mullinax, Y. Li, G. Niu, C. J. Marshall, P. W. Marshall, H. S. Kim, and M. J. Palmer, "The effects of proton irradiation on the lateral and vertical scaling of UHV/CVD SiGe HBT BiCMOS technology," *IEEE Trans. Nucl. Sci.*, vol. 47, pp. 2515–2520, Dec. 2000.

[2] S. Zhang, G. Niu, J. D. Cressler, S. J. Mathew, U. Gogineni, S. D. Clark, P. Zampardi, and R. L. Pierson, "A comparison of the effects of gamma irradiation on SiGe HBT and GaAs HBT technologies," *IEEE Trans. Nucl. Sci.*, vol. 47, pp. 2521–2527, Dec. 2000.

[3] J. M. Roldan, G. Niu, W. E. Ansley, J. D. Cressler, S. D. Clark, and D. C. Ahlgren, "An investigation of the spatial location of proton-induced traps in SiGe HBTs," *IEEE Trans. Nucl. Sci.*, vol. 45, pp. 2424–2429, Dec. 1998.

[4] J. A. Babcock, J. D. Cressler, L. S. Vempati, S. D. Clark, R. C. Jaeger, and D. L. Harame, "Ionizing radiation tolerance and low-frequency noise degradation in UHV/CVD SiGe HBT's," *IEEE Electron Device Lett.*, vol. 16, pp. 351–353.

[5] S. B. Witmer, S. D. Mittleman, D. Lehy, and R. Ren *et al.*, "The effects of ionizing radiation on GaAs/AlGaAs and InGaAs/AlInAs heterojunction bipolar transistors," *Mater. Sci. Eng.*, vol. B2, pp. 280–291, 1993.

[6] Y. Song, M. E. Kim, A. K. Oki, and M. E. Hafizi, "Effects of neutron irradiation on GaAs/AlGaAs heterojunction bipolar transistors," *IEEE Trans. Nucl. Sci.*, vol. 36, pp. 2155–2160, Dec. 1989.

[7] G. L. Hash, J. R. Schwank, M. R. Shaneyfelt, C. E. Sandoval, M. P. Connors, T. J. Sheridan, F. W. Sexton, E. M. Slayton, J. A. Heise, and C. C. Foster, "Proton irradiation effects on advanced digital and microwave III–V components," *IEEE Trans. Nucl. Sci.*, vol. 41, pp. 2259–2266, Dec. 1994.

[8] J. F. Ziegler, J. P. Biersack, and U. Littmark, *The Stopping and Range of Ions in Solids*, 2nd ed. New York: Pergamon Press, 1996.

[9] W. Liu, *Handbook of III–V Heterojunction Bipolar Transistors*. New York: Wiley, 1998.

[10] M. A. Listvan, P. J. Vold, and D. K. Arch, "Ionizing radiation hardness of GaAs Technologies," *IEEE Trans. Nucl. Sci.*, vol. NS-34, p. 1664, 1987.

[11] S. L. Kosier, A. Wei, R. D. Schrimpf, D. M. Fleetwood, M. DeLaus, R. L. Pease, and W. E. Combs, "Physically-based comparison of hot-carrier-induced and ionizing-radiation-induced degradation in BJTs," *IEEE Trans. Electron Devices*, vol. 42, pp. 436–444, 1995.

[12] G. A. Schrantz *et al.*, "Neutron irradiation effects on AlGaAs/GaAs heterojunction bipolar transistors," *IEEE. Trans. Nucl. Sci.*, vol. NS-35, pp. 1657–1661, June 1988.